INSTITUTO POTOSINO DE INVESTIGACIÓN CIENTÍFICA Y TECNOLÓGICA, A.C.

POSGRADO EN CIENCIAS AMBIENTALES

Enhancing the removal of styrene vapors and greenhouse gases using ionic liquids and deep eutectic solvents

Mariana Candía Lomelí

Para obtener el grado de
Doctora en Ciencias Ambientales

Directora de la Tesis
Dra. Sonia Lorena Arriaga García

San Luis Potosí, S.L.P., Septiembre del 2023

Constancia de aprobación de la tesis

La tesis **"Enhancing the removal of styrene vapors and greenhouse gases using ionic liquids and deep eutectic solvents"** presentada para obtener el Grado de Doctora en Ciencias Ambientales fue elaborada por **Mariana Candia Lomelí** y aprobada el 22 de Septiembre de 2023 por los suscritos, designados por el Colegio de Profesores de la División de Ciencias Ambientales del Instituto Potosino de Investigación Científica y Tecnológica, A.C.

_____

Dra. Sonia Lorena Arriaga García
(Directora de tesis)

_____

Dr. César Nieto Delgado
(Miembro del Comité Tutoral)

_____

Dr. Aitor Aizpuru
(Miembro del Comité Tutoral)

_____

Dr. Guillermo Quijano Govantes
(Miembro del Comité Tutoral)

Créditos Institucionales

Esta tesis fue elaborada en los laboratorios de la División de Ciencias Ambientales del Instituto Potosino de Investigación Científica y Tecnológica, A.C., bajo la dirección de la Dra. Sonia Lorena Arriaga García**.**

Durante la realización de este trabajo de investigación la autora recibió una beca académica del Consejo Nacional de Ciencia y Tecnología 736303

Página en blanco que se va a utilizar para colocar la copia del acta de examen

Dedicatoria

Este trabajo está dedicado a mis padres Gerardo y Graciela por todo su apoyo y amor incondicional,

A mis hermanas Sarai, Andrea y Sofía y a mi hermano Gerardo por acompañarme con alegría y cariño en este trayecto.

Agradecimientos

Me complace extender mi más profundo agradecimiento a la Dra. Sonia Lorena Arriaga García por permitirme trabajar bajo su dirección, por compartir su conocimiento y experiencia y también por su paciencia y dedicación. Así como a los miembros de mi comité tutoral Dr. Guillermo Quijano Govantes, al Dr. Aitor Aizpuru, a la Dra. Fátima Pérez Rodríguez y al Dr. César Nieto Delgado por sus valiosos aportes, sus críticas constructivas y su tiempo.

Al Dr. Antonio Avalos Ramírez por el apoyo y las facilidades otorgadas para la realización de la estancia en el CNETE, así como a la Dra. Beatriz Delgado Cano por sus atenciones prestadas durante mi estancia en los laboratorios del CNETE.

Agradezco al IPICYT y al CNETE por la infraestructura, equipo y materiales brindados para realizar mi doctorado.

Agradezco a CONAHCYT por la beca otorgada.

A los técnicos académicos de la División de Ciencias Ambientales, el M. en C. Guillermo Vidriales Escobar, el M. en C. Juan Pablo Rodas Ortiz y la Dra. Elizabeth Isaacs por su apoyo técnico.

Gracias a Itzel Covarrubias por su asesoría con los experimentos y en la revisión de resultados, a mis compañeras que hicieron muy amena la convivencia dentro y fuera de los laboratorios: Mariana, Lilia, Mónica, Estheisy, Dulce, Joel y Noelia

A mis amigas Anaí, Karime, Marisol por todos los buenos momentos que compartimos en el transcurso de estos años.

Gracias a mi Sofis que me ayudó con el diseño de la presentación y los graphical abstracts.

Finalmente, agradezco a mis padres, mis hermanas y mi hermano, por su acompañamiento, su apoyo incondicional, por creer en mí y por todo su amor.

Contenido

Table of Figures

Table of Tables

Resumen

Mejora en la eliminación de vapores de estireno y gases de efecto invernadero utilizando líquidos iónicos y mezclas eutécticas de bajo punto de fusión

Palabras clave: ILs, DESs, NADESs, biodegradación de estireno, captura de gases de efecto invernadero

La calidad del aire tiene un impacto significativo en la salud humana. Según el informe State of Global Air 2020 del Health Effects Institute, en 2019, la contaminación del aire se clasificó como el cuarto factor de riesgo principal de muerte prematura a nivel mundial. Entre las actividades antropogénicas responsables de la contaminación del aire se encuentran la quema de combustibles fósiles, las actividades industriales y agrícolas, y la gestión de residuos. Estas actividades liberan una serie de contaminantes al medio ambiente, incluyendo dióxido de carbono (CO_2), los óxidos de nitrógeno (NO_x), los compuestos orgánicos volátiles (COVs), el dióxido de azufre (SO_2), el monóxido de carbono (CO), las partículas en suspensión y el ozono (O_3). La exposición al aire contaminado tiene efectos adversos tanto en la salud humana (problemas respiratorios, enfermedades cardiovasculares, alergias e irritaciones), así como en el medio ambiente, contribuyendo al calentamiento global, la lluvia ácida y la formación de ozono a nivel del suelo. Por lo tanto, es de suma importancia desarrollar tecnologías para controlar las emisiones de contaminantes atmosféricos. Actualmente existen diversas técnicas para el control de las emisiones de contaminantes atmosféricos, tales como la adsorción, la absorción, la destrucción térmica y los tratamientos biológicos.

Recientemente, se está investigando cada vez más el uso de líquidos iónicos (LI), de mezclas eutécticas de bajo punto de fusión (DES, por sus siglas en inglés) y de mezclas eutécticas de bajo punto de fusión naturales (NADES, por sus siglas en inglés) para la mitigación de los contaminantes atmosféricos. Los LI son sales líquidas que consisten únicamente en iones y tienen bajo punto de fusión (<100°C). Los DES y los NADES, por otro lado, son solventes formados por mezclas eutécticas de donantes de enlaces de hidrógeno (HBD) y aceptores de enlaces de hidrógeno (HBA). Estos solventes poseen varias propiedades que los hacen atractivos para el control de la contaminación del aire: baja presión de vapor, alta estabilidad térmica, excelentes propiedades de disolución y capacidad para disolver una amplia gama de gases y COVs. También pueden ser regenerados y reutilizados, lo que los hace más sostenibles desde el punto de vista ambiental en comparación con los procesos tradicionales basados en solventes

orgánicos. En este contexto, esta tesis doctoral se enfoca a estudiar el uso de estos nuevos disolventes como absorbentes de COVs en particular el estireno. En primer lugar, se realizó una evaluación de las principales características fisicoquímicas de los solventes, como densidad, viscosidad, polaridad, ángulo de contacto, estabilidad térmica y solubilidad en agua. También se evaluó la biodegradabilidad de los solventes y su toxicidad hacia lodo activado. Los experimentos de absorción de estireno revelaron que los mejores solventes fueron el DES formado con bromuro de tetrabutilamonio y ácido decanoico, así como los LIs [C_6mim][FAP], [C_4mim][NTf_2] y [C_4mim][PF_6], debido a sus bajos valores de coeficiente de partición de estireno. A continuación, se seleccionó el IL [C_6mim][FAP] como una fase líquida no acuosa (NAPL, por sus siglas en inglés) en un biorreactor de partición (TPPB, por sus siglas en inglés) debido a su alta afinidad por el estireno, baja solubilidad en agua y que es no biodegradable; la mineralización del estireno fue tres veces mayor en el TPPB en comparación con el control. La segunda parte de esta tesis consiste en usar estos nuevos solventes en la captura de gases de efecto invernadero (GEI). Dado que la utilización de IL, DES y NADES en el proceso de absorción de GEI presenta limitaciones de transferencia de masa debido a su elevada viscosidad, este estudio propuso la impregnación de estos disolventes en un material de soporte poroso como silica gel (SiO_2) para superar esta limitación. Se investigó la influencia del tamaño de partícula de SiO_2 impregnada en la captura de CO_2 y N_2O a presión y temperatura ambiente. El material impregnado se caracterizó mediante espectroscopia infrarroja por transformada de Fourier (FTIR), análisis termogravimétrico (TGA) y difracción de rayos X (XRD). El coeficiente de partición del CO_2 y el N_2O se determinó mediante un método estático de espacio de cabeza. El análisis de FTIR y TGA de las partículas impregnadas indicó una impregnación exitosa del silica gel con los solventes. El coeficiente de partición del CO_2 en SiO_2 impregnada mostró un rango de 0.46 a 4.75, mientras que el coeficiente de partición del N_2O en SiO_2 impregnado osciló entre 0.50 y 2.21. Esto indica que las partículas impregnadas tienen una mayor afinidad por el N_2O en comparación con el CO_2. El proceso de impregnación demostró la capacidad de reducir el consumo de solvente en un 60% mientras se preserva la capacidad de captura de gases de efecto invernadero. Por último, se realizó la predicción de los coeficientes de ley de Henry en varios líquidos iónicos basados en imidazol con aniones fluorado a través de cálculos de mecánica cuántica.

Abstract

Enhancing the removal of styrene vapors and greenhouse gases using ionic liquids and deep eutectic solvents

Keywords: ILs, DESs, NADESs, styrene biodegradation, greenhouse gases capture

Air quality significantly influences human health. According to the State of Global Air 2020 report by the Health Effects Institute, air pollution was the fourth leading cause of premature death worldwide in 2019. Various anthropogenic activities contribute to air pollution, including the burning of fossil fuels, industrial and agricultural operations, and waste management. These activities release pollutants such as carbon dioxide (CO_2), nitrogen oxides (NOx), volatile organic compounds (VOCs), sulfur dioxide (SO_2), carbon monoxide (CO), particulate matter, and ozone (O_3) into the atmosphere. Exposure to polluted air can have adverse effects on human health, including respiratory problems, cardiovascular diseases, allergies, and irritation. Moreover, these pollutants also have environmental impacts such as global warming, acid rain, and the formation of ground-level ozone.

To address these issues, it is crucial to develop technologies for controlling air pollutant emissions. Several techniques have been developed for this purpose, including adsorption, absorption, thermal destruction, and biological treatments. In recent years, the use of ILs, DES, and NADES has gained prominence for air pollution mitigation. ILs are unique molten salts composed entirely of ions and have a low melting point below 100 °Celsius. DES and NADES, on the other hand, are solvent systems formed by eutectic mixtures of hydrogen bond donors (HBDs) and hydrogen bond acceptors (HBAs). These solvents possess advantageous properties for air pollution control, including low vapor pressure, high thermal stability, excellent solvent properties, and the ability to dissolve a wide range of gases and VOCs. Additionally, they can be regenerated and reused, making them environmentally sustainable compared to traditional solvent-based processes. One focus of this doctoral dissertation was the study of these emerging solvents as absorbents for VOCs, specifically styrene. The physicochemical characteristics of the solvents, such as density, viscosity, polarity, contact angle, thermostability, and water solubility, were assessed, along with their biodegradability and toxicity towards activated sludge. The absorption experiments revealed that DESs formed with tetrabutylammonium bromide and decanoic acid, as well as the ILs [C_6mim][FAP], [C_4mim][NTf_2], and [C_4mim][PF_6], exhibited the lowest styrene partition coefficients, making them the most suitable solvents. Subsequently, the IL [C_6mim][FAP] was selected as a non-aqueous phase liquid (NAPL) in a TPPB (Two-Phase Partitioning Bioreactor) batch

process, demonstrating high styrene affinity, low solubility in water, and non-biodegradability. The TPPB process achieved three times higher styrene mineralization compared to the control. The second part of this research was to explore the use of ILs, DESs, and NADESs for greenhouse gas (GHG) capture. However, the high viscosity of these solvents presents mass transfer limitations in GHG absorption processes. To overcome this limitation, the impregnation of these solvents onto a porous support material, such as silica gel, was proposed. The influence of particle size of the impregnated silica on the capture of CO_2 and N_2O at atmospheric pressure and temperature was investigated. The impregnated material was characterized using thermogravimetric analysis (TGA), X-ray diffraction (XRD), and Fourier-transform infrared spectroscopy (FTIR). The determination of CO_2 and N_2O partition coefficient was carried out using a static headspace method. The FTIR and TGA analyses confirmed the successful impregnation of silica gel with the solvents. The impregnated silica exhibited CO_2 partition coefficient ranging from 0.46 to 4.75, while N_2O partition coefficient ranged from 0.50 to 2.21. This indicates that the impregnated particles have a higher affinity for N_2O compared to CO_2. Moreover, the impregnation process demonstrated a significant reduction of solvent consumption by 60% while maintaining the greenhouse gas capture capacity. Finally, the prediction of Henry's law constants of CO_2 and N_2O for several fluorinated imidazolium-based ionic liquids using quantum mechanics was performed in the last part of this thesis.

1. General Background

1.1. Introduction

Air pollution is the presence of contaminants or substances in the air that interfere with human health or welfare or produce other harmful environmental effects (Vallero, 2019). Categorizing air pollutants based on their physical attributes yields three distinct groupings: 1) Coarse Particulate Matter (PM), these are either solid particles or liquid droplets with an average diameter exceedingly approximately 10 µm. 2) Aerosols, this category encompasses solid particles or liquid droplets that generally fall within an average diameter range of less than 10 µm. 3) Gases, this grouping involves contaminants existing in a gaseous or vapor state, such as carbon monoxide, carbon dioxide, sulfur dioxide, nitric oxide (NO), nitrogen dioxide (NO_2), and ozone. Additionally, it includes substances that are not typically in gaseous form, such as vapors from volatile organic compounds (VOCs) and volatile nonmetal or metal vapors like arsenic, mercury, and zinc when they exist in a vaporized state (Hocking, 2005).

Among this air pollutant last category air pollutants such as VOCs and GHGs, given their impact in health and environment are mainly discussed. VOCs according to the United States Environmental Protection Agency (USEPA), are defined as organic chemicals that have a high vapor pressure at room temperature, which allows them to easily evaporate into the air, some examples are styrene, benzene, toluene, acetone, formaldehyde, xylene, trichloroethylene and perchloro ethylene, while GHGs are gases that can absorb long-wavelength thermal radiation emitted from the Earth's surface, such as CO_2, N_2O, CH_4 and hydrofluorocarbons (HFCs), perfluorocarbons (PFCs), and sulfur hexafluoride (SF_6) (Sonwani & Saxena, 2022).

In terms of environmental impact, VOCs formed ground-level ozone when they react with nitrogen oxides (NOx) in the presence of sunlight. Ground-level ozone presents health problems in humans and causes damage to vegetation and wildlife (Vallero, 2014). GHGs, on the other hand, contribute to global warming, a significant environmental concern. Gaseous pollutants have both natural and anthropogenic sources. Natural sources include respiration from plants and animals, decomposition of organic matter, volcanoes, and naturally occurring forest fires. Various plant species, such as cedar, pine, eucalyptus, lavender, mint, and sage, emit VOCs (Hocking, 2005). Anthropogenic sources of air pollutants, including VOCs, come from consumer products like room air deodorants, building materials such as paints and adhesives, and personal activities like

smoking, driving, and showering. Traditional outdoor sources such as chemical plants, petroleum refineries, automobiles, and hazardous waste sites also contribute, but to a lesser extent, typically accounting for less than 25% of personal exposure to VOCs. In terms of GHG emissions, transportation, electricity production, industries, the commercial and residential sectors, agriculture, land use, and forestry are the major contributors (Bloemen & Burn, 1993).

The adverse effects of air pollution on human health include impairment of lung function in children, inflammation in airways, lung aging, and the development of chronic obstructive pulmonary disease (COPD). Air pollution is also responsible for a significant number of cardiovascular and stroke deaths. It affects the immune system, contributing to the development and exacerbation of allergic and potentially autoimmune diseases. Emerging evidence suggests links between air pollution and cognitive function, neurological diseases, diabetes, obesity, and endocrine changes (Xiao & Gao, 2021).

Hence, it is imperative to tackle air pollution to alleviate its detrimental impact on both the ecosystem and human health. Different methods have been developed for the removal of gaseous pollutants, including absorption, adsorption, condensation, thermal destruction, and biological processes. Among these methods, biological systems offer several advantages. They operate at relatively low costs since they can be operated under ambient temperature and pressure conditions. Additionally, biological systems typically generate minimal toxic by-products and have low emissions of greenhouse gases like NOx and CO_2, which sets them apart from thermal systems. Biological systems are suitable for treating waste streams with low to moderate concentrations of VOCs. The VOC concentrations must be high enough to serve as food sources for microbes but not toxic to them. In these systems, the air or gas containing VOCs is passed through a biologically active medium, where microbes break down the compounds into simpler forms, ultimately converting them to CO_2 (in aerobic conditions) or methane (in anaerobic conditions) and water. Furthermore, biological systems have demonstrated effectiveness in removing various vapor-phase inorganic compounds, including ammonia, hydrogen sulfide, sulfides (such as carbon disulfide), and mercaptans, in addition to a wide range of volatile chain and aromatic organic compounds (Pham & Pakrasi, 2017).

Unfortunately, biological processes face challenges when the transfer of hydrophobic pollutants and oxygen from the gaseous phase to the microorganisms in the aqueous phase is slow, limiting

their effectiveness. To overcome these limitations and expand the scope of biological treatment for contaminated air, two-phase partitioning reactors (TPPBs) have been proposed. TPPBs incorporate both an aqueous phase and a non-aqueous phase. The presence of the non-aqueous phase facilitates the transfer of hydrophobic VOCs and oxygen to the microorganisms, while also reducing the exposure of microorganisms to inhibitory substances by diluting their concentration in the aqueous phase (Muñoz et al., 2007). The absorption of pollutant gases in a liquid, requires a selective liquid that is tailored to the specific gas being targeted. The choice of absorption liquid is crucial, as it should possess high gas solubility to ensure efficient removal while minimizing the amount of solvent required. Additionally, the ideal solvent for absorption should have a low vapor pressure to prevent significant losses, as well as exhibit noncorrosive, inexpensive, nontoxic, nonflammable, and chemically stable properties. It is also advantageous for the solvent to have a low freezing point (Pham & Pakrasi, 2017).

Novel solvents had been proposed for the capture of different gases, among them ILs, DES and NADES present characteristics such as low volatility, high thermal stability, and the ability to dissolve a wide range of gases. Additionally, ILs, DESs and NADESs can be designed and tailored to have specific properties, such as high gas solubility and low viscosity, making them well-suited for gas capture applications. They can be modified by changing their components, allowing for customization based on the specific gas being targeted. Moreover, ILs, DESs and NADESs are considered more environmentally friendly compared to traditional organic solvents used in gas capture processes. They have low volatility, reducing the risk of emissions, and can be recycled and reused, minimizing waste generation. Their inherent stability and non-flammability further enhance their safety profile.

Overall, the unique properties and versatility of ILs, DESs and NADESs make them attractive options for gas capture applications, offering efficient and environmentally sustainable solutions for gas separation and purification processes, as well as an alternative for NAPL in a TPPB.

1.2. Objectives

The general objective of this study was to investigate the viability and effectiveness of ILs, DESs, and NADESs in the elimination of air pollutants, such as VOCs and GHG (CO_2 and N_2O). The physicochemical properties of these ILs, DESs, NADESs were evaluated, the toxicity and biodegradability, their capacity for absorbing a VOC such as styrene and was explored their

potential to enhance the biodegradation of VOCs in a partitioning bioreactor. Additionally, the developed porous materials impregnated with ILs, DESs, and NADESs to improve the capture of greenhouse gases such as CO_2 and N_2O was studied.

This general objective is based on the following previously established specific objectives:

1. Prepare and characterize different ILs, DESs, and NADESs physicochemically.

2. Determine the toxicity towards activated sludge and the biodegradability of different ILs, DESs, and NADESs.

3. Evaluate the absorbption of styrene as a model VOC in different ILs, DESs, and NADESs through gas/liquid partition coefficient measurements.

4. Enhance the biodegradation of a model VOC (styrene) using an ionic liquid as a mass transfer vector in a partitioning bioreactor.

5. Prepare and characterize porous materials (SiO_2) impregnated with ILs, DESs, and NADESs.

6. Measure the affinity of impregnated materials towards greenhouse gases (CO_2 and N_2O) through experimental determination of the partition coefficient.

By achieving these specific objectives, a deeper understanding of the use of ILs, DESs, and NADESs in air pollutant mitigation and their potential for environmental applications is expected to be obtained.

1.3. Hypothesis

Firstly, we expect that ILs, DESs, and NADESs, are effective absorbents for VOCs like styrene. Secondly, we hypothesize that the physicochemical characteristics, toxicity and biodegradability profile of ILs, DESs, and NADESs, as well as their affinity towards styrene, will make them suitable solvents to be used as NAPL in a TPPB that biodegrades styrene. Thirdly, we hypothesize that the utilization of an ionic liquid as a mass transfer vector in a TPPB will enhance the biodegradation of styrene. The presence of the ionic liquid is expected to facilitate the transfer of styrene to the biodegradation phase, resulting in an increase of styrene mineralization. Lastly, we propose that the impregnation of porous materials, such as SiO_2, with ILs, DESs, and NADESs will enhance the gas capture capacity for GHGs, specifically CO_2 and N_2O. This impregnation

technique is predicted to improve the sorption capacity of the solvents towards these gases, by increasing the area surface that it is in contact with the gaseous phase.

1.4. Structure of the thesis

The accomplishment of these objectives and the assessment of these hypothesis, leads to the arrange of this doctoral dissertation as follows:

Chapter 2. Potential of ILs, DESs, and NADESs to enhance VOCs removal: progress and challenges.

This chapter defines the concepts of ILs, DESs, and NADESs, and provides a summary of their key physicochemical characteristics, including density, viscosity, and thermal stability. It also presents information regarding their toxicity and biodegradability. Additionally, the chapter describes the application of ILs, DESs, and NADESs in the removal of various VOCs through both physicochemical and biological technologies.

Chapter 3. Preparation and physicochemical characterization of deep eutectic solvents and ionic liquids for the potential absorption and biodegradation of styrene vapors

The chapter investigates the potential use of ILs, DESs, and NADESs as absorbents for styrene vapors in a TPPBs process. Initially, the prepared NAPLs were subjected to characterization to evaluate their physicochemical properties, including density, viscosity, polarity, contact angle, thermostability, and water solubility. Subsequently, their biodegradability and toxicity towards activated sludge were assessed. The partition coefficient of styrene in the solvents was measured, and based on the results, [C_4MIM][FAP] exhibited the most favorable characteristics for NAPL use. Finally, it was employed in a TPPB system for styrene biodegradation.

Chapter 4. Greenhouse gases capture applying impregnated silica with IL, DES and NADES

This chapter focuses on the preparation and characterization (using FTIR, TGA, XRD) of impregnated silica with three distinct solvents, (IL, DES, and NADES). Subsequently, the CO_2 and N_2O partition coefficients were determined for both the pure solvents and the impregnated silica. The measurements were conducted using a static headspace method under atmospheric temperature and pressure conditions.

Chapter 5. Greenhouse gases solubility in fluorinated imidazolium based ionic liquids: a computational modeling approach.

The prediction of the CO_2 and N_2O Henry's law constants in fluorinated imidazolium-based ionic liquids using a computational model is addressed in this chapter.

Chapter 6. Global conclusions and perspectives

General considerations regarding the obtained results and future research directions are proposed in this chapter**.**

1.5. References

Bloemen, H. J. T., & Burn, J. (Eds.). (1993). *Chemistry and Analysis of Volatile Organic Compounds in the Environment*. Springer Netherlands. https://doi.org/10.1007/978-94-011-2152-1

Hocking, M. B. (2005). Air Quality Measurement and Effects of Pollution. *Handbook of Chemical Technology and Pollution Control*, 33–70. https://doi.org/10.1016/b978-012088796-5/50005-3

Muñoz, R., Villaverde, S., Guieysse, B., & Revah, S. (2007). Two-phase partitioning bioreactors for treatment of volatile organic compounds. In *Biotechnology Advances* (Vol. 25, Issue 4, pp. 410–422). https://doi.org/10.1016/j.biotechadv.2007.03.005

Pham, M., & Pakrasi, A. (2017). Air pollution control technologies. In *Proceedings of the Air and Waste Management Association's Annual Conference and Exhibition, AWMA*. https://doi.org/10.1016/b978-0-12-814934-8.00013-2

Sonwani, S., & Saxena, P. (2022). Greenhouse Gases: Sources, Sinks and Mitigation. In *Greenhouse Gases: Sources, Sinks and Mitigation*. https://doi.org/10.1007/978-981-16-4482-5

Vallero, D. (2014). The Science of Air Pollution. In *Fundamentals of Air Pollution*. https://doi.org/10.1016/b978-0-12-401733-7.00003-7

Vallero, D. A. (2019). Introduction. *Air Pollution Calculations*, 1–27. https://doi.org/10.1016/b978-0-12-814934-8.00001-6

2. Potential of ILs, DESs, and NADESs to enhance VOCs removal: progress and challenges

2.1. Abstract

Every year, around 7 million deaths are due to exposure from both outdoor and indoor air pollution. Air quality determines to a high extent the quality of human health. Volatile organic compounds (VOCs) are air pollutants widely spread from several industries such as chemical, automotive and food-related. Humans are mainly exposed to VOCs through inhalation of polluted air; thus, it is important to develop technologies to control air pollutant emissions. Ionic liquids (ILs), deep eutectic solvents (DESs), and natural deep eutectic solvents (NADESs) are compounds which can be used to treat VOCs emissions. They are non-volatile and stable at high temperatures. They can be hydrophilic or hydrophobic and their selection will depend on the nature of VOCs. This review article is devoted to show the potentialities of novel solvents such as ILs, DESs and NADESs to absorb VOCs based on the analysis of their physicochemical characteristics and level of toxicity and biodegradability. The application of such novel phases in partition bioreactors for VOCs abatement is specially discussed.

Keywords: VOCs, ILs, DES, NADES, absorption, biodegradation.

2.2. Introduction

Volatile organic compounds (VOC) are organic compounds with a vapor pressure between 1 and 760 torr at 20 °C, under normal conditions of pressure and temperature (1 atm, 0 °C) they are liquids or solids (Derwent, 1995). VOCs are air pollutants that can affect the human health, causing symptoms of asthma, chronic diseases, and premature death from respiratory diseases, heart, and lung cancer. In 2017, the Global Burden of Disease ranked exposure to air pollution as the fifth largest risk factor for human mortality worldwide (Health Effects Institute, 2019). The VOCs are emitted from anthropogenic and natural sources (Fig. 2.1). Anthropogenic origins include the combustion of fuel, landfill, agriculture, and chemical compounds. Natural sources encompass emissions from plants, forest fires, and anaerobic processes.

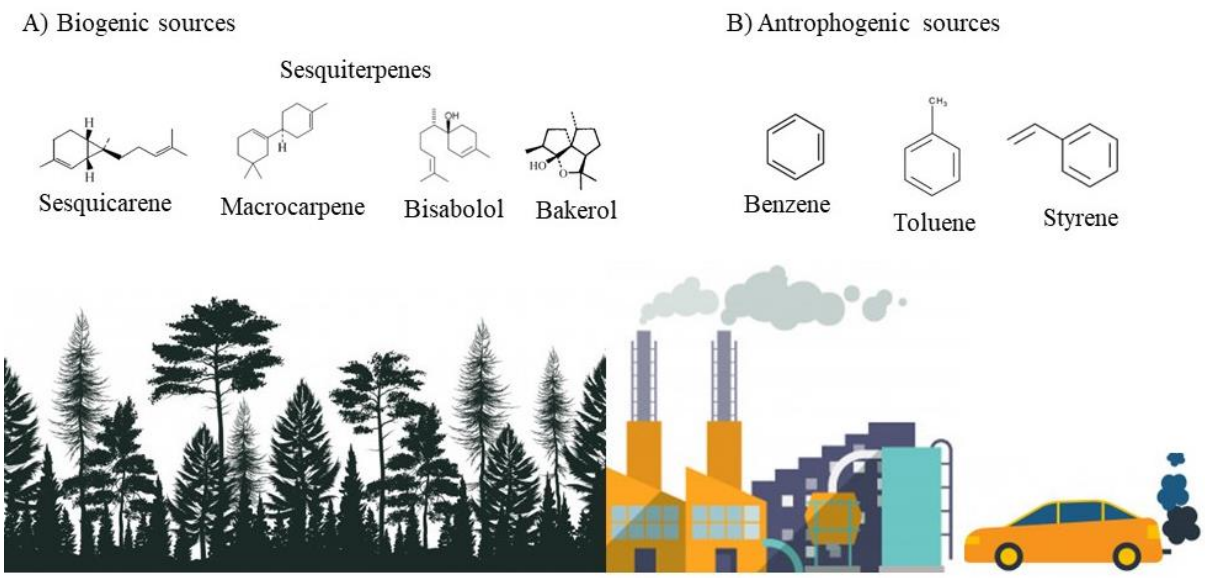

Fig. 2.1 Volatile organic compounds and their emission source A) Biogenic B) Anthropogenic

Several processes have been developed to control VOC emissions, they are based on physical, chemical and biological principles (condensation, membranes, absorption, adsorption, combustion, precipitation, oxidation, biofilters, trickling biofilters, bio-scrubbers, membrane bioreactors, suspended bioreactors, and partition bioreactors). The selection of the technology to remove VOCs is based on the chemical nature and the conditions of the stream. For example, physical treatments are applied when the flow rate (10-10000 m^3/h) and the concentration of pollutants are high (>1 g/m^3 to 100 g/m^3) (Revah and Morgan-Sagastume, 2005). Some advantages of biological processes are that they occurs at mild temperatures (10 to 40 ºC), and atmospheric pressure, making them cost-effective, easy to operate, and environmentally friendly (Le Cloirec et al., 2005). Biological systems are based on the ability of microorganisms to use VOCs as a source of carbon and energy, carrying out their cellular metabolism through the complete mineralization of VOCs (CO_2 + H_2O) or through a partial degradation (by-products, CO_2, H_2O, biomass). The performance of biological technologies is poor for hydrophobic VOCs treatment (Fig. 2.2A), because of their low mass transfer from the gas phase to the aqueous phase where microorganisms prevail, limiting microbial activity (Muñoz et al., 2012). For these cases, partitioning bioreactors (TPPBs) have been developed (Fig. 2.2B). TPPBs consists in the addition of a non-aqueous phase liquid (NAPL), which increases the mass transfer of VOC and oxygen from the gas phase to microorganisms.

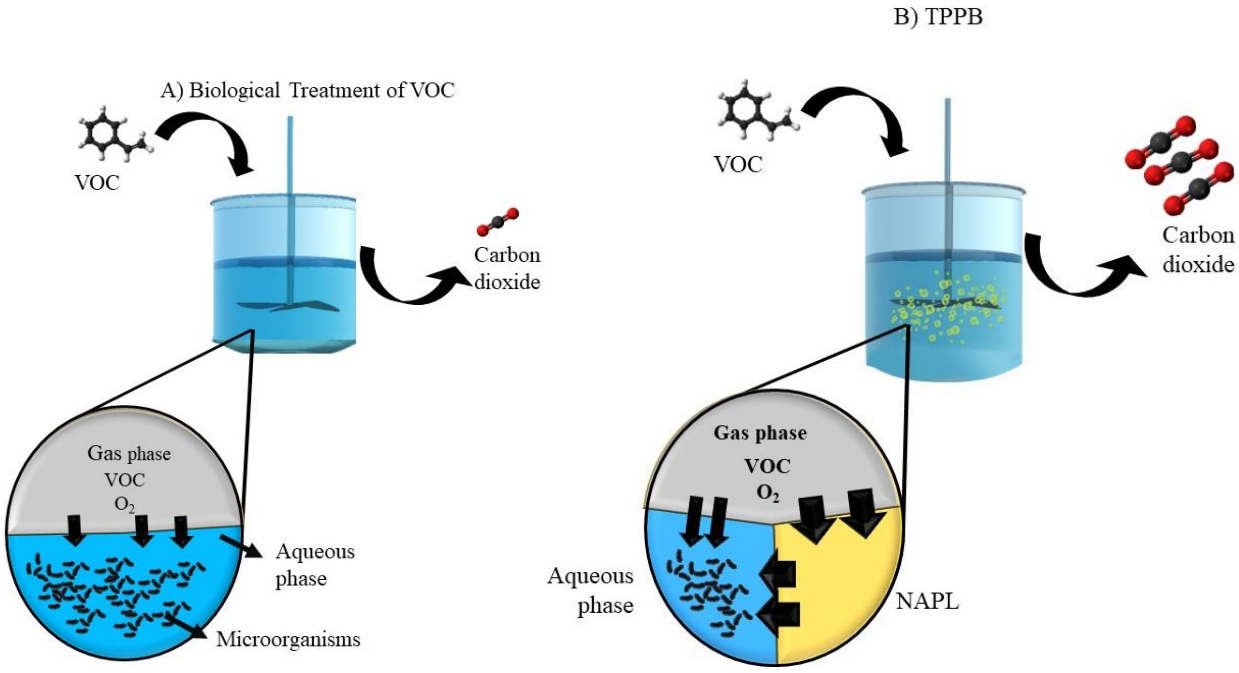

Fig. 2.2 A) Biological treatment of hydrophobic VOCs present low mass transfer, limiting their solubilizationin aqueous phase and thus lowering the biodegradation. B) Two phase partitioning bioreactor. Modified from Muñoz et al., (2007)

Some of the NAPLs already tested are silicone oil, hexadecane, and perfluorocarbons (Muñoz et al., 2007). An ideal NAPL should have the following characteristics: innocuous, non-biodegradable, high affinity for the target VOC, low tendency to form emulsion, immiscible in water and low vapor pressure (Muñoz et al., 2012). The application of ILs as absorbents for VOCs has been reported (Bedia et al., 2013; Cheng et al., 2009; Quijano et al., 2011a, 2013; Rodriguez Castillo et al., 2019; Wang et al., 2017; Yu et al., 2018, 2020; Zhao et al., 2019). Also, the use of ILs as NAPL has been investigated in TPPBs (Quijano et al., 2011a, 2013; Rodriguez Castillo et al., 2016, 2018b, 2018a, 2019). Other potential solvents for VOCs removal are DESs and NADESs (Chen et al., 2021, 2022; Indra et al., 2022; Li et al., 2022; Moufawad et al., 2022; Moura et al., 2017; Mu et al., 2022; Song et al., 2020) given their low cost, low toxicity, high biodegradability, and tailor-made ability.

Even though (Muñoz et al., 2012) recommended a non-biodegradable solvent as NAPL, the DESs and NADESs can be an alternative to expensive NAPL. In this case, the NAPL could be biodegraded, thus, competing with the VOCs degradation, but the NAPL could be replenish given

its low cost and due to its level of biodegradability this process will not generate wastes such as occur when non-biodegradable NAPL are used. The objective of this review is to analyze and summarize the potential of ILs, DESs, and NADESs to mitigate VOCs emissions through physicochemical and biological technologies.

2.3. ILs, DESs and NADESs

ILs are composed of cationic and anionic species, they are organic salts that are liquid at room temperature. ILs comprise large organic cations, resulting in an asymmetric structure, giving them a low tendency to crystallize. The cation commonly has a cyclic structure (e.g., imidazolium, pyrrolidinium, or pyridinium) or quaternary nitrogen or phosphorus atoms, all have attached alkyl chains and they can be combined with different anions, some of them are listed in Fig. 2.3 (Mallakpour & Dinari, 2012; Marcus, 2016). They have negligible vapor pressure and are recyclable, hence ILs are considered as green solvents. They are also known as "designer solvents" given the wide combinations of cations and anions, which leads to the possibility of tailoring the properties of ILs such as density, viscosity, polarity, acid/base character and coordination capacity (Mallakpour & Dinari, 2012). They are classified into 4 types (Fig. 2.3) according to their cationic segment: 1) alkylammonium, 2) dialkylimidazolium, 3) phosphonium and 4) ILs based on N-alkylpyridinium and, according to their anion, ILs are classified into 3 groups: (1) Chloride based systems and organic sales such as 1-butyl-3-methylimidazolium chloride [bmim] [Cl]; (2) non organic anion systems like hexafluorophosphate $[PF_6]^-$, tetrafluoroborate $[BF_4]^-$ and hexafluoroantimonate $[SbF_6]^-$; (3) organic-based systems such as triflate $[CF_3SO_3]^-$, bistrifluoromethylsulfonyl imide $[Tf_2N]^-$ and similar (Mallakpour & Dinari, 2012).

DESs consist in a mixture of hydrogen bond donors (HBDs) with hydrogen bond acceptors (HBAs) and are classified in five types (I to V) (Abranches & Coutinho, 2022). DESs I to IV are formed by a quaternary ammonium or phosphonium salts (HBAs) with an inorganic metal salt or an amide or an alcohol as HBDs, where the charge on the anion is delocalized and the freezing point of the mixture decreases because of complexation of the inorganic salt with the halide anion. Type V DESs comprise only non-ionic precursors (Abranches & Coutinho, 2022; El Achkar et al., 2021).

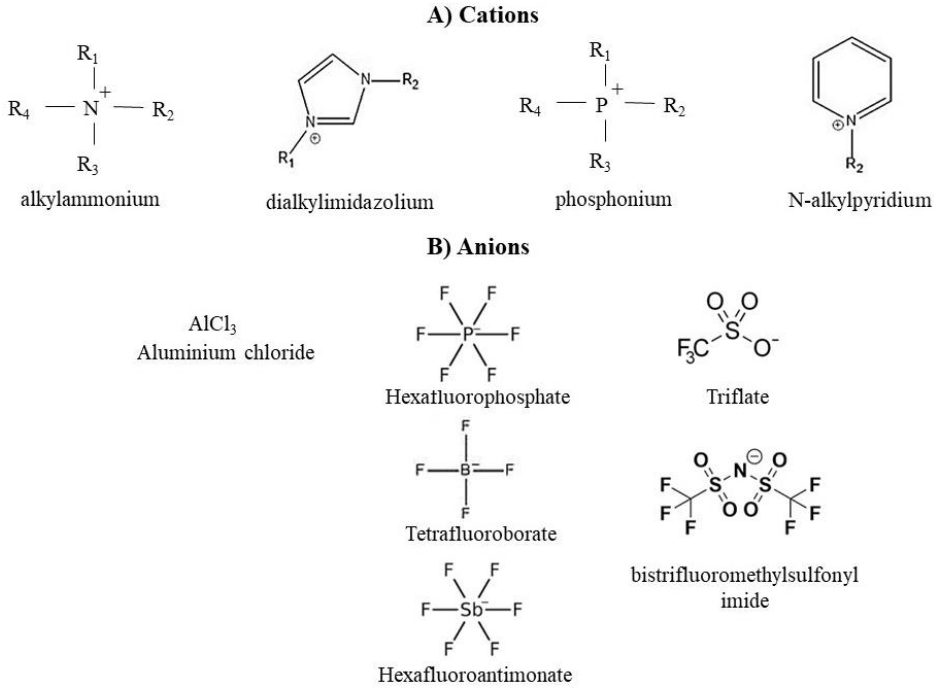

Fig. 2.3 A) Most common cations used to synthesize ionic liquids. B) Most common anions used to synthesize ionic liquids

DESs were discovered by Abbott et al., (2004) when they mixed choline chloride (ChCl) and urea, both solids, in a 1: 2 molar ratio, forming a liquid mixture that was frozen at 12 °C. As pure compounds, choline chloride and urea melt at 302 °C and 133 °C, respectively. Most of the reported eutectic solvents have been formed by a mixture of ChCl, or other quaternary substitutes for ammonium salts, and metal halides (Freemantle, 2009). Although most DESs are prepared from ChCl as ionic species, DESs are not considered ILs because DESs are not only composed of ionic species. Compared to IL, ChCl-derived DESs have advantages such as low cost, they are easily prepared, do not require purification and most of them are biodegradable and non-toxic (Zhang et al., 2012).

DESs are solvents that can be designed by combining properly several quaternary ammonium salts (i.e., ChCl) with different HBDs (Fig. 2.4). Therefore, DESs can be prepared with specific physicochemical properties, such as viscosity, conductivity, pH, hydrophobicity and hydrophilicity (Zhang et al., 2012). DESs can also be obtained from natural sources and in this case, they are named NADESs and represent a subclass of DESs. NADESs are mixtures of two or three natural compounds, such as choline chloride (as HBA) and primary metabolites such as organic acids, amino acids, and sugars alcohols (as HBDs). Applications of DESs and NADESs

include organic synthesis, catalysis, biodiesel transformation, electrochemistry, nanotechnology and separation technologies. There are also reports about the potential use of DESs as absorbents of VOCs (Chen et al., 2021, 2022; Indra et al., 2022; Li et al., 2022; Moufawad et al., 2022; Moura et al., 2017; Mu et al., 2022; Song et al., 2020).

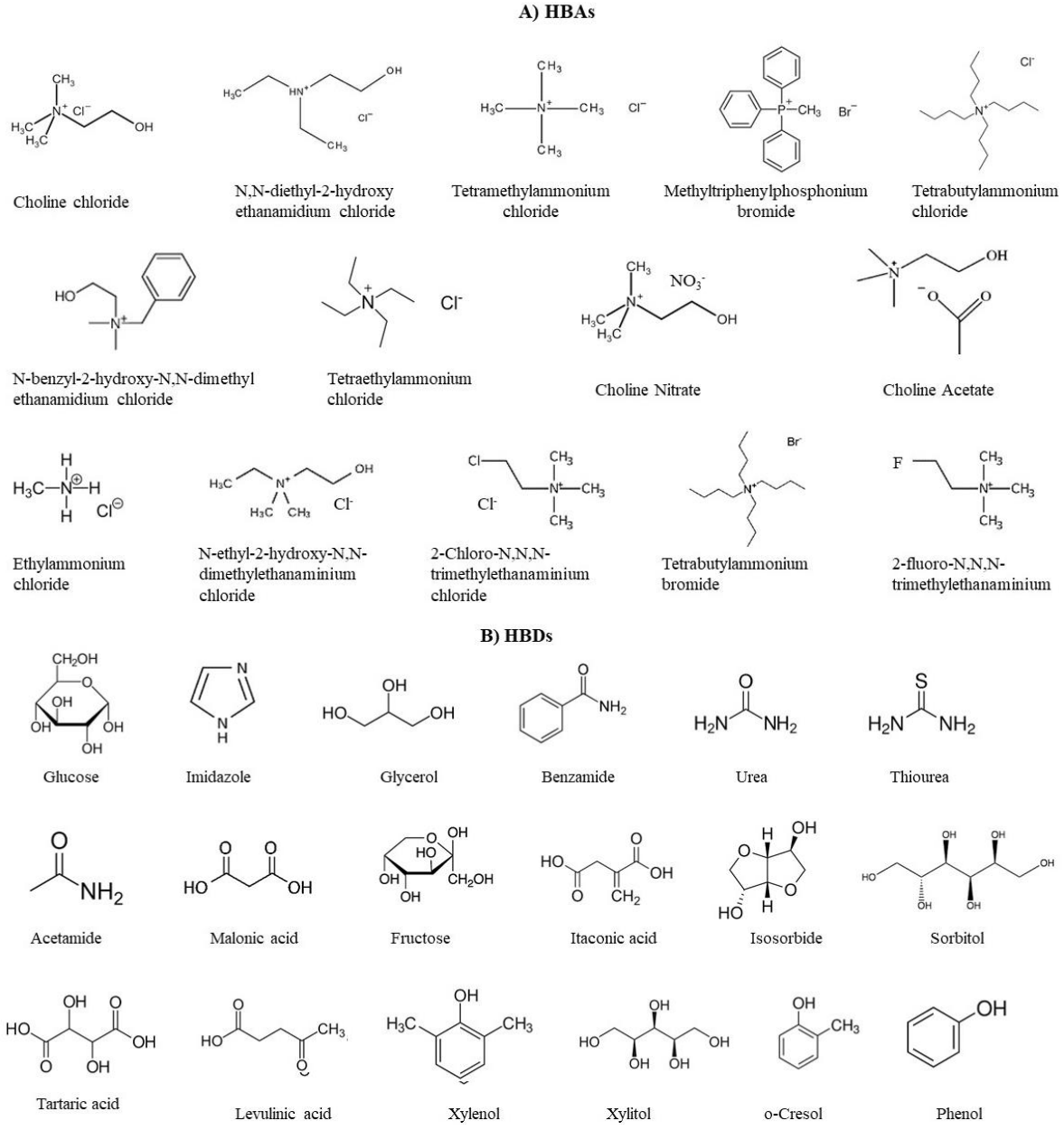

Fig. 2.4 Most common hydrogen bond acceptors (A) and hydrogen bond donors (B) used in the preparation of DESs.

2.4. Physicochemical properties of ILs, DES and NADESs

The selection of a solvent to remove air pollutants must consider the physicochemical properties such as viscosity, density, thermal stability, toxicity, among others. Some of them are shown in Fig. 2.5, Fig. 2.6 and Fig. 2.7.

Viscosity values in ILs range commonly from 15 to 480 mPa/s at ambient temperature (Fig. 2.5) and it is determined by their tendency to form hydrogen bonds, and by the strength of electrostatic forces and Van der Waals interactions (Mallakpour & Dinari, 2012; Marcus, 2016; Zhou et al., 2004). Anions with the capacity to generate hydrogen bonds (i.e. $[BF_4]^-$, $[PF_6]^-$) will form highly viscous ILs (254-312 mPa*s). Imidazolium-based ILs increase their viscosity with the increase of the alkyl chain due to the stronger Van der Waals interactions. The symmetry of the anion also influences viscosity, when the anion has an irregular shape ($[Al_2Cl_7]^-$ and $[(CF_3SO_2)_2N]^-$) the ILs viscosity is low (32.9-41.7 mPa*s). Instead of, ILs with symmetry forms ($[BF_4]^-$, $[PF_6]^-$, $[AsF_6]^-$ and $[SbF_6]^-$) containing salts are highly viscous (254-312 mPa*s). The viscosity decreases with temperature (Mallakpour & Dinari, 2012; Marcus, 2016; Zhou et al., 2004)

The density of ILs ranges from 1.05 to 1.69 g/cm^3 (Fig. 2.6), being denser than water. The ILs density decreases with temperature and increases with the alkyl-substituted chain length (Fredlake et al., 2004). The water content is another aspect to consider since most ILs are highly hygroscopic and the presence of water causes changes in the density, increase in water content leads to a decrease in density (Porcedda et al., 2014).

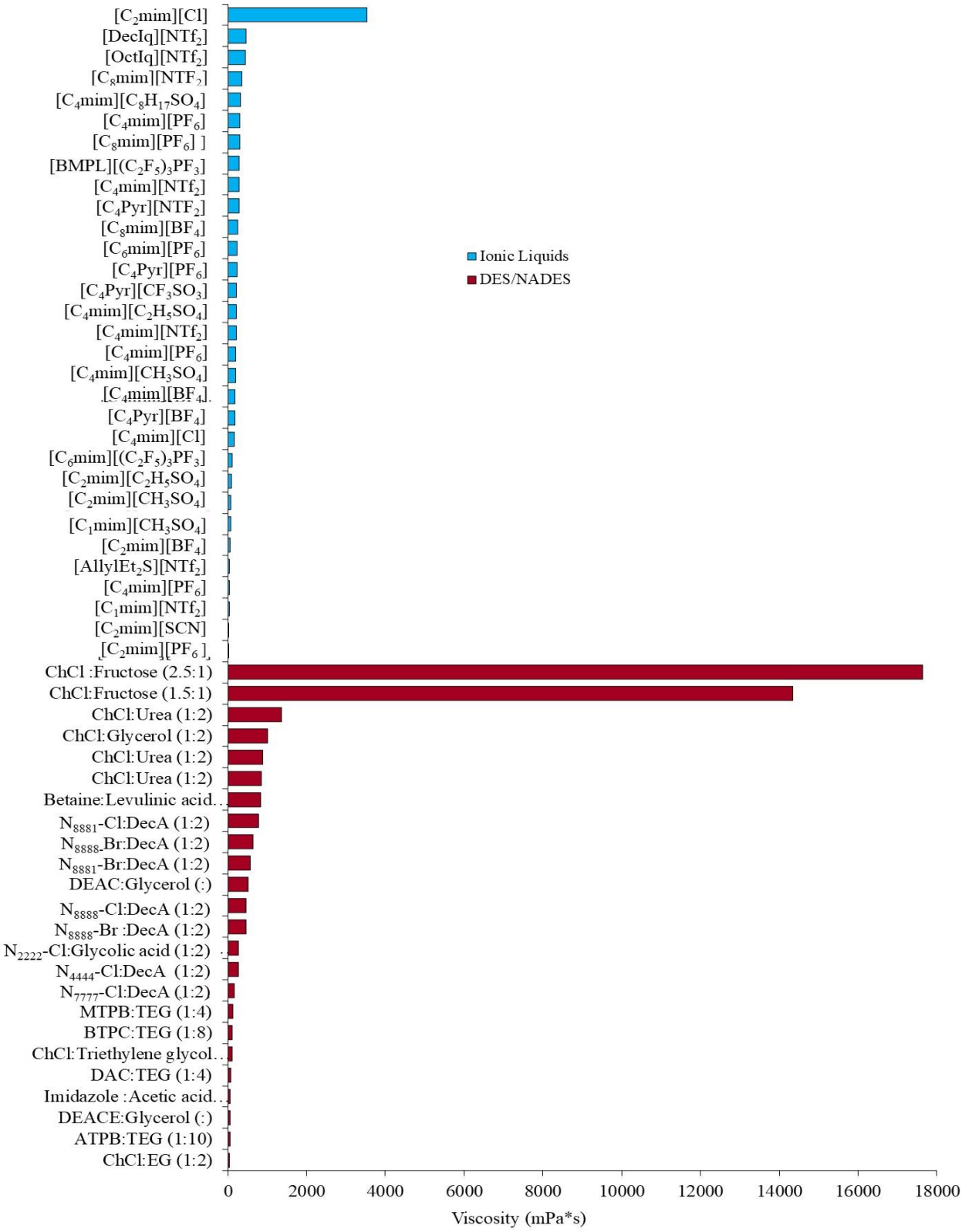

Fig. 2.5 Viscosity comparison between ILs, DESs and NADESs. Based on Table 8.1 of the Appendix

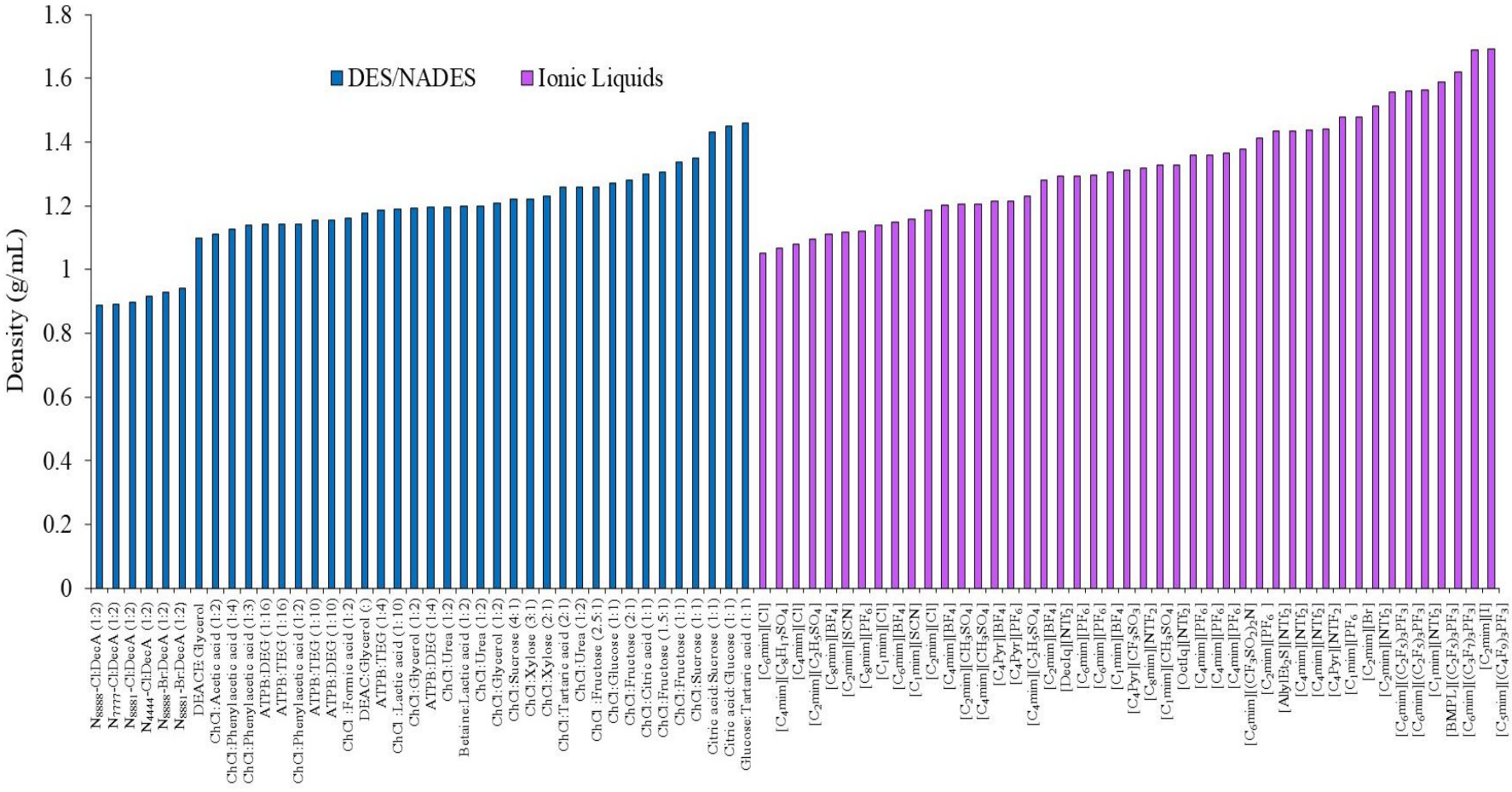

Fig. 2.6 Density comparison between ILs, DESs and NADESs. Based on Table 8.2 of the Appendix

Thermogravimetric analysis indicates high thermal stability for many ILs above 300°C (Fig. 2.7). For instance, the family of $[C_n mim][NTf_2]$ (n=2–8) starts to decompose at 327°C. The thermal decomposition of ILs relies upon the anion rather than on the cation and the relative anion stabilities follow the trend $[PF_6]^- > [BETI]^- > [TFSI]^- > [CF_3SO_3]^- > [BF_4]^- > Me[(CF_3SO_2)_3C]^- >> [I]^-, [Br]^-, [Cl]$ (Ludwig & Kragl, 2007; Zhang et al., 2006). The vapor pressure of ILs is negligible at ambient temperature, being ILs nonvolatile and non-flammable at ambient conditions. However the distillation of pure ILs ($[C_2mim][NTf_2]$,$[C_{10}mim][NTf_2]$ and $[C_{16}mim][NTf_2]$) have been achieved under vacuum (0.1-5 mbar) and at 200–300 °C and without decomposition of those ILs (Earle et al., 2006).

Hydrophobic ILs contain fluorinated ($[PF_6]^-$, $[BF_4]^-$, $[Tf_2N]^-$, $[FAP]^-$) anions and long alkyl side chain cations. In the presence of water, ILs containing $[PF_6]^-$ and $[BF_4]^-$ can release $[F]^-$ and produce HF. $[NTf_2]^-$ is more stable in water and it is highly hydrophobic. ILs that are immiscible in water tend to be hygroscopic. ILs with fluorinated anions ($[PF_6]$ $[NTf_2]$) are less stable in water and thus less environmentally benign. Therefore, it is necessary to synthethyze highly water stable ILs such as ILs containing tris(perfluoroalkyl)trifluorophosphate anion $[FAP]^-$ which is produced thermally. The ILs formed with $[FAP]^-$ anion uptake water 10 times less than the ILs formed with $[PF_6]^-$ (Ge & Lee, 2015).

DESs and NADEs have similar properties, they are non-volatile, thermally stable, highly conductive and they possess a stable liquid state over a wide range of temperatures. They can be used as solvents in a range of temperature from 0 to 100 °C, and present high solvation capacity. The most studied DESs are based on choline chloride [ChCl: (2-hydroxyethyl)trimethylammonium chloride]. ChCl is the quaternary ammonium salt, which is biodegradable, non-toxic, and relatively cheap. The most investigated DES is reline which is prepared using choline chloride and urea in a 1:2 molar ratio (Abdullah & Kadhom, 2016; Dietz et al., 2017; Shekaari et al., 2017; Yadav & Pandey, 2014). Other constituents of common DES like H-bond donor are alcohols, amides or carboxylic acids (Siongco et al., 2013; Yadav & Pandey, 2014).

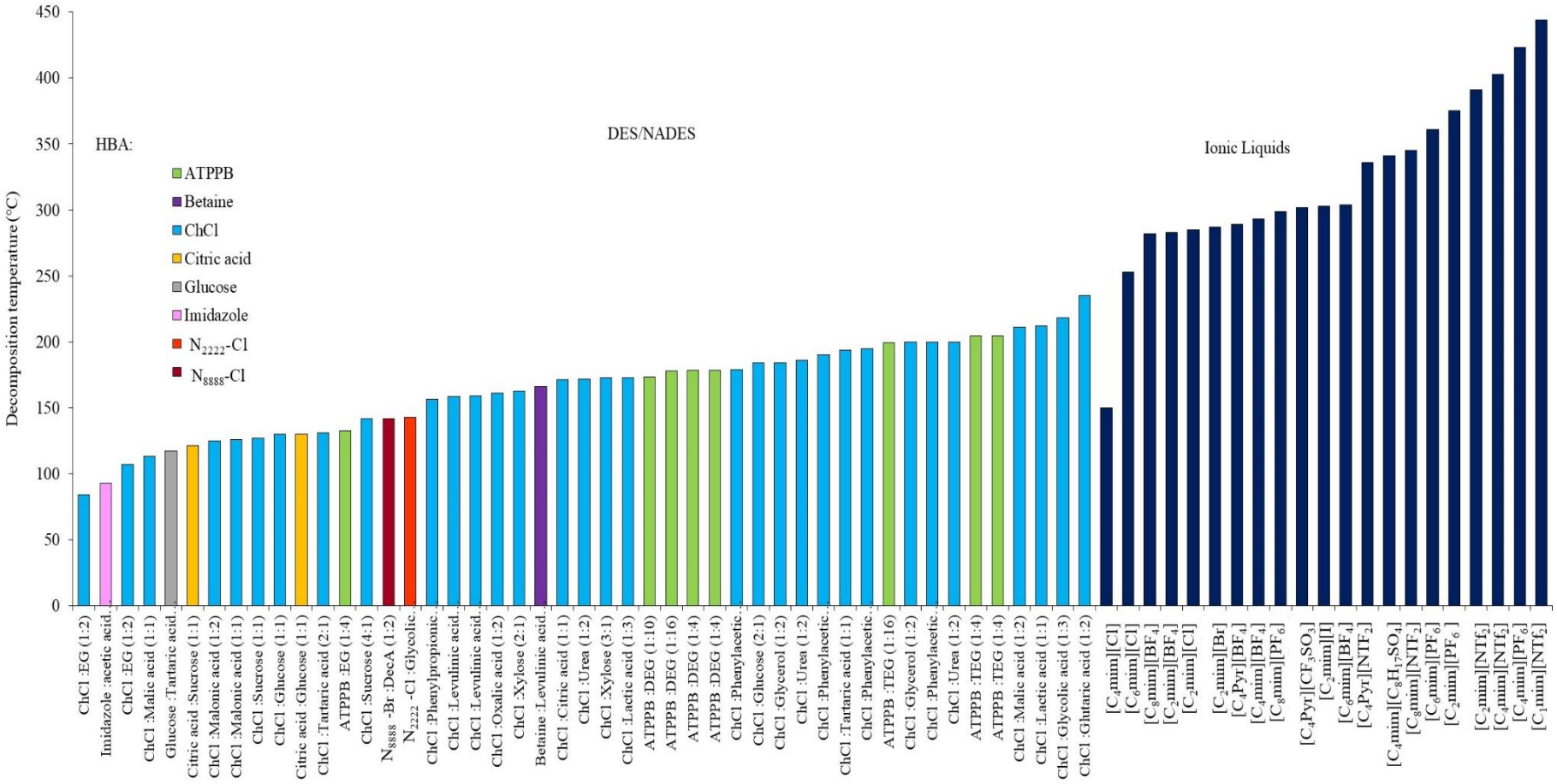

Fig. 2.7 Decomposition temperatures (°C) of common ILs, DESs and NADESs. Based on Table 8.3 of the Appendix

Most DESs and NADESs exhibit densities in the range of 0.88 to 1.34 g/cm^3 (Fig. 2.6). They also exhibit high viscosities between 35 and 17645 mPa/s at room temperature (Fig. 2.5). The high viscosity of DESs and NADESs is due to the extensive hydrogen bond network between each component, which results in a low mobility of free species within the DESs or NADES. The large ion size and small void volume of most DESs but electrostatic forces or van der Waals interactions between the ion and the HBD may contribute to the high viscosity of DESs. Viscosity may also be explained by the "hole theory". In this theory, the viscosity is correlated with the availability of holes in the fluid that allows proper ionic motion and thus, the viscosity is mainly controlled by volumetric factors despite the strong intermolecular interactions. Although ion−HBD interactions play a pivotal role in determining the DESs viscosity, steric effects should also play some role, which may be quantified by the hole theory approach (García et al., 2015; Ruesgas-Ramón et al., 2017).

DESs and NADESs density and viscosity are mainly influenced by the nature of HBA and HBD, molar ratio, temperature, and water content. For example the effect of DESs components (functional groups, carbon chain, halogen ions of components) over the density and viscosity values was assessed (Cao et al., 2022), finding that DESs densities and viscosities increased with the amount of functional groups of HBDs, given that the formation of DESs is due to the formation of hydrogen bonds between HBAs and HBDs, the hydrogen bond interactions will be increased with the type and amount of functional groups, resulting in the increase of densities and viscosities of DESs. Thus, when the interaction between HBAs and HBDs diminish due to a large HBD structure, the density of the DESs will decrease. Also, the densities and viscosities of hydrophilic DESs are higher than the hydrophobic ones (Cao et al., 2022).

The viscosity of six hydrophobic DESs formed by decanoic acid (DecA) and six different quaternary ammonium salt as HBAs was measured (van Osch et al., 2015), the results indicated that (i) the longer the alkyl chain length of the salt is, the higher the viscosity, and (ii) salts containing a bromide anion had higher viscosities than those containing a chloride anion.

The effect of molar ratios (1:4, 1:10 and 1:16) of HBA:HBD on the density and viscosity of different DESs was reported (Ghaedi et al., 2017), where DESs with molar ratios of 1:4 had the highest density in comparison with DESs with molar ratios of 1:10 and 1:16. Thus, high molar content of HBD leads to a decrease in the density when using ATPPB as HBA and DEG, and TEG

as HBDs. Another study (Cao et al., 2022) found that when prepared ChCl-based DESs the increase in the HBA molar content leads to a decreased in the density and viscosity. Also, when hydrophobic DESs (menthol and DecA-based) were tested the increase in the HBA molar content leads to an increased density. Generally, under higher molar content of HBAs higher values of DESs viscosities were obtained (Cao et al., 2022). Density and viscosity of DESs and NADESs decrease with temperature (Dietz et al., 2017; Ghaedi et al., 2017; Hayyan et al., 2012, 2015; Shekaari et al., 2017; Siongco et al., 2013; Yadav et al., 2014; Yadav & Pandey, 2014). This can be explained by the increase in the mobility of the molecules of the liquid which causes volume expansion. DESs density also decreases with water ratio (Abdullah & Kadhom, 2016; Hayyan et al., 2012; Jablonský et al., 2018; Yadav et al., 2014).

Thermal stability of some DESs have been evaluated through thermogravimetric analysis (TGA) indicating that DESs mixtures at 0% water content started to decompose around 125-200 ºC (Fig. 2.5). Some studies reported two types of temperatures of decomposition (T_{onset}), the first one indicate the temperature of decomposition (T_{dcp}) of HBDs and the second one is pertinent to the T_{dcp} of salts HBAs (Abdullah & Kadhom, 2016; Delgado-Mellado et al., 2018; Dietz et al., 2017; Kroon & Binnemans, 2019).

The thermal stability of DESs prepared with DEG, TEG as HBDs and with ATPPB as a HBA at different mole ratios (1:4, 1:10 and 1:16) was investigated (Ghaedi et al., 2018) , the increase in the quantity of HBDs (DEG and TEG) in DESs, leads to a decrease in the thermal decomposition temperature of DESs, indicating that DESs with high molar ratios of HBDs are less stable. The Fourier Transform Infrared Spectroscopy (FT-IR) showed that the hydrogen bonding in ATPPB-DEG DESs decreases by increasing the amount of DEG in ATPPB-DEG DESs (Ghaedi et al., 2018). Similarly, when increased the amount of TEG in ATPPB-TEG DESs, the strengths of hydrogen bonding between ion Br and hydroxyl group of HBD (Br-H) decreases (Ghaedi et al., 2018). While DESs prepared from GL, EG, DEG, TEG as HBDs with ATPPB as a HBA at a molar ratio of 1:4 showed the next trend according to the thermal stability of HBDs: GL > TEG > DEG > EG, which may be attributed to the viscosity of the DES (Ghaedi et al., 2017). Regarding the thermal stability of DESs the trend was ATPPB-GL > ATPPB-TEG > ATPPB-DEG > ATPPB-EG like the trend of HBDs. Thus, it can be stated that the type of HBD has a significant effect on the thermal stability of DESs (Ghaedi et al., 2017).

Three different DESs were prepared by mixing malonic, lactic and tartaric acid as HBD with ChCl at a molar ratio 1:1, they performed long-term isothermal stability through thermogravimetric method (Skulcova et al., 2017), DESs were stable under 60°C (Skulcova et al., 2017). The performance of isothermal TGA at different temperatures to determine the long-term stability of mixtures based on ChCl in combination with oxalic acid dehydrate (molar ratio 1:1); GL (1:2); glycolic acid (1:3); malic acid (1:1); and citric acid monohydrate (1:1) revealed that the most stable DES was ChCl DES with malic acid (weight loss of 4.4%) > GL(5.0%) > citric acid monohydrate (5.2%) > oxalic acid dihydrate (7.3%) > glycolic acid (11.7%), while applying isothermal methods at 80 °C. The trend of thermal stability of DESs follows: DES choline chloride with oxalic acid dehydrate (4.0%), malic acid (8.8%), glycolic acid (10.4%), GL (12.6%), and citric acid monohydrate (27.8%) at 120 °C during 10 h (Jablonsky et al., 2018).

The degradation of carboxylic acid−ChCl DESs via dynamic TGA was investigated (Kroon & Binnemans, 2019) and decomposition temperatures of DESs were found between 125 °C and 235 °C (Kroon & Binnemans, 2019). The decomposition (T_d) is associated with an esterification reaction between the OH group of the choline cation and the carboxylic acid or self-esterification for DESs containing an acid with an alcohol group, since this esterification reaction is promoted under high temperature. Preparing DESs via the heating method at temperatures above of 80 °C produce an esterified DES. While the test of thermal stability of DESs prepared with ChCl: phenylacetic acid at different molar ratios (1:2, 1:3 and 1:4) showed that the acid ratio did not affect the T_{onset} or T_d of the mixture (Altamash et al., 2017).

The thermal stability of DESs prepared from organic compounds as HBDs: LevA, MalA, GL, EG, Phenylac, Phenylprop, urea, and glucose with ChCl were assessed (Delgado-Mellado et al., 2018). Two degradation steps were reported, the first one related to the complete vaporization of the HBDs and the second one associated with the complete ChCl decomposition. The order of the thermal stability of the evaluated DESs increased in the next order: ChCl:EG < ChCl:MalA < ChCl:LevA < ChCl:Phenylac < ChCl: Phenylprop < ChCl:GL < ChCl:Urea < ChCl:Glucose. Also, they observed that DESs formed from HBDs had high thermal stabilities and high boiling points such as urea, glycerol, and glucose. Thus, to obtain DESs with high stability, they recommended to use HBD with low volatility and high thermal stability.

The thermal stability of NADES composed of different sugars, organic acids and ChCl was assessed by Differential Scanning Calorimetry (DSC) using temperatures up to 250 °C (Craveiro et al., 2016). All NADES presented a single degradation peak at temperatures above 120 °C. According to the mentioned above and in terms of thermal stability of DES and NADES, it is more recommended to use temperatures below 80 °C in order to decrease viscosity and density of the DESs/NADESs and to maintain the chemical composition of the solvent.

2.5. Biodegradability and toxicity of ILs, DESs and NADESs

According to the Test No. 301 of the OECD Guidelines for the Testing of Chemicals (OECD, 1992), a chemical is considered readily biodegradable once reached a 70% removal of dissolved organic carbon (DOC) and 60% of CO_2 production for respirometric methods in 28 days aerobic assay under dark or diffuse light conditions.

Generally, ILs are considered non-biodegradable, different authors reported no biodegradation in long term biodegradability tests (30 days) of 1-n-butyl-3-methylimidazolium (bmim) based ILs ([bmim][Cl], [bmim][Tf_2N], ([bmim][Br], [bmim][BF_4], ([bmim][PF_6]) (Gathergood et al., 2004; Mena et al., 2020; Quijano et al., 2011b).

Imidazolium-based ILs like [hmim][Br] and [omim][Br], were partially mineralized by activated sludge in 28 days (Docherty et al., 2007). The imidazolium ring remained intact and it was not used as carbon source by microorganisms. Pyridinium based ILs as [omPyr][Br] were fully biodegradable with more than 70% of carbon removal within 10 days period in activated sludge. Whereas [bmPyr][Br] and [hmPyr][Br] were not readily biodegradable with less than 70% removal of carbon within 10 days period. Although, [hmPyr][Br] cannot be classified as readily biodegradable, it was fully mineralized after 49 days of incubation with activated sludge. The application of "CO_2 Headspace'' technique was used to evaluate the ultimate aerobic biodegradability of 1-butylpyridinium ILs (Harjani et al., 2009) and revealed that the salts with $[Br]^-$, $[PF_6]^-$ and $[NTf_2]^-$ ions were non-biodegradable with 1 to 3% biodegradability in 1 month. When used octyl sulfate ion the biodegradability increased up to 40%. While 1-alkylpyridinium IL with linear C_4, C_{10}, and C_{16} achieved low levels of biodegradability (0-9%).

The biological oxygen demand tests (BOD_5, BOD_{28}) and long-term biodegradability tests (LTB) proved that imidazolium-based IL ([bmim][PF_6] and [bmim][NTF_2]) can not be metabolized by microorganisms. The BOD_{28} tests indicated that ILs with $[NTf_2]^-$, $[PF_6]^-$ and $[NfO]^-$ ions are not biodegradable (Quijano et al., 2011b, 2013; Rodriguez Castillo et al., 2016).

The biodegradability of DESs have been determined (Juneidi et al., 2015; Radošević et al., 2015; Wen et al., 2015), where ChCl-based DESs with different HBDs (urea, acetamide, glucose, oxalic acid, GL, EG) and DESs formed by EAC with EG, MalA, GL, urea, zinc chloride and zinc nitrate hexahydrate as HBDs have been reported as readily biodegradable (Juneidi et al., 2015; Radošević et al., 2015; Wen et al., 2015), since they reached a biodegradation of 60% in 10 days during a test of 28 days.

While ChCl:glycerol (1:1) and ChCl:ethylene glycol (1:1) and DESs prepared with choline acetate ChAc with different HBDs (urea, acetamide, glycerol, and ethylenglycol) at a molar ratio of 1:1, were considered no readily biodegradable since it did not reached a 60% biodegradation in 10 days (Wen et al., 2015).

Particularly ChCl:GL (2:1) and ChCl:GL (1:2) reached a biodegradability of 96% and 91 %, respectively. ChCl:Glucose (2:1), ChCl:Urea (1:1), ChCl:Urea (1:2) and ChCl:acetamide (1:1) achieved at least 80% biodegradation and, DESs prepared with organic acids such as ChCl:oxalic acid (1:1) (Juneidi et al., 2015; Radošević et al., 2015; Wen et al., 2015) and EAC:MalA (1:1) showed a biodegradation of 68% and 61%, respectively. When EAC was used as HBA with GL, EG, urea, zinc chloride and MalA the biodegradation varied from 61 to 75% (Juneidi et al., 2015), thus are considered as readily biodegradable. The variations in aerobic biodegradability observed between ChCl and EAC-based DESs could be attributed to ChCl having fewer carbon atoms in its methyl groups (CH_3) compared to the ethyl groups in EAC (C_2H_5).

Toxicity is a molecular sequence of events ranging from the absorption of an effective dose to the production of a specific biological response. A mode of toxic action is a set of physiological and behavioral signs that characterize an adverse biological response (McCarty & Borgert, 2006). The potential environmental risk of a compound in the aquatic environment is usually evaluated with a bioluminescence assay with *Vibrio fischeri* (Microtox ®). This bioassay is based on the production of light per unit time by living luminescent bacteria (De Zwart & Slooff, 1983). The

criterion in this test is defined as the attenuation of the light emission about a standard emission obtained from a toxicity-free solution. Toxicity by Microtox ® assay is expressed as the concentration that causes 50% inhibition of luminescence (EC_{50}) (De Zwart & Slooff, 1983).
The toxicity of IL expressed in terms of EC_{50} has been determined with Microtox® bioassay (Fig. 2.8) (Hernández-Fernández et al., 2015; Mena et al., 2020; Montalbán et al., 2016; Oliveira et al., 2016; Romero et al., 2008). The EC_{50} of ILs based on 1-alkylimidazolium (C_1, C_2, C_4, C_6, C_8) correlates directly with the length of the n-alkyl substitute in the methyl imidazolium cation while the anion has a low effect (Hernández-Fernández et al., 2015; Montalbán et al., 2016; Oliveira et al., 2016; Romero et al., 2008). Whereas, for three bmim-based ILs the highest toxicity occurred when the anion $[NTf_2]^-$ was present with an EC_{50} equal to 108 mg/L (257mM), and it seems to be attributed to its high hydrophobicity and the ability of the anion to penetrate the cell membrane which is considered non-polar (Mena et al., 2020). The lowest toxicity occurred with pyrrolidinium cations based IL and the highest with IL containing aromatic cations, such as imidazolium and pyridinium cations and $[NTF_2]^-$ anion (Hernández-Fernández et al., 2015).

The toxicity test of imidazolium, pyridinium, and ammonium-based IL revealed that pyridinium-based ILs are more toxic than imidazolium-based ILs (Montalbán et al., 2016). Imidazolium IL is less toxic when the alkyl chain is functionalized with a hydroxyl group or a double bond, or when a second short alkyl chain is present in the cation. When four ammonium-based IL were tested (Oliveira et al., 2016) (m-2-HEAA, m-2-HEAPr, m-2-HEAB, and m-2-HEAP), was observed that the microbial toxicity increased with the alkyl chain length of the anion increase.

Ecotoxicologic effect of cholinium based-IL using the standard Microtox® test have been reported (Fig. 2.8) (Ventura et al., 2014), where the EC_{50} of IL followed the next order:

[Chol][Bic] < [BzChol]Cl < [Chol][But] < [Chol][Ac] < [Chol][Sal] < [Chol][Bit] < [Chol][DHCit] < [Chol][Cl] < [Chol][Prop] < [Chol][DHPhosp] < [Chol][Sal] < [Chol][Bit] < [Chol][DHCit].

They compared the ecotoxicity of this cholinium-based IL to atrazine, dichloromethane and ethyl acetate and observed that the EC_{50} of the most toxic cholinium compounds [Chol][DHCit] and [Chol][Bit] are comparable to that of the pesticide atrazine and the EC_{50} value of most cholinium-based ILs fell between the toxicity of dichloromethane and ethyl acetate, a correlation between the

toxicity and the anion hydrophobicity was observed, indicating that the permeation through the cell membrane plays an important role in the toxicity.

Another approach to assess ILs toxicity is through the glucose-uptake inhibition by activated sludge test (Quijano et al., 2011b, 2013). This test showed that [BMtriaz][NTf_2], [Butenylmim][NfO], [MeOEmim][NfO] and Aliquat 366® completely inhibited the microbial glucose uptake at a concentration of 5% v/v. For [bmim][PF_6], [bmim][NTF_2] and [PEGMIM][PF_6] an acclimation time (lag phase) of approximately 24 h at a concentration of 5 and 10 % (v/v) were observed, after the lag phase complete consumption of glucose were reported. When 10% (v/v) of IL was used a decrease in the metabolic activity of microorganisms of 30% was attained, thus 5% (v/v) concentration of IL was considered as non-toxic for the microbial metabolism once the lag phase was over. It has been reported that the alkyl chain length and the number of carbon atoms influence ILs toxicity and contrary to other reports, the lapsed time of lag phase was reduced when the alkyl chain length increased (Rodriguez Castillo et al., 2016). The lag phase duration for ILs with $[NTf_2]^-$ follows the order [Triaz] > [Morph] > [S] > [Pyrr] ≥ [Im] > [Iq]. The acclimation lapsed time showed that ILs toxicity was as follows: $[NfO]^-$ > $[PF_6]^-$ > $[NTf_2]^-$, and the time needed for glucose consumption followed the next order: $[PF_6]^-$ > $[NfO]^-$ > $[NTf_2]^-$. The $[NTf_2]^-$ anion seemed to be the less toxic to activated sludge.

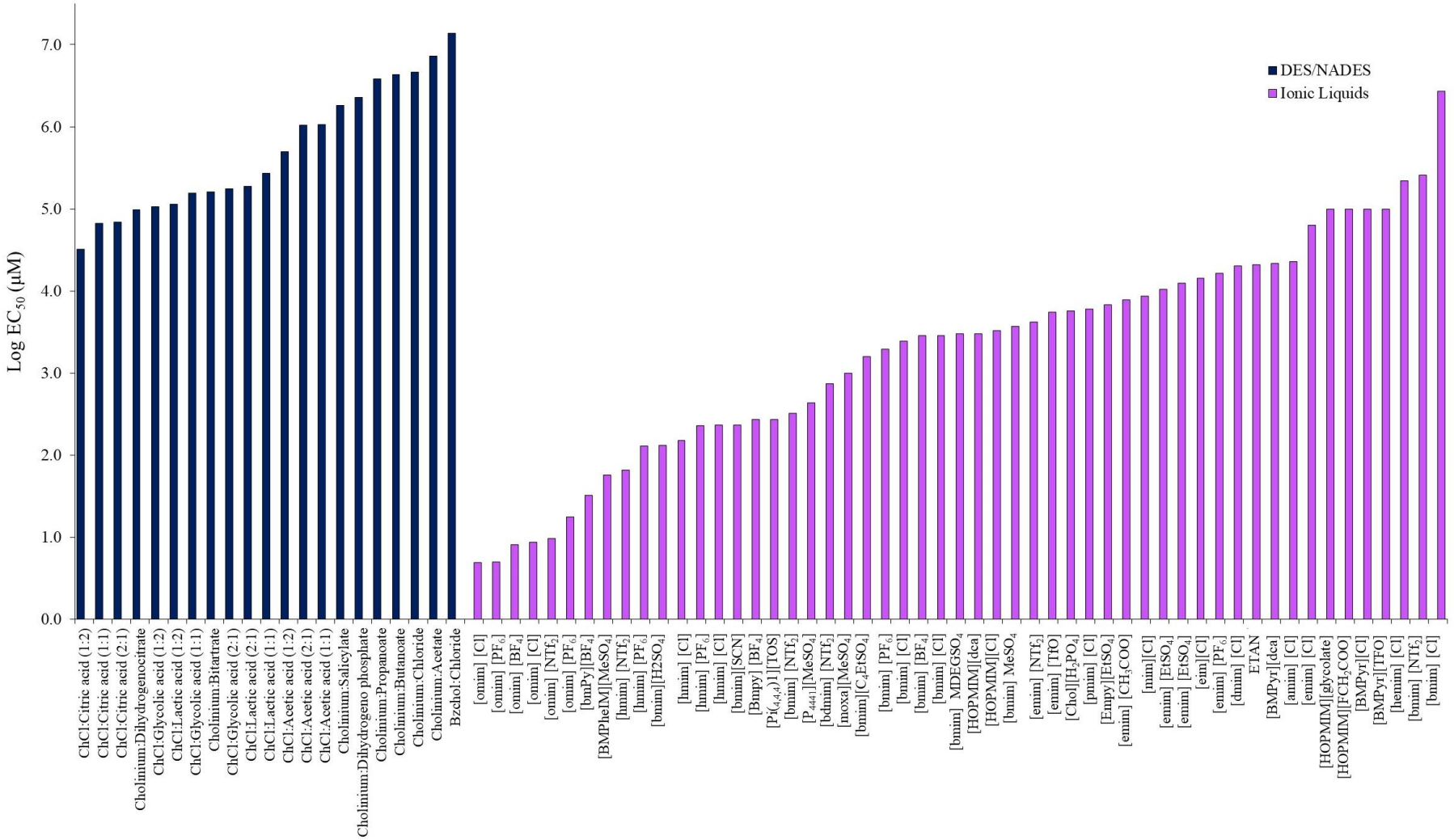

Fig. 2.8 Log EC_{50} (µM) values for some ILs, DESs and NADESs using Microtox® bioassay. Based on Table 8.4 of the Appendix

The assessment of toxicity of DESs has been evaluated towards different microorganisms (Hayyan et al., 2013; Juneidi et al., 2016; Radošević et al., 2015, 2016; Ventura et al., 2014; Wen et al., 2015), where the Microtox toxicity test (Fig. 2.8) using ChCl-based DESs with different organic acids as HBDs (acetic acid, citric acid, lactic acid and the glycolic acid) (De Morais et al., 2015) was used, the toxicity increased with the acid content. The degree of toxicity of these different acids toward *V. fischeri* was similar, except for acetic acid for which the toxicity was 4 to 5 times lower than for the other acids. The authors classified the DES with "moderate toxicity", suggesting that their toxicity was dominated by the corresponding acid. Since organic acids were used as HBDs, pH values of the DES were low (<3), leading to the denaturation of proteins, this could explain their negative effect.

Phosphonium-based DESs toxicity towards *Bacillus subtilis*, *Staphylococcus aureus, Escherichia coli* and *Pseudomonas aeruginosa* was investigated. DESs prepared with MTPB and with three HBDs, glycerine, EG and TEG did not inhibit the growth of any of the bacteria selected (Hayyan et al., 2013).

The toxicity of ChCl and ChAc-based DESs with four HBDs (urea, acetamide, GL and EG) at three molar ratios (1:2, 1:1, 2:1) were evaluated towards *E. coli* (Wen et al., 2015). At low DES concentrations (<75 mM) an inhibition index on bacterial growth lower than 10 % was observed. Higher DESs concentrations (0.75 mM) showed an inhibition index of 72.8–93.8% on bacterial growth. The toxicity of DES in aqueous solution towards bacteria can be explained by the interaction of the DES partially dissociated with the peptidoglycan which is located immediately outside of the cytoplasmic membrane through H-bonding or electrostatic interaction, leading to cell wall distortion or disruption.

The antifungal *Aspergillus niger* activity of ChCl and EAC-based DESs was evaluated (Juneidi et al., 2015). ChCl-based DESs had lower toxicity compared with EAC-based DESs. The highest toxicity came from EAC: $ZnCl_2$ and EAC: zinc nitrate hexahydrate with a MIC <2.2 mg/mL, followed by EAC: MalA with a MIC= 64.42 mg/mL for *A. niger*. The toxicity exhibited by EAC: MalA was explained by its acidity (pH 4.14), while the toxicity of EAC and metal (Zinc chloride/ zinc nitrate hexahydrate) was advocated to the ionic interaction, which presented a high toxic effect

on the cell surface and inhibition of growth and sporulation. DESs possess anti-fungal properties higher than their original components and most DESs did not show inhibition at low concentrations.

Toxicological assessment of ten ChCl-based DES towards fungi strains: *P. chrysosporium, A. niger, L. tigrinus and Candida cylindracea*, was conducted (Juneidi et al., 2016). ChCl was combined with different HBDs such as alcohols, sugars, acids, and others to form DESs. DESs synthesized exhibited low toxicity towards all fungal strains, and they presented a higher toxicological behavior than their individual components. The highest inhibition for the four fungal strains were presented with ChCl:Zinc chloride.

The antimicrobial activity of 10 NADES based on choline chloride, betaine and citric acid as HBAs with different sugars, organic acids and aminoacids as HBDs towards *Staphylococcus aureus, Escherichia coli, Proteus mirabilis, Salmonella typhimurium, Pseudomonas aeruginosa* and *Candida albicans* was performed (Radošević et al., 2018). Between the tested NADES, ChCl:xylitol, ChCl:sorbitol and Betaine:glucose did not present antimicrobial activity against the selected microorganisms. Of ChCl-based NADES only ChCl:urea at 10% of water content was effective against *E. coli,* indicating the low toxicity of urea towards the microorganisms (Radošević et al., 2018). All NADES containing citric acid showed growth inhibition of bacteria and the highest toxicity was presented by citric acid:glucose:glycerol and citric acid:fructose:glycerol. ChCl:oxalic acid at 10% water content was capable of inhibit all microorganisms. They also reported that DESs were more toxic in comparison with their original components (Radošević et al., 2018).

Generally DESs and NADESs containing organic acids presented higher antimicrobial activity than having alcohol-, amine-, and sugars (Hayyan et al., 2013; Juneidi et al., 2016; Radošević et al., 2015, 2016; Ventura et al., 2014; Wen et al., 2015). Also, DES showed higher toxicity than their individual components, due to the charge delocalization occurring through hydrogen bonding. Chemicals having delocalized charges are more toxic than chemicals with localized charges and when DES concentration increase, DES became more hazardous to the tested microorganisms (Hayyan et al., 2013; Juneidi et al., 2016; Radošević et al., 2015, 2016; Ventura et al., 2014; Wen et al., 2015).

2.6. VOC removal using ILs, DES and NADES

Absorption stands out as one of the methodologies employed for mitigating VOCs in the atmosphere. Air pollutants are taken up by a solution, typically water or solvents. A critical factor within this technology involves the choice of the sorbent (Le Cloirec et al., 2005). Various VOCs, including toluene, vinyl chloride, dimethyl sulfide (DMS), dimethyl disulfide (DMDS), dichloromethane (DCM), benzene, p-xylene, dimethoxymethane (DMM), methanol, methyl ethyl ketone, acetone, ethanol, styrene, and 1-butanol, have undergone evaluation for their absorption behavior in different ILs and DESs (Bedia et al., 2013; Candia-Lomelí et al., 2023; Chen et al., 2021; Cheng et al., 2009; Fahri et al., 2020; Li et al., 2015; Li et al., 2022; Ma et al., 2019; Moufawad et al., 2022; Moura et al., 2017; Mu et al., 2022; Praus et al., 2022; Quijano et al., 2011a, 2013; Rodriguez Castillo et al., 2019; Song et al., 2020; Wang et al., 2017; Yu et al., 2018, 2020; Zhao et al., 2019)

Various methods, both static and dynamic, along with several parameters such as partition coefficient, Henry's constants, and absorption capacity, have been employed to characterize the affinity between the IL or DESs and VOCs. For example, researchers have employed the static headspace method to determine the dimensionless partition coefficient at various temperatures (25-30 °C) and atmospheric pressure. The majority of ILs investigated in these studies belong to the imidazolium family and feature fluorinated anions such as $[PF_6]^-$,$[BF_4]$, $[NfO]^-$, $[NTf_2]$, and [FAP] (Fig 2.9) (Bedia et al., 2013; Candia-Lomelí et al., 2023; Cheng et al.,, 2009; Fahri et al., 2020; Gui et al., 2022; Li et al., 2015; Ma et al., 2019; Praus et al., 2022; Quijano et al., 2011a, 2013; Rodriguez Castillo et al., 2019; Wang et al., 2017; Yu et al., 2018, 2020; Zhao et al., 2019). VOCs affinity towards DESs has also been tested through the measure of the dimensionless partition coefficient using the headspace method (Fahri et al., 2020; Moufawad et al., 2022; Moura et al., 2017).

This dimensionless partition coefficient (K) is defined as the ratio of VOC concentration in the gas phase (C_g) to VOC concentration in the IL/DES phase (C_L). An elevated partition coefficient suggests a reduced solubility of the VOCs in the IL or DES.

.

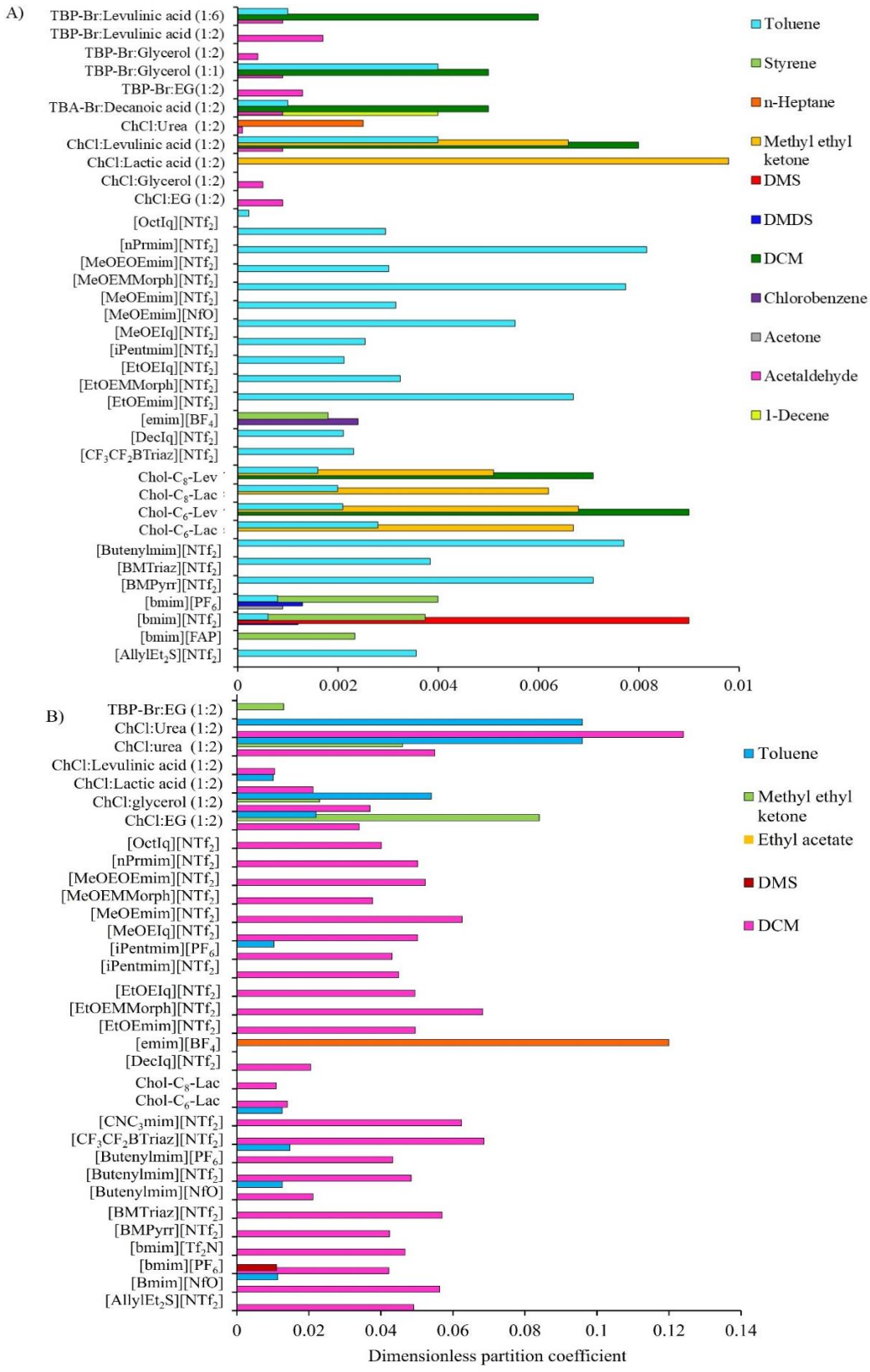

Fig. 2.9 Dimensionless partition coefficient of different VOCs in ILs or DESs A) K values lower than 0.01 B) K values between 0.01 to 0.12. Based on Table 8.5 of the Appendix

When toluene affinity towards different ILs through the measurement of partition coefficient was assessed, it was observed that the K values varied between 0.00022 to 0.015 at 25 °C. Remarkably, among the 27 ILs investigated, [OctIq][NTf_2] demonstrated superior absorbent capabilities (K=0.00022). For ILs based on the [NTf_2] anion, the K values for toluene varied from 0.00022 for [OctIq][NTf_2] to 0.0126 for [CNC_3mim][NTf_2]. For [PF_6]$^-$ based ILs, the IL based on [bmim][PF_6] was the more proficient absorbent given its toluene K value which was threefold lower than [Emim][PF_6] and 1.5-fold lower than [iPentmim][PF_6]. Regarding the ILs with [NfO]$^-$, the order of affinity to toluene was [MeOEmim][NfO]>[Bmim][NfO]> [Butenylmim][NfO], the IL based on [emim][BF_4] presented one of the highest K values (0.024) for toluene absorption (Fig. 2.9) (Ma et al., 2019, 2021; Quijano et al., 2011a; Rodriguez Castillo et al., 2019).

When bio-based ILs (Chol-C_6-Lev; Chol-C_8-Lev, Chol-C_6-Lac, and Chol-C_8-Lac) (Fahri et al., 2020) were tested for toluene absorption, Chol-C_8-Lev emerged as the most efficacious absorbent, yielding a K value of 0.0016. Notably, Chol-C_8-Lev demonstrated a K value that was 4% to 20.37% lower in comparison to those acquired for Chol-C_8-Lac, Chol-C_6-Lev, and Chol-C_6-Lac.

The toluene K values in various DESs ranged from 0.0009 to 0.096. Among these DESs, the most effective absorbent was TBA-Br:Decanoic acid (1:2) with a K value of 0.0009, while the least effective was ChCl (1:2) at 30 °C. It is evident that DESs based on TBP-Br exhibited better toluene absorption performance compared to those based on ChCl. Specifically, the toluene K values for TBP-Br based DESs ranged from 0.0009 to 0.004, while ChCl based DESs had toluene K values ranging from 0.0045 to 0.096, as shown in Figure 2.9 (Fahri et al., 2020; Moufawad et al., 2022; Moura et al., 2017).

For DESs formed using TBA-Br along with decanoic and levulinic acids, the toluene K values varied from 0.0009 to 0.0013, these values are comparable to the toluene K value obtained with [bmim][PF_6], which was 0.00096 (Quijano et al., 2011a).

K values for DCM in different ILs (Fig. 2.9) ranged from 0.0071 to 0.0686. Notably, Chol-C_8-Lev emerged as the preeminent absorbent for DCM, demonstrating its high affinity. Among the range of bio-based ILs examined, DCM K values displayed a narrower range from 0.0071 to 0.0141, establishing them as the group with the lowest K values for DCM, these bio-based ILs exhibited DCM K values sixfold lower in magnitude than their [PF_6]-based counterparts. For [NTf_2]-based

ILs, DCM K values spanned from 0.0205 to 0.0686 and [Butenylmim][NfO] and [Bmim][NfO] presented DCM K values of 0.021 and 0.056 respectively (Fahri et al., 2020; Rodriguez Castillo et al., 2019).

According to K values for toluene and DCM in different ILs, toluene showed a better solubility in all ILs than DCM with K values between 4 to 32 times lower than those observed for DCM.

The DCM K values within DESs displayed a range from 0.004 to 0.124. Among these DESs, the most effective absorbent was TBP-Br: EG (1:2), with a K value of 0.004. This trend closely resembles the absorption pattern observed for toluene, as DESs based on TBP-Br also demonstrated better DCM absorption performance than ChCl based ones. Specifically, the DCM K values for TBP-Br based DESs varied from 0.004 to 0.006, while ChCl based DESs had DCM K values ranging from 0.008 to 0.124 at the same temperature.

When comparing DESs performance with ILs, it is evident that DESs exhibited better absorption characteristics for DCM. K values for DCM in ILs were 0.0071 for Chol-C_8-Lev and 0.02052 for [DecIq][NTf_2], which are 1.8 and 5 times higher, respectively, than the DCM K values (around 0.005) observed for TBP-Br based DESs.

ILs and DESs affinity towards VOCs such as acetone, acetaldehyde, DMDS, DMS, styrene, chlorobenzene, methyl ethyl ketone, dimethylbenzene, ethyl acetate and hexane has been investigated by determining the partition coefficients using the headspace static method (Fig 2.9). The IL [bmim][NTf_2] was employed to absorb DMDS, styrene, and DMS, showing superior absorbent properties for DMDS with a K of 0.0012. This value is 3 and 7.5 times lower than the partition coefficients observed for styrene (0.0037) and DMS (0.009), respectively. Similarly, the IL [bmim][PF_6] was utilized to absorb acetone, DMDS, DMS, and styrene, demonstrating better absorption capabilities for acetone with a K value of 0.0009, while for DMDS, styrene, and DMS values were around (0.0013 to 0.011) Also, [emim][BF_4] was tested with styrene, chlorobenzene, ethyl acetate, and hexane, exhibiting optimal absorption for styrene and chlorobenzene with K values of 0.0018 and 0.0024, respectively. However, ethyl acetate and hexane exhibited K values in [emim][BF_4] 50 and 156 times higher than those observed for aromatic compounds.

Bio-based ILs such as Chol-C_6-Lev; Chol-C_8-Lev, Chol-C_6-Lac, and Chol-C_8-Lac displayed K values for methyl ethyl ketone ranging from 0.0051 to 0.0067. These K values were 1.7 to 41 times

lower than those obtained for DMS, ethyl acetate, and hexane in [bmim][NTf_2], [bmim][PF_6], and [emim][BF_4] (Candia-Lomelí et al., 2023; Fahri et al., 2020; Ma et al., 2019, 2021; Quijano et al., 2011a).

The methyl ethyl ketone K values obtained for DESs ranged from 0.0023 to 0.084. Notably, DESs based on TBP-Br demonstrated superior absorbent capabilities compared to those based on ChCl. Specifically, TBP-Br based DESs exhibited K values that were 2.8 to 6.6 times lower than those reported for ChCl-based DESs (Fahri et al., 2020; Moufawad et al., 2022).

When it comes to acetaldehyde absorption, the K values in DESs were all below 0.001 at 30 °C. Notably, ChCl:urea (1:2) demonstrated the highest absorbent capability, with a K value of 0.00001. This indicates that DESs formed using alcohols as HBDs exhibited superior absorption performance for acetaldehyde in comparison to those formed with organic acids.

For the absorption of n-heptane and 1-decene, the DES consisting of TBA-Br:Decanoic acid (1:2) demonstrated superior absorbent properties with K values of 0.0033 and 0.0004, respectively. Interestingly, the solubility of 1-decene was 8 to 9 times higher than the n-heptane in all the tested DESs (Moufawad et al., 2022; Moura et al., 2017).

The impact of temperature on VOC absorption is evident in the increase (1.5 times) in the partition coefficient of toluene and acetone for [Bmim][PF_6] as the temperature rises from 20 °C to 60 °C. The temperature increases reduced VOC solubility in the ILs. The phenomenon can be explained by the elevation of VOC vapor pressure with temperature, resulting in a high vaporization of VOC (Ma et al., 2021).

The solubility of VOCs in ILs has been characterized using Henry's constant, which has been determined through thermogravimetric or gravimetric methods (Bedia et al., 2013; Praus et al., 2022), as well as by measuring the pressure variation in an absorption vessel containing the IL (Li et al., 2015). The Henry's law constant (K_H) is calculated using the mole fraction of VOC in the IL and the equilibrium pressure. Thus, lower K_H values indicate higher solubility in the solvent. Table 2.1 shows Henry's constant values obtained for different VOCs and ILs or DESs.

Table 2.1 Henry's constant of different VOCs in ILs or DESs.

IL	VOC	H, kPa	T, K	Reference
[bmim][BF_4]	Benzene	26.81	303	Li et al., 2015
	Acetone	34.71	303	Li et al., 2015
	Benzene	91.97	333	Li et al., 2015
	Acetone	109.72	333	Li et al., 2015
[bmim][PF_6]	Acetone	25.04	303	Li et al., 2015
	Benzene	25.37	303	Li et al., 2015
	Acetone	79.21	333	Li et al., 2015
	Benzene	87.24	333	Li et al., 2015
[bmim][Tf_2N]	1-butanol	4.7	313	Praus et al., 2022
	p-xylene	11	313	Praus et al., 2022
	Benzene	14.05	303	Li et al., 2015
	Acetone	14.92	303	Li et al., 2015
	Ethanol	28	313	Praus et al., 2022
	Acetone	36.4	313	Praus et al., 2022
	Methanol	38	313	Praus et al., 2022
	Acetone	48.48	333	Li et al., 2015
	Benzene	49.15	333	Li et al., 2015
[bmim][TfO]	1-butanol	5.4	313	Praus et al., 2022
	p-xylene	8.6	313	Praus et al., 2022
	Ethanol	18.2	313	Praus et al., 2022
	Methanol	23.5	313	Praus et al., 2022
	Acetone	42	313	Praus et al., 2022
[BMPy][Tf_2N]	p-xylene	5.8	313	Praus et al., 2022
	1-butanol	9.1	313	Praus et al., 2022
	Acetone	37	313	Praus et al., 2022
	Ethanol	45	313	Praus et al., 2022
	Methanol	45.4	313	Praus et al., 2022
[BMPyr][TfO]	1-butanol	3.2	313	Praus et al., 2022
	p-xylene	8.1	313	Praus et al., 2022
	Ethanol	15.8	313	Praus et al., 2022
	Methanol	24.4	313	Praus et al., 2022
	Acetone	48	313	Praus et al., 2022
[dcmim][NTf_2]	Toluene	4	298	Bedia et al., 2013
[emim][BF_4]	Benzene	33.04	303	Li et al., 2015
	Acetone	45.71	303	Li et al., 2015
	Benzene	113.29	333	Li et al., 2015
	Acetone	144.99	333	Li et al., 2015

IL	VOC	H, kPa	T, K	Reference
[emim][Tf_2N]	Toluene	11	298	Bedia et al., 2013
	Acetone	15.74	303	Li et al., 2015
	Benzene	17.45	303	Li et al., 2015
	Acetone	51.74	333	Li et al., 2015
	Benzene	60.55	333	Li et al., 2015
[hmim][Tf_2N]	Benzene	11.75	303	Li et al., 2015
	Acetone	14.04	303	Li et al., 2015
	Benzene	41.17	333	Li et al., 2015
	Acetone	46.49	333	Li et al., 2015
[hxmim][BF_4]	Benzene	24.4	303	Li et al., 2015
	Acetone	30	303	Li et al., 2015
	Benzene	83.88	333	Li et al., 2015
	Acetone	93.48	333	Li et al., 2015
[hxmim][NTf_2]	Toluene	6	298	Bedia et al., 2013
[hxmim][PF_6]	Benzene	19.78	303	Li et al., 2015
	Acetone	21.99	303	Li et al., 2015
	Benzene	68.65	333	Li et al., 2015
	Acetone	72.53	333	Li et al., 2015
[omim][NTf_2]	Toluene	5	298	Bedia et al., 2013
Thy:DecA (1:1)	acetone	8.58	303	Chen 2022
ChCl:EG (1:1)	Cyclohexane	7260	303	Li et al., 2022
		13790	323	Li et al., 2022
		23580	343	Li et al., 2022
ChCl:EG (1:2)	Cyclohexane	26040	303	Li et al., 2022
		46080	323	Li et al., 2022
		71470	343	Li et al., 2022
ChCl:EG (1:3)	Cyclohexane	56220	303	Li et al., 2022
		90970	323	Li et al., 2022
		130660	343	Li et al., 2022
ChCl:Urea (1:1)	Cyclohexane	1440	303	Li et al., 2022
		3050	323	Li et al., 2022
		5700	343	Li et al., 2022
ChCl:Urea (1:2)	Cyclohexane	1500	303	Li et al., 2022
		3830	323	Li et al., 2022
		6850	343	Li et al., 2022
ChCl:Urea (1:3)	Cyclohexane	1930	303	Li et al., 2022
		4050	323	Li et al., 2022
		7140	343	Li et al., 2022

For instance, K_H values were obtained for toluene in [NTf_2]-based ILs with different alkyl chain lengths (2, 6, 8, 10) in the 3-methyl-imidazolium cation following the next trend in toluene solubility: [dcmim][NTf_2] > [omim][NTf_2] > [hxmim][NTf_2] > [emim][NTf_2]. Similarly, for benzene and acetone in various fluorinated imidazolium-based ILs, the trend for the absorption capacity based on the type of anion used was as follows: $[Tf_2N]^-$ > $[PF_6]^-$ > $[BF_4]^-$. It's noteworthy that increasing the length of alkyl substitutions in the imidazolium cation led to improve the solubility for toluene, benzene, and acetone (Table 2.1) (Bedia et al., 2013; Li et al., 2015).

ILs with [bmPy] and [bmim] cations and [NTf_2] and [TfO] anions were assessed for methanol, ethanol, 1-butanol, acetone, and p-xylene absorption through K_H measurements. The K_H values for methanol, ethanol and 1-butanol ranged from 3.2 to 48 kPa demonstrating greater solubility in [TfO]-based ILs, while acetone and p-xylene exhibited higher solubilities in [Tf_2N]-based ILs (Table 2.1). An increase in temperature led to an elevation in K_H values, indicating a decrease in the solubility of the VOCs in the ILs (Bedia et al., 2013; Li et al., 2015; Praus et al., 2022).

The Henry's constant of cyclohexane in DESs formed with ChCl and urea and EG at different molar ratios indicated that solubility decreases when both the molar ratios of HBA to HBD decrease and temperature increases (Table 2.1).

Dynamic absorption experiments between VOCs such as benzene, toluene, p-xylene, DMM, methanol, DCM, ethanol, and vinyl chloride using various imidazolium fluorinated ILs ([dcmim][NTf_2], [omim][NTf_2], [hxmim][NTf_2], , [dcmim][BF_4], [emim] [$C_2H_5SO_4$] ,TMGL, [$TMGHPO_2$][BF_4], [Emim][PF_6],[Hnmp][HSO_4], [Bmim][PF_6], [$PhCH_2$mim][Tf_2N], [Amim][Tf_2N], [Emim][Tf_2N], [Emim][BF_4], [Emim][Ac] and [Bmim][NTf_2]) have been conducted (Bedia et al., 2013; Cheng, et al., 2009; Gui et al., 2022; Ma et al., 2019; Wang et al., 2017; Yu et al., 2018, 2020; Zhao et al., 2019). VOCs dynamic absorption experiments in columns using DESs have also been performed, assessing different conditions of inlet VOC concentration, flow rate and temperature (Chen et al., 2021, 2022; Gui et al., 2023; Li et al., 2022; Moufawad et al., 2022; Mu et al., 2022; Song et al., 2020).

The results of continuous VOC absorption experiments conducted under various conditions (temperature initial, gas flow rate, and initial VOC concentration) revealed an interesting trend. Specifically, as the temperature increased, there was a noticeable reduction in VOC absorption.

For instance, in the case of toluene absorption, its absorptivity decreased from 97.1% at 20 °C to 93.8% at 80 °C when utilizing [bmim][NTf_2] (Wang et al., 2017). the saturated absorption of toluene by [Emim][BF_4], declined from 4.5 mg/g at 303 K to 0.0045 mg/g at 90 °C (Ma et al., 2019). In another study, the absorptivity of toluene diminished from 97.6% to 83.4% within the temperature range of 20 °C to 60 °C Similarly, acetone exhibited a similar behavior with an initial absorptivity of 88% at 20 °C, dropping to 78.5% at 60 °C (Ma et al., 2021).

Toluene absorption by thermogravimetric analysis in [dcmim][NTf_2], [omim][NTf_2], [hxmim][NTf_2], [emim][NTf_2], [dcmim][BF_4], and [emim] [$C_2H_5SO_4$] at different temperatures 20, 30, 40 °C, and a toluene initial concentration of 20000 ppmv and a toluene initial concentration of 20000 ppmv and at 100 flow rate of cm^3/mL, showed a decreased in toluene absorption when temperature increase for all the ILs analyzed (Bedia et al., 2013).

When using DESs, the DCM absorption capacity in [P_{4444}][Cl]-LevA (1:2) decreased from 1512 to 646 mg/g as the temperature changed from 25 to 35 °C (Mu et al., 2022). The solubility of toluene significantly decreased from nearly 100% removal to 80% removal at 25 and 45 °C, respectively, when utilizing TEACl-OA (1:3) as an absorbent in a dynamic absorption experiment (Song et al., 2020). The toluene absorption capacity of LauA:DecA (1:3) was 5.69 mg toluene/g of DES at 20 °C, but it decreased to 1.68 mg toluene/g of DES at 45 °C (Chen et al., 2021).

For acetone absorption, the Thy:DecA (1:1) system achieved an absorption capacity of 6.57 mg acetone/g of DES at 20 °C, whereas the saturated absorption capacity decreased to 1.14 mg acetone/g of DES at 40 °C (Chen et al., 2022). The heptane absorption capacity in TBABr:Dec decreased from 0.51 mg to 0.26 mg of heptane per gram of DES (Moufawad et al., 2022). In the case of DMC absorption, the capacity of TEBAC-TEG (1:3) was 263.62 mg/g at 40 °C which is less than half of the capacity at 30 °C (581.72 mg/g) (Gui et al., 2023). The decrease in the solubility of VOCs in solvents could be due to the increased of the evaporation of the VOC when temperature increase.

The impact of gas flow on continuous VOC absorption experiments revealed a noteworthy trend, the absorption of VOCs was high at lower gas flow rates within the ILs. This phenomenon can be attributed to the prolonged interaction time between VOCs and the absorbent at slower gas flow

rates, facilitating a more effective dissolution of VOCs into the ILs. Conversely, higher gas flow rates result in shorter contact times, limiting the capacity of organic pollutants to dissolve in ILs.

The investigation into the effects of varying toluene and acetone flow rates (300, 600, and 900 mL/min) within [bmim][PF_6] yielded intriguing results. At a temperature of 20°C and an initial concentration of 1200 mg/m^3, the toluene absorption capacity was observed to be 2.967, 1.599, and 1.437 mg/g for flow rates of 300, 600, and 900 mL/min, respectively. Similarly, for acetone under the same conditions, the absorption capacity was found to be 0.773, 0.758, and 0.591 mg/g for the corresponding flow rates of 300, 600, and 900 mL/min (Ma et al., 2021). When using DES TEACl-OA (1:3) as absorbent in a column, the removal efficiency change from almost 100% removal to 90% removal at 200 and 400 mL/min, respectively (Song et al., 2020).

Concerning the initial VOC concentration, an increase in the initial VOC concentration has not demonstrated any impact on the absorption rate or absorption capacity in continuous VOC absorption experiments. When evaluating the variations in initial toluene concentrations (2, 4, 8, 12, 16, 20 g/m^3), the absorption rate remained unaffected in [emim][BF_4] (Ma et al., 2019). Similarly, when the initial concentrations of toluene and acetone were altered from 1200 mg/m^3 to 3000 mg/m^3, there was a slight influence on the initial absorption of toluene and acetone, which ranged from 97% to 93% and 93% to 88%, respectively. However, noteworthy changes were observed in the saturation absorption capacity, increasing from 2.967 mg/g to 5.162 mg/g for toluene and from 0.718 mg/g to 2.225 mg/g for acetone in [bmim][PF_6] (Ma et al., 2021).

In continuous experiments involving DESs, the toluene absorption capacity in LauA:DecA (1:3) increased from 2.00 to 9.94 mg of toluene/g DES when the inlet toluene concentration increased from 250 ppm to 800 ppm (Chen et al., 2021). Additionally, the toluene absorption capacities of various DESs, such as ChCl:Lev, TBPBr:LevA, and TBABr:DecA, reached 5.7, 13.3, and 24.9 mg of toluene/g DES, respectively, for initial toluene concentrations of 1200, 2700, and 5150 g/m^3 (Moufawad et al., 2022). Similarly, the DCM absorption capacity in [P_{4444}][Cl]-LevA (1:2) and in DESs based on TEBAC demonstrated an increase with the rise in DCM partial pressure (Gui et al., 2023; Mu et al., 2022).

The increase in absorption capacity attained under high initial VOC concentration is attributed to the formation of a VOC film and a solvent (IL/DES) film at the gas-liquid interface, following the

principles of the two-film theory[12]. For VOC molecules to dissolve in the liquid phase, they must traverse the gas-liquid interface. As the VOC concentration rises, the concentration gradient between the gas and liquid phases intensifies, enhancing the driving force for mass transfer. This phenomenon is advantageous for VOC absorption in the liquid, ultimately enhancing absorptivity (Wang et al., 2017).

Regenerated ILs have been used in continuous VOC absorption experiments, the thermal distillation at 75 °C of [bmim][NTf_2] was used for regeneration, the absorptivity of toluene remained between 92% and 97% during the five reuse cycles (Wang et al., 2017). In the case of [emim][BF_4], the solubility of toluene remained largely unchanged after three cycles (Ma et al., 2019). Regarding [bmim][PF_6], its recycling performance demonstrated satisfactory reusability over five cycles for absorbing either toluene or acetone (Ma et al., 2021).

Regeneration of DES in continuous VOC absorption experiments, showed that after regeneration through heat, TEACl-OA (1:3) the removal efficiency was maintained (93-99%) after ten cycles (Song et al., 2020). Also DESs LauA;DecA and Thy:DecA (1:1) showed a stable toluene, acetone absorptivity (96 -99%) during five consecutive reuse cycles after regeneration (Chen et al., 2021, 2022). TBPBr:LevA and [P_{4444}][Cl]-LevA (1:2) ,and TEBAC-TEG (1:3) showed stable absorption capacities after five or ten absorption/desorption cycles (Gui et al., 2023; Moufawad et al., 2022; Mu et al., 2022).

Gravimetric dynamic absorption experiments showed that [$TMGHPO_2$][BF_4] was the best absorbent of gaseous vinyl chloride comparing with the ILs [bmim][PF_6], [bmi][BF_4], TMGL and [$TMGHPO_2$][BF_4]) in a range of temperatures from 15 to 50 °C. The vinyl chloride was physically absorbed with weak interactions (hydrogen bonds) in ILs, this was proved by proton nuclear magnetic resonance spectra (^{1}H-NMR). Moreover, the regeneration of IL through vacuum and/or heat was performed (Cheng et al., 2009).

Absorption experiments in packed columns operated in countercurrent mode have also been conducted for benzene, toluene, and p-xylene in [emim][Tf_2N] (Yu et al., 2018). For toluene in ILs based on [$PhCH_2$mim][Tf_2N] and [Amim][Tf_2N] (Yu et al., 2020) and for DCM and ethanol in IL based on [emim][Ac] (Gui et al., 2022).

Absorption experiments in packed columns operated in countercurrent mode, showed that higher values of IL flow rate (F_{IL}) improve VOCs absorption, for instance when F_{IL} is more than 15 mL/min the removal of benzene, toluene and p-xylene reached 97.7%, 94.1% and 83.5% removal (Yu et al., 2018). Toluene absorption increased slowly with the increase of F_{IL} and when F_{IL} increased from 5 mL/min to 20 mL/min. Also, the removal of DCM and ethanol increased rapidly, and with a F_{IL} of 20 mL/min, the removal ratios of DCM and ethanol reached 91.82% and 97.01%, respectively (Gui et al., 2022).

Interestingly, the gas flow rate (F_{Feed}) was found to have not significant impact on VOC removal. For instance, the absorptivity of toluene remained consistently high regardless of F_{Feed} variations. In specific conditions, toluene absorptivity was 99.329% for F_{Feed} = 500 mL/min and 99.288% for F_{Feed} = 100 mL/min (Yu et al., 2020).

Furthermore, the regeneration of various ionic liquids ([Emim][Tf_2N], [$PhCH_2$mim][Tf_2N], and [Amim][Tf_2N]) was achieved using vacuum and temperature (80°C or 140°C) or solely vacuum. These regeneration methods maintained the volatile organic compound captured efficiently in ILs by using multiple cycles like 5 or 20 cycles (Gui et al., 2022; Yu et al., 2018, 2020).

Packed absorption column operated in countercurrent using DESs ChCl:EG and ChCl:urea at molar ratio 1:2 were used as absorbents for cyclohexane gas (Li et al., 2022)**.** The packed column absorption experiment showed that the maximum cyclohexane recovery with ChCl:EG (96.0 %) was obtained at 15 mL/min and an inlet concentration of 400 ppm. The highest cyclohexane recovery (96.2%) with ChCl:urea was obtained at 30 mL/min and an inlet concentration of 380 ppm. The regeneration of the absorbents applying vacuum (0.1kPa) for 2 h was achieved, after 10 cycles no changes in the solubility of cyclohexane was observed (Li et al., 2022).

2.7. VOCs removal using ILs in biological systems

For the control of air pollution, various biological systems are used (e.g. biofilters, biotrickling filters, TPPBs) which are considered cost-effective solutions treating high air flow rate at low concentration of pollutants (Muñoz et al., 2007). TPPBs has been used to treat hydrophobic VOCs. The principle of operation of the TPPB consists of absorbing a specific compound in a non-aqueous liquid phase (NALP) that shows great affinity for the hydrophobic pollutant and coexists with an aqueous phase containing microorganisms capable to degrade the VOCs (Nguyen et al.,

2017). Imidazolium and pyridinium based ILs with fluorinated anions such as $[NTf_2]^-$ and $[PF_6]^-$ has been used for NAPL in a TPPB due to their immiscibility in water, their low melting point and their high thermal, chemical and hydrolytic stability (Nguyen et al., 2017; Quijano et al., 2013a; Rodriguez Castillo et al., 2018a, 2019). The effect of using IL in the biodegradation of toluene and dimethyl disulfide was studied (Quijano et al., 2011a, 2013a). Toluene and dimethyl disulfide biodegradation were inhibited by [bmim][NTf_2] with non-acclimated activated sludge. The use of [bmim][PF_6] produced a lag phase of 60 h in the biodegradation of toluene, whereas the control without IL required 19 h to reach a complete toluene biodegradation, when [bmim][PF_6] was used the biodegradation of dimethyl disulfide was inhibited. In addition, the acclimation process to dimethyl disulfide did not improve its biodegradation in the presence of ILs, while sludge acclimated to toluene, depleted toluene in 20 and 72 h in the presence of [bmim][PF_6] and [bmim][NTf_2], respectively, when the control without IL were able to deplete toluene in 15 h.

The use of [OctIq] [NTf2] at a ratio of 5% v/v as a possible NAPL to treat toluene was studied in a pilot-scale TPPB (12 L). Using and toluene-acclimated activated sludge (Nguyen et al., 2017), where a biodegradation rate of 14.3 g VOCs/m^3h was achieved at an initial toluene amount of 9 g. Other study tested four hydrophobic IL at a ratio of 5% v/v in batch tests for toluene degradation with activated sludge acclimated to both toluene and IL (Rodriguez Castillo et al., 2018), where isoquinolinium IL appeared to be the most suitable NAPL for toluene biodegradation in a TPPB. An improvement in toluene biodegradation was observed when the activated sludge was acclimated to the toluene substrate and IL. (Rodriguez Castillo et al., 2018).

2.8. Perspectives

The reports on the use of DES or NADES for VOCs absorption are scarce, which makes them novel systems for the elimination of air pollutants. Given they share relevant advantages with ILs as low vapor pressure, thermal stability and some of their properties can be tailored when choosing their components, it is interesting to prove these solvents in the same way that ILs have been proven as absorbents for remove VOCs. Also, it would be interesting to investigate DES/NADES performance in TPPBs taking advantages of their low cost and negligible impact to the environment due to their biodegradability and low level of toxicity. DESs/NADESs are less expensive than ILs. For instance, the prices of most imidazolium ILs ranged in 2019 between

$587.56 to 5875.60 per kilogram (Abushammala & Mao, 2020), whereas the price of ChCl:urea (1:2) is approximately $132.8 per kilogram. Thus, the use of DESs/NADESs presents better economic feasibility than ILs.

Table 2.2 Bioreactor experiments using ILs as non-aqueous phase for the removal of various VOCs

VOC	Operation mode	IL ratio (%v/v)	Microorganism	IL	Results	Reference
Toluene	Batch	5	Activated sludge	[OctIq][NTf_2], [$AllylEt_2S$][NTf_2], [DecIq][NTf_2] and [Bmim][NTf_2]	Non-acclimated AS: [OctIq][NTf_2]: 1.11 mg/L*h [$AllylEt_2S$][NTf_2]: 0.92 mg/L*h [DecIq][NTf_2]: 0.77 mg/L*h [Bmim][NTf_2]: 0.50 mg/L*h AS acclimated to toluene: [OctIq][NTf_2]: 59.9 mg/L*h [$AllylEt_2S$][NTf_2]: 32.3 mg/L*h AS acclimated to toluene and IL: [OctIq][NTf_2]: 54.8 mg/L*h [$AllylEt_2S$][NTf_2]: 14.3 mg/L*h	Rodriguez Castillo et al., 2018a
Toluene	CSTR 12 L	5	Activated sludge	[OctIq] [NTf_2]	14.3 g Toluene/m^3*h	Nguyen et al., 2017

VOC	Operation mode	IL ratio (%v/v)	Microorganism	IL	Results	Reference
Toluene and DMDS	Batch	5	Activated sludge	[BMIM][PF_6], [BMIM][NTf_2], [PEGMIM][PF_6], [C_2OHMIm][PF_6] and Aliquat 336®	Non-acclimated AS: [BMIM][PF_6]: 0.13 g Toluene/m^3*h; 0.023 g DMDS /m^3*h. [BMIM][NTf_2]: 0.01 g toluene/m^3*h; 0.023 g DMDS/m3*h. Acclimated AS: [BMIM][PF_6]: 0.48 g toluene/m^3*h. [BMIM][NTf_2]: 0.11 g Toluene/m^3*h.	Quijano et al., 2013
Toluene, DMS and DMDS	Batch	5	Activated sludge	[C_4mim][PF_6] and [C_4mim][NTf_2]	Control without IL: 0.48 g toluene/m^3*h [BMIM][PF_6]: 0.36 g toluene/m^3*h [BMIM][NTf_2]: 0.1 g toluene/m^3*h	Quijano et al., 2011a

DMDS: Dimethyl Disulfide, DMS: Dimethyl Sulfide, AS: Activated sludge

It is worth mentioning that DESs and NADESs have been scarcely tested in TPPBs for the elimination of VOCs from gas streams, thus it will be open a research window to evaluate the effectiveness of these novel phases. It will be necessary to evaluate if there will be competition between the degradation of VOCs and DESs/NADESs by microorganisms due to both are biodegradable, or from when this competition occurs during TPPBs operation because it is unknown since they have not been used for this purpose. Considering that most DESs/NADESs are biodegradable this could bring advantages such as diminish their environmental impact and cost of disposition of the used NAP, and finally the TPPB could be operated as fed batch mode, in order to replenish the DESs/NADESs biodegrades and a the same time it will permit to enhance the biodegradation of the pollutant.

2.9. Conclusions

Ionic liquids present characteristics such as low vapor pressure, thermal stability, and a wide variety of solubilities (hydrophilic/hydrophobic) making them an alternative of organic solvents for the absorption of VOCs from air. However, limitations such as their high viscosity, toxicity as well as their persistence in the environment must be considered in order to design a process that allows to diminish such limitations and take advantage of the maximum benefit they can provide. The use of ILs as reservoir of VOC in biologically system have been demonstrated. However, more information is needed about the convenience of using ILs since they present some drawbacks in this process due to their high cost and toxicity.

An alternative to the use of ILs are DES and NADES that present similarities with ILs (low vapor pressure, thermal stability, and the wide variety of solubilities (hydrophilic/hydrophobic)). Also, they have a series of characteristics such as low toxicity and high biodegradability that makes them benign for the environment. Not to mention the lower cost that DESs/NADEs could have compared to ILs. However, there are still few reports in their use for the absorption of VOCs from air, thus, more research is needed in this area.

2.10. Abbreviations

Table 2.3 Abbreviations used in this chapter.

Abbreviation	Name
$[N(CN)_2]$-	dicyanamide
$[(CF_3SO_2)(CF_3CO)N]$-	2,2,2-(trifluoromethylsulfonyl)acetamide
$[Al_2Cl_7]$-	Dialuminum;heptachloride
$[AllylEt_2S][NTf_2]$	Allyl-diethylsulfonium bis(trifluoromethylsulfonyl)imide
[Amim][Tf2N]	1-allyl-3-methylimidazolium bis(trifluoromethylsulfonyl)imide
$[AsF_6]$-	hexafluoroarsenic
$[BF_4]$-	tetrafluoroborate
[bmim]	1-n-butyl-3-methylimidazolium
$[bmim][BF_4]$	1-butyl-3-methylimidazolium tetrafluoroborate
[bmim][Br]	1-butyl-3-methylimidazolium Bromide
[bmim][Cl]	1-butyl-3-methylimidazolium Chloride
[bmim][NfO]	1-butyl-3-Methylimidazoliumno nafluorobutane sulfonate
$[bmim][NTf_2]$, [Bmim][TFSI]	1-butyl-3-methylimidazolium bis(trifluoromethylsulfonyl)imide
$[bmim][PF_6]$	1-butyl-3-methylimidazolium hexafluorophosphate
[bmim][TfO]	1-butyl-3-methylimidazolium trifluoromethanesulfonate
[bmPyr][Br]	N-butyl-N-methylpyrrolidinium bromide
$[bmPyrr][NTf_2]$	1-Butyl-1-methylpyrrolidinium bis(trifluoromethylsulfonyl)imide
[bmPyrr][TfO]	1-Butyl-1-methylpyrrolidinium trifluoromethanesulfonate
$[bmTriaz][NTf_2]$	1-butyl-3-methyl-1H-[1,2,4]triazolium bis(trifluoromethylsulfonyl)imide
[Br]-	bromide
[ButenylMim][NfO]	3-Butenyl-1-methylimidazolium nonafluorobutylsulfonate
$[ButenylMim][NTf_2]$	3-Butenyl-1-methylimidazolium bis(trifluoromethylsulfonyl)imide
$[ButenylMim][PF_6]$	3-Butenyl-1-methylimidazolium hexafluorophosphate
[BzChol]Cl	benzyldimethyl(2-hydro- xyethyl)ammonium chloride
$[C(CN)_3]$-	tricyanomethanide
$[C_{10}Iq][NTf_2]$	1-decylisoquinoliniumbis(trifluoromethylsulfonyl)imide
$[C_{10}mim][NTf_2]$/ $[dcmim][NTf_2]$	1-decyl--3-methylimidazolium bis(trifluoromethylsulfonyl)imide
$[C_{16}mim][NTf_2]$	1-hexadecyl--3-methylimidazolium bis(trifluoromethylsulfonyl)imide
$[C_2mim][NTf_2]$/[emim][NTf_2]	1-ethyl--3-methylimidazolium bis(trifluoromethylsulfonyl)imide
$[CF_2CFEBTriaz][NTf_2]$	1-butyl-3-(1,1,2-trifluoro-1-butenyl)-1H-[1,2,4]triazolium bis(trifluoromethylsulfonyl)imide
$[CF_3CF_2BTriaz][NTf_2]$	1-butyl-3-(1,1,2-trifluoro-1-butenyl)-1H-[1,2,4]triazolium bis(trifluoromethylsulfonyl)imide
$[CF_3SO_3]-$	triflate
[Chol][Ac]	cholinium acetate
[Chol][Bic]	cholinium bicarbonate
[Chol][Bit]	cholinium bitartrate
[Chol][But]	cholinium butanoato
[Chol][Cl]	cholinium cloride
[Chol][DHCit]	cholinium dihydrogenocitrate
[Chol][DHPhosp]	cholinium dihydrogenophosphate
[Chol][Prop]	cholinium propanoate
[Chol][Sal]	cholinium salicylate
[Cl]-	cloride

Abbreviation	Name
$[CNC_{3m}im][NTf_2]$	3-(4-butyronitrile)-1-methylimidazolium bis(trifluoromethylsulfonyl)imide
$[dcmim][BF_4]$	1-decyl--3-methylimidazolium tetrafluoroborate
[dcmim][Cl]	1-decyl--3-methylimidazolium chloride
$[dcmim][NTf_2]$	1-decyl-3-methylimidazolium bis(trifluoromethylsulfonyl)imide
$[decIq][NTf_2]$	1-decyl-3-methyisoquinolium bis(trifluoromethylsulfonyl)imide
$[emim]$ $[C_2H_5SO_4]$	1-ethyl-3-methylimidazolium ethylsulfate
[Emim][Ac]	1-ethyl-3-Methylimidazoliumno acetate
$[Emim][BF_4]$	1-ethyl-3-methylimidazolium tetrafluoroborate
$[emim][C_2H_5SO_4]$	1-ethyl--3-methylimidazolium
[emim][NTf2].	1-ethyl-3-Methylimidazoliumno acetate bis(trifluoromethylsulfonyl)imide
$[Emim][PF_6]$	1-ethyl-3-methylimidazolium hexafluorophosphate
$[EtOEIq][NTf_2]$	1-(-1- ethoxyethyl)-isoquinolinium bis(trifluoromethylsulfonyl)imide
$[EtOEMim][NTf_2]$	3-(1-ethoxyethyl)-1-methylimidazolium bis(trifluoromethylsulfonyl)imide
$[EtOEMMorph][NTf_2]$	4-Ethoxyethyl-4-methylmorpholinium bis(trifluoromethylsulfonyl)imide
[FAP]-	tris(perfluoroalkyl)trifluorophosphate
[hmim][Br]	1-hexyl--3-methylimidazolium bromide
[hmPyr][Br]	N-hexyl-N-methylpyrrolidinium bromide
$[Hnmp][HSO_4]$	1-methyl-2-pyrrolidonium hydrogen sulphate
$[hxmim][NTf_2]$	1-hexyl--3-methylimidazolium bis(trifluoromethylsulfonyl)imide
[I]-	iodide
[Im]	Imidazolium
$[iPtMim][NTf_2]$	3-Isopentyl-1-methylimidazolium bis(trifluoromethylsulfonyl)imide
$[iPtMim][PF_6]$	3-Isopentyl-1-methylimidazolium hexafluorophosphate
[Iq]	Isoquinolinium
$[MeOC_2OC_2Emim][NTf_2]$	3-(1-methoxyethoxyethyl)-1-methylimidazolium bis(trifluoromethylsulfonyl)imid
$[MeOEIq][NTf_2]$	1-(-1-methoxyethyl)-isoquinolinium bis(trifluoromethylsulfonyl)imide
[MeOEMim][NfO]	3-(1-methoxyethyl)-1-methylimidazolium nonafluorobutylsulfonate
$[MeOEmim][NTf_2]$	3-(1-methoxyethyl)-1-methylimidazolium bis(trifluoromethylsulfonyl)imide
$[MeOEMMorph][NTf_2]$	4-Methoxyethyl-4-methylmorpholinium bis(trifluoromethylsulfonyl)imide
[Morph]	Morpholium
[NfO]-	nonafluorobutylsulfonate
$[nPrMim][NTf_2]$	3-Propyl-1-methylimidazolium bis(trifluoromethylsulfonyl)imide
$[NTf_2]^-$, [TFSI], $[(CF_3SO_2)_2N]$-	bistrifluoromethylsulfonyl imide
$[OctIq][NTf_2]$	1-octylisoquinolinium bis (trifluoromethyl-sulfonyl)imide
[omim][Br]	1-octyl--3-methylimidazolium bromide
$[omim][NTf_2]$	1-octyl--3-methylimidazolium bis(trifluoromethylsulfonyl)imide
[omPyr][Br]	N-octyl-N-methylpyrrolidinium bromide
$[P_{4443}][BF_4]$	tributyl(propyl)phosphonium tetrafluoroborate
$[P_{4444}][Cl]$:LevA	Tetrabutylphosphonium chloride: levulinic acid
$[PEGMIM][PF_6]$	1-(2-Hydroxyethyl)-3-methylimidazolium hexafluorophosphate
$[PF_6]$-	hexafluorophosphate
$[PhCH_2mim][NTf_2]$	1-benzyl-3-methylimidazolium bis(trifluoromethylsulfonyl)imide
[Pyrr]	Pyrrolidinium

Abbreviation	Name
[S]	Sulfonium
$[SbF_6]^-$	hexafluoroantimonate
$[TMGHPO_2][BF_4]$	2,4-bis(2-hydroxypropyl)-1,1,3,3-tetramethyl guanidinium tetrafluoroborate
[Triaz]	Triazolium
ATPPB	allyltriphenylphosphonium bromide
BETI	bis(pentafluoroethylsulfonyl)imide
BTPC	Benzyltriphenylphosphonium chloride
ChA	choline acetate
ChCl	Choline chloride
Chol-C_6-Lac	Hexylcholinium lactate
Chol-C_6-Lev	Hexylcholinium levulinate
Chol-C_8-Lac	Octylcholinium lactate
Chol-C_8-Lev	Octylcholinium levulinate
$C_n$mim][NTf_2]	N-alkyl-3-methylimidazolium bis(trifluoromethylsulfonyl)imide
DEACEG	N,N-diethylethanol ammonium chloride–ethylene glycol
DEACG	N,N-diethylethanol ammonium chloride-glycerol
DecA	Decanoic acid
DEG	diethylene glycol
EAC	N,N-Diethyl ethanol ammonium chloride
EG	ethylene glycol
GL	glycerol
LauA	lauric acid
LevA	levulinic acid
m-2-HEAA	N-methyl-2-hydroxyethylammonium acetate
m-2-HEAB	N-methyl- 2-hydroxyethylammonium butyrate
m-2-HEAP	N- methyl-2-hydroxyethylammonium pentanoate
m-2-HEAPr	N-methyl-2- hydroxyethylammonium propionate
MalA	malonic acid
$Me[(CF_3SO_2)_3C]^-$	tris(trifluoromethylsulfonyl)methide
MTPB	methyltriphenylphosphonium bromide
N_{4444}-Cl	tetrabutylammonium chloride
N_{7777}-Cl	tetraheptylammonium chloride
N_{8881}-Br	methyltrioctylammonium bromide
N_{8881}-Cl	methyltrioctylammonium chloride
N_{8888}- B	tetraoctylammonium bromide
N_{8888}-Cl	tetraoctylamonium chloride
OA	oleic acid
Phenylac	phenylacetic acid
Phenylpr	phenylpropionic acid
TBA-Br	tetrabutylammonium bromide
TBP-Br	tetrabutylphosphonium bromide

Abbreviation	Name
TEACl	tetraethylammonium chloride
TEBAC	benzyltriethylammonium chloride
TEG	triethyleneglycol
Thy	thymol
TMGL	1,1,3,3-tetramethyl guanidinium lactate
$ZnCl_2$	zinc chloride
ZnN	zinc nitrate hexahydrate

2.11. References

Abbott, A. P., Boothby, D., Capper, G., Davies, D. L., & Rasheed, R. K. (2004). Deep Eutectic Solvents formed between choline chloride and carboxylic acids: Versatile alternatives to ionic liquids. *Journal of the American Chemical Society*, *126*(29), 9142–9147. https://doi.org/10.1021/ja048266j

Abdullah, G. H., & Kadhom, M. A. (2016). Studying of two choline chloride's deep eutectic solvents in their aqueous mixtures. In *International Journal of Engineering Research* (Vol. 12, Issue 9).

Abranches, D. O., & Coutinho, J. A. P. (2022). Type V deep eutectic solvents: Design and applications. *Current Opinion in Green and Sustainable Chemistry*, *35*, 100612. https://doi.org/10.1016/j.cogsc.2022.100612

Abushammala, H., & Mao, J. (2020). A Review on the Partial and Complete Dissolution and Fractionation of Wood and Lignocelluloses Using Imidazolium Ionic Liquids. *Polymers*, *12*(1). https://doi.org/10.3390/polym12010195

Altamash, T., Atilhan, M., Aliyan, A., Ullah, R., Nasser, M., & Aparicio, S. (2017). Rheological, Thermodynamic, and Gas Solubility Properties of Phenylacetic Acid-Based Deep Eutectic Solvents. *Chemical Engineering and Technology*, *40*(4), 778–790. https://doi.org/10.1002/ceat.201600475

Bedia, J., Ruiz, E., de Riva, J., Ferro, V. R., Palomar, J., & Rodriguez, J. J. (2013). Optimized ionic liquids for toluene absorption. *AIChE Journal*, *59*(5), 1648–1656. https://doi.org/10.1002/aic.13926

Candia-Lomelí, M., Covarrubias-Garcia, I., Aizpuru, A., & Arriaga, S. (2023). Preparation and physicochemical characterization of deep eutectic solvents and ionic liquids for the potential absorption and biodegradation of styrene vapors. *Journal of Hazardous Materials*, *441*(April 2022), 129835. https://doi.org/10.1016/j.jhazmat.2022.129835

Cao, J., Zhu, F., Dong, Q., Wu, R., & Su, E. (2022). Insight into the physicochemical properties of deep eutectic solvents by systematically investigating the components. *Journal of Molecular Liquids*, *346*, 118315. https://doi.org/10.1016/j.molliq.2021.118315

Chen, C. C., Huang, Y. H., & Fang, J. Y. (2022). Hydrophobic deep eutectic solvents as green absorbents for hydrophilic VOC elimination. *Journal of Hazardous Materials*, *424*(PB), 127366. https://doi.org/10.1016/j.jhazmat.2021.127366

Chen, C. C., Huang, Y. H., Hung, S. M., Chen, C., Lin, C. W., & Yang, H. H. (2021). Hydrophobic deep eutectic solvents as attractive media for low-concentration hydrophobic VOC capture. *Chemical Engineering Journal*, *424*. https://doi.org/10.1016/j.cej.2021.130420

Cheng, X., Yang, G., Mu, T., Guo, X., & Wang, X. (2009). Absorption of vinyl chloride by room temperature ionic liquids. *Clean - Soil, Air, Water*, *37*(3), 245–248. https://doi.org/10.1002/clen.200800188

Craveiro, R., Aroso, I., Flammia, V., Carvalho, T., Viciosa, M. T., Dionísio, M., Barreiros, S., Reis, R. L., Duarte, A. R. C., & Paiva, A. (2016). Properties and thermal behavior of natural deep eutectic solvents. *Journal of Molecular Liquids*, *215*, 534–540. https://doi.org/10.1016/j.molliq.2016.01.038

De Morais, P., Gonçalves, F., Coutinho, J. A. P., & Ventura, S. P. M. (2015). Ecotoxicity of Cholinium-Based Deep Eutectic Solvents. *ACS Sustainable Chemistry and Engineering*, *3*(12), 3398–3404. https://doi.org/10.1021/acssuschemeng.5b01124

De Zwart, D., & Slooff, W. (1983). The Microtox as an alternative assay in the acute toxicity assessment of water pollutants. *Aquatic Toxicology*, *4*(2), 129–138. https://doi.org/10.1016/0166-445X(83)90050-4

Delgado-Mellado, N., Larriba, M., Navarro, P., Rigual, V., Ayuso, M., García, J., & Rodríguez, F. (2018). Thermal stability of choline chloride deep eutectic solvents by TGA/FTIR-ATR analysis. *Journal of Molecular Liquids*, *260*, 37–43. https://doi.org/10.1016/j.molliq.2018.03.076

Derwent, R. G. (1995). Sources, distributions, and fates of VOCs in the atmosphere. In R. E. Hester & R. M. Harrison (Eds.), *Volatile Organic Compounds in the Atmosphere* (pp. 1–16). The Royal Society of Chemistry. https://doi.org/10.1039/9781847552310-00001

Dietz, C. H. J. T., Kroon, M. C., Van Sint Annaland, M., & Gallucci, F. (2017). Thermophysical Properties and Solubility of Different Sugar-Derived Molecules in Deep Eutectic Solvents. *Journal of Chemical and Engineering Data*, *62*(11), 3633–3641. https://doi.org/10.1021/acs.jced.7b00184

Docherty, K. M., Dixon, J. K., & Kulpa, C. F. (2007). Biodegradability of imidazolium and pyridinium ionic liquids by an activated sludge microbial community. *Biodegradation*, *18*(4), 481–493. https://doi.org/10.1007/s10532-006-9081-7

Earle, M., Esperança, J., Gilea, M. A., Magee, J. W., Seddon, K. R., & Widegren, J. A. (2006). The distillation and volatility of ionic liquids. *Nature*, *439*, 831–834. https://doi.org/10.1038/nature04451

El Achkar, T., Greige-Gerges, H., & Fourmentin, S. (2021). Basics and properties of deep eutectic solvents: a review. *Environmental Chemistry Letters*, *19*(4), 3397–3408. https://doi.org/10.1007/s10311-021-01225-8

Fahri, F., Bacha, K., Chiki, F. F., Mbakidi, J. P., Panda, S., Bouquillon, S., & Fourmentin, S. (2020). Air pollution: new bio-based ionic liquids absorb both hydrophobic and hydrophilic volatile organic compounds with high efficiency. *Environmental Chemistry Letters*, *18*(4), 1403–1411. https://doi.org/10.1007/s10311-020-01007-8

Fredlake, C. P., Crosthwaite, J. M., Hert, D. G., Aki, S. N. V. K., & Brennecke, J. F. (2004). Thermophysical Properties of Imidazolium-Based Ionic Liquids. *Journal of Chemical and Engineering Data*, *49*, 954–964. https://doi.org/10.1021/je034261a

Freemantle, M. (2009). *An Introduction to Ionic Liquids*. The Royal Society of Chemistry.

García, G., Aparicio, S., Ullah, R., & Atilhan, M. (2015). Deep eutectic solvents: Physicochemical properties and gas separation applications. *Energy and Fuels*, *29*(4), 2616–2644. https://doi.org/10.1021/ef5028873

Gathergood, N., Garcia, M. T., & Scammells, P. J. (2004). Biodegradable ionic liquids: Part I. Concept, preliminary targets and evaluation. *Green Chemistry*, *6*(3), 166–175. https://doi.org/10.1039/b315270g

Ge, D., & Lee, H. K. (2015). Ultra-hydrophobic ionic liquid 1-hexyl-3-methylimidazolium tris(pentafluoroethyl)trifluorophosphate supported hollow-fiber membrane liquid-liquid-liquid microextraction of chlorophenols. *Talanta*, *132*, 132–136. https://doi.org/10.1016/j.talanta.2014.08.074

Ghaedi, H., Ayoub, M., Sufian, S., Hailegiorgis, S. M., Murshid, G., & Khan, S. N. (2018). Thermal stability analysis, experimental conductivity and pH of phosphonium-based deep eutectic solvents and their prediction by a new empirical equation. *Journal of Chemical Thermodynamics*, *116*, 50–60. https://doi.org/10.1016/j.jct.2017.08.029

Ghaedi, H., Ayoub, M., Sufian, S., Lal, B., & Shariff, A. M. (2017). Measurement and correlation of physicochemical properties of phosphonium-based deep eutectic solvents at several temperatures (293.15 K–343.15 K) for CO2 capture. *Journal of Chemical Thermodynamics*, *113*, 41–51. https://doi.org/10.1016/j.jct.2017.05.020

Ghaedi, H., Ayoub, M., Sufian, S., Lal, B., & Uemura, Y. (2017). Thermal stability and FT-IR analysis of Phosphonium-based deep eutectic solvents with different hydrogen bond donors. *Journal of Molecular Liquids*, *242*, 395–403. https://doi.org/10.1016/j.molliq.2017.07.016

Gui, C., Li, G., Song, M., & Lei, Z. (2023). Absorption of dichloromethane in deep eutectic solvents: Experimental and computational thermodynamics. *Separation and Purification Technology*, *311*(February), 123281. https://doi.org/10.1016/j.seppur.2023.123281

Gui, C., Li, G., Zhu, R., Lei, Z., & Dong, Y. (2022). Capturing VOCs in the pharmaceutical industry with ionic liquids. *Chemical Engineering Science*, *252*. https://doi.org/10.1016/j.ces.2022.117504

Harjani, J. R., Singer, R. D., Garcia, M. T., & Scammells, P. J. (2009). Biodegradable pyridinium ionic liquids: Design, synthesis and evaluation. *Green Chemistry*, *11*(1), 83–90. https://doi.org/10.1039/b811814k

Hayyan, A., Mjalli, F. S., Alnashef, I. M., Al-Wahaibi, T., Al-Wahaibi, Y. M., & Hashim, M. A. (2012). Fruit sugar-based deep eutectic solvents and their physical properties. *Thermochimica Acta*, *541*, 70–75. https://doi.org/10.1016/j.tca.2012.04.030

Hayyan, M., Aissaoui, T., Hashim, M. A., AlSaadi, M. A. H., & Hayyan, A. (2015). Triethylene glycol based deep eutectic solvents and their physical properties. *Journal of the Taiwan Institute of Chemical Engineers*, *50*, 24–30. https://doi.org/10.1016/j.jtice.2015.03.001

Hayyan, M., Hashim, M. A., Al-Saadi, M. A., Hayyan, A., AlNashef, I. M., & Mirghani, M. E. S. (2013). Assessment of cytotoxicity and toxicity for phosphonium-based deep eutectic solvents. *Chemosphere*, *93*(2), 455–459. https://doi.org/10.1016/j.chemosphere.2013.05.013

Health Effects Institute. (2019). State of Global Air 2019. Special Report. In *Health Effects Institute*. MA:Health Effects Institute.

Hernández-Fernández, F. J., Bayo, J., Pérez de los Ríos, A., Vicente, M. A., Bernal, F. J., & Quesada-Medina, J. (2015). Discovering less toxic ionic liquids by using the Microtox® toxicity test. *Ecotoxicology and Environmental Safety*, *116*, 29–33. https://doi.org/10.1016/j.ecoenv.2015.02.034

Indra, S., Subramanian, R., & Daschakraborty, S. (2022). Absorption of Volatile Organic Compounds Toluene and Acetaldehyde in Choline Chloride-Based Deep Eutectic Solvents. *Journal of Physical Chemistry B*, *126*(20), 3705–3716. https://doi.org/10.1021/acs.jpcb.2c00076

Jablonsky, M., Skulcova, A., Haz, A., Sima, J., & Majova, V. (2018). Long-term Isothermal Stability of Deep Eutectic Solvents. *BioResources*, *13*(4), 7545–7559. https://doi.org/10.15376/biores.13.4.7545-7559

Jablonský, M., Škulcová, A., Ház, A., Šima, J., & Majová, V. (2018). Stability of eutectic solvents. In *BioResources* (Vol. 13, Issue 4).

Juneidi, I., Hayyan, M., & Hashim, M. A. (2015). Evaluation of toxicity and biodegradability for cholinium-based deep eutectic solvents. *RSC Advances*, *5*(102), 83636–83647. https://doi.org/10.1039/c5ra12425e

Juneidi, I., Hayyan, M., & Mohd Ali, O. (2016). Toxicity profile of choline chloride-based deep eutectic solvents for fungi and Cyprinus carpio fish. *Environmental Science and Pollution Research*, *23*(8), 7648–7659. https://doi.org/10.1007/s11356-015-6003-4

Kroon, M. C., & Binnemans, K. (2019). Degradation of Deep-Eutectic Solvents Based on Choline Chloride and Carboxylic Acids [Research-article]. *ACS Sustainable Chemistry & Engineering*, *7*, 11521–11528. https://doi.org/10.1021/acssuschemeng.9b01378

Le Cloirec, P., Andrès, Y., Gérente, C., & Pré, P. (2005). Biological Treatment of Waste Gases Containing Volatile Organic Compounds. In Z. Shareefdeen & A. Singh (Eds.), *Biotechnology for Odor and Air Pollution Control*. Springer Berlin Heidelberg. https://doi.org/10.1007/3-540-27007-8_13

Li, C. H., Gao, K. X., Meng, Y. N., Wu, X. K., Zhang, F., & Wang, Z. X. (2015). Solution Thermodynamics of Imidazolium-Based Ionic Liquids and Volatile Organic Compounds: Benzene and Acetone. *Journal of Chemical and Engineering Data*, *60*(6), 1600–1607. https://doi.org/10.1021/je500986b

Li, G., Gui, C., Zhu, R., & Lei, Z. (2022). Deep eutectic solvents for efficient capture of cyclohexane in volatile organic compound : Thermodynamic and molecular mechanism. *AIChE Journal*, *68*(3), 1–6. https://doi.org/10.1002/aic.17535

Ludwig, R., & Kragl, U. (2007). Do We Understand the Volatility of Ionic Liquids? *Angewandte Chemie International Edition*, *46*(35), 6582–6584. https://doi.org/10.1002/anie.200702157

Ma, X., Wang, W., Sun, C., & Sun, J. (2021). Comprehensive evaluation of ionic liquid [Bmim][PF6] for absorbing toluene and acetone. *Environmental Pollution*, *285*, 117675. https://doi.org/10.1016/j.envpol.2021.117675

Ma, X., Wu, M., Liu, S., Huang, J., Sun, B., Zhou, Y., Zhu, Q., & Lu, H. (2019). Concentration control of volatile organic compounds by ionic liquid absorption and desorption. *Chinese Journal of Chemical Engineering*, *27*(10), 2383–2389. https://doi.org/10.1016/j.cjche.2018.12.019

Mallakpour, S., & Dinari, M. (2012). Ionic Liquids as Green Solvents: Progress and Prospects. In A. Mohammad & D. Inamuddin (Eds.), *Green Solvents II: Properties and Applications of Ionic Liquids* (pp. 1–32). Springer Netherlands. https://doi.org/10.1007/978-94-007-2891-2_1

Marcus, Y. (2016). Ionic liquid properties: From molten salts to RTILs. In *Ionic Liquid Properties: From Molten Salts to RTILs*. https://doi.org/10.1007/978-3-319-30313-0

McCarty, L. S., & Borgert, C. J. (2006). Review of the toxicity of chemical mixtures: Theory, policy, and regulatory practice. *Regulatory Toxicology and Pharmacology*, *45*(2), 119–143. https://doi.org/10.1016/j.yrtph.2006.03.004

Mena, I. F., Diaz, E., Palomar, J., Rodriguez, J. J., & Mohedano, A. F. (2020). Cation and anion effect on the biodegradability and toxicity of imidazolium– and choline–based ionic liquids. *Chemosphere*, *240*. https://doi.org/10.1016/j.chemosphere.2019.124947

Montalbán, M. G., Hidalgo, J. M., Collado-González, M., Díaz Baños, F. G., & Víllora, G. (2016). Assessing chemical toxicity of ionic liquids on Vibrio fischeri: Correlation with structure and composition. *Chemosphere*, *155*, 405–414. https://doi.org/10.1016/j.chemosphere.2016.04.042

Moufawad, T., Costa Gomes, M., & Fourmentin, S. (2022). Deep eutectic solvents as absorbents for VOC and VOC mixtures in static and dynamic processes. *Chemical Engineering Journal*, *448*(June), 137619. https://doi.org/10.1016/j.cej.2022.137619

Moura, L., Moufawad, T., Ferreira, M., Bricout, H., Tilloy, S., Monflier, E., Costa Gomes, M. F., Landy, D., & Fourmentin, S. (2017). Deep eutectic solvents as green absorbents of volatile organic pollutants. *Environmental Chemistry Letters*, *15*(4), 747–753. https://doi.org/10.1007/s10311-017-0654-y

Mu, M., Zhang, X., Yu, G., Xu, R., Liu, N., Wang, N., & Chen, B. (2022). Effective absorption of dichloromethane using deep eutectic solvents. *Journal of Hazardous Materials*, *439*(May), 129666. https://doi.org/10.1016/j.jhazmat.2022.129666

Muñoz, R., Daugulis, A. J., Hernández, M., & Quijano, G. (2012). Recent advances in two-phase partitioning bioreactors for the treatment of volatile organic compounds. In *Biotechnology Advances* (Vol. 30, Issue 6, pp. 1707–1720). https://doi.org/10.1016/j.biotechadv.2012.08.009

Muñoz, R., Villaverde, S., Guieysse, B., & Revah, S. (2007). Two-phase partitioning bioreactors for treatment of volatile organic compounds. In *Biotechnology Advances* (Vol. 25, Issue 4, pp. 410–422). https://doi.org/10.1016/j.biotechadv.2007.03.005

Nguyen, T. V. N., Rodriguez Castillo, A. S., Guihéneuf, S., Biard, P. F., Paquin, L., Amrane, A., & Couvert, A. (2017). Toluene degradation in a two-phase partitioning bioreactor involving a hydrophobic ionic liquid as a non-aqueous phase liquid. *International Biodeterioration and Biodegradation*, *117*, 31–38. https://doi.org/10.1016/j.ibiod.2016.11.011

OECD. (1992). OECD 301 - Ready Biodegradability. *OECD Guidelines for the Testing of Chemicals*, *301*(July), 1–62.

Oliveira, M. V. S., Vidal, B. T., Melo, C. M., Miranda, R. D. C. M. De, Ventura, P. M., Mattedi, S., & Soares, C. M. F. (2016). *Chemosphere (Eco) toxicity and biodegradability of protic ionic liquids*. *147*, 460–466. https://doi.org/10.1016/j.chemosphere.2015.11.016

Porcedda, S., Usula, M., & Marongiu, B. (2014). Physical-Chemical Properties of Ionic Liquid-Containing Mixtures. In R. Caminiti & L. Gontrani (Eds.), *The Structure of Ionic Liquids. Soft and Biological Matter*. Springer. https://doi.org/10.1007/978-3-319-01698-6

Praus, J., Pokorný, P., Číhal, P., & Vopička, O. (2022). Solubility and diffusivity of six volatile compounds in ionic liquids [BMIM][Tf2N], [BMPy][Tf2N], [BMIM][TfO] and [BMPy][TfO]. *Fluid Phase Equilibria*, *557*. https://doi.org/10.1016/j.fluid.2022.113418

Quijano, G., Couvert, A., Amrane, A., Darracq, G., Couriol, C., Le Cloirec, P., Paquin, L., & Carrié, D. (2011a).

Potential of ionic liquids for VOC absorption and biodegradation in multiphase systems. *Chemical Engineering Science*, *66*(12), 2707–2712. https://doi.org/10.1016/j.ces.2011.01.047

Quijano, G., Couvert, A., Amrane, A., Darracq, G., Couriol, C., Le Cloirec, P., Paquin, L., & Carrié, D. (2011b). Toxicity and biodegradability of ionic liquids: New perspectives towards whole-cell biotechnological applications. *Chemical Engineering Journal*, *174*(1), 27–32. https://doi.org/10.1016/j.cej.2011.07.055

Quijano, G., Couvert, A., Amrane, A., Darracq, G., Couriol, C., Le Cloirec, P., Paquin, L., & Carrié, D. (2013). Absorption and biodegradation of hydrophobic volatile organic compounds in ionic liquids. *Water, Air, and Soil Pollution*, *224*(5). https://doi.org/10.1007/s11270-013-1528-y

Radošević, K., Čanak, I., Panić, M., Markov, K., Bubalo, M. C., Frece, J., Srček, V. G., & Redovniković, I. R. (2018). Antimicrobial, cytotoxic and antioxidative evaluation of natural deep eutectic solvents. *Environmental Science and Pollution Research*, *25*(14), 14188–14196. https://doi.org/10.1007/s11356-018-1669-z

Radošević, K., Cvjetko Bubalo, M., Gaurina Srček, V., Grgas, D., Landeka Dragičević, T., & Redovniković, R. I. (2015). Evaluation of toxicity and biodegradability of choline chloride based deep eutectic solvents. *Ecotoxicology and Environmental Safety*, *112*, 46–53. https://doi.org/10.1016/j.ecoenv.2014.09.034

Radošević, K., Železnjak, J., Cvjetko Bubalo, M., Radojčić Redovniković, I., Slivac, I., & Gaurina Srček, V. (2016). Comparative in vitro study of cholinium-based ionic liquids and deep eutectic solvents toward fish cell line. *Ecotoxicology and Environmental Safety*, *131*, 30–36. https://doi.org/10.1016/j.ecoenv.2016.05.005

Revah Sergioand Morgan-Sagastume, J. M. (2005). Methods of Odor and VOC Control. In A. Shareefdeen Zarookand Singh (Ed.), *Biotechnology for Odor and Air Pollution Control* (pp. 29–63). Springer Berlin Heidelberg. https://doi.org/10.1007/3-540-27007-8_3

Rodriguez Castillo, A. S., Biard, P. F., Guihéneuf, S., Paquin, L., Amrane, A., & Couvert, A. (2019). Assessment of VOC absorption in hydrophobic ionic liquids: Measurement of partition and diffusion coefficients and simulation of a packed column. *Chemical Engineering Journal*, *360*(July 2018), 1416–1426. https://doi.org/10.1016/j.cej.2018.10.146

Rodriguez Castillo, A. S., Guihéneuf, S., Biard, P. F., Paquin, L., Amrane, A., & Couvert, A. (2018a). Impact of activated sludge acclimation on the biodegradation of toluene absorbed in a hydrophobic ionic liquid. *International Journal of Environmental Science and Technology*, *15*(3), 621–630. https://doi.org/10.1007/s13762-017-1429-5

Rodriguez Castillo, A. S., Guihéneuf, S., Biard, P. F., Paquin, L., Amrane, A., & Couvert, A. (2018b). Physicochemical properties of some hydrophobic room-temperature ionic liquids applied to volatile organic compounds biodegradation processes. *Journal of Chemical Technology and Biotechnology*, *93*(1), 215–223. https://doi.org/10.1002/jctb.5343

Rodriguez Castillo, A. S., Guihéneuf, S., Le Guével, R., Biard, P. F., Paquin, L., Amrane, A., & Couvert, A. (2016). Synthesis and toxicity evaluation of hydrophobic ionic liquids for volatile organic compounds biodegradation in a two-phase partitioning bioreactor. *Journal of Hazardous Materials*, *307*, 221–230. https://doi.org/10.1016/j.jhazmat.2015.12.043

Romero, A., Santos, A., Tojo, J., & Rodríguez, A. (2008). Toxicity and biodegradability of imidazolium ionic liquids. *Journal of Hazardous Materials*, *151*(1), 268–273. https://doi.org/10.1016/j.jhazmat.2007.10.079

Ruesgas-Ramón, M., Figueroa-Espinoza, M. C., & Durand, E. (2017). Application of Deep Eutectic Solvents (DES) for Phenolic Compounds Extraction: Overview, Challenges, and Opportunities. *Journal of Agricultural and Food Chemistry*, *65*(18), 3591–3601. https://doi.org/10.1021/acs.jafc.7b01054

Shekaari, H., Zafarani-Moattar, M. T., & Mohammadi, B. (2017). Thermophysical characterization of aqueous deep eutectic solvent (choline chloride/urea) solutions in full ranges of concentration at T = (293.15–323.15) K. *Journal of Molecular Liquids*, *243*, 451–461. https://doi.org/10.1016/j.molliq.2017.08.051

Siongco, K. R., Leron, R. B., & Li, M. H. (2013). Densities, refractive indices, and viscosities of N,N-diethylethanol ammonium chloride-glycerol or -ethylene glycol deep eutectic solvents and their aqueous solutions. *Journal of Chemical Thermodynamics*, *65*, 65–72. https://doi.org/10.1016/j.jct.2013.05.041

Skulcova, A., Majova, V., Haz, A., Kreps, F., Russ, A., & Jablonsky, M. (2017). Long-term isothermal stability of deep eutectic solvents based on choline chloride with malonic or lactic or tartaric acid. *International Journal of Scientific & Engineering Research*, *8*(7), 2249–2252.

Song, Y., Chen, S., Luo, F., & Sun, L. (2020). Absorption of Toluene Using Deep Eutectic Solvents: Quantum Chemical Calculations and Experimental Investigation. *Industrial and Engineering Chemistry Research*, *59*(52), 22605–22618. https://doi.org/10.1021/acs.iecr.0c04986

van Osch, D. J. G. P., Zubeir, L. F., van den Bruinhorst, A., Rocha, M. A. A., & Kroon, M. C. (2015). Hydrophobic deep eutectic solvents as water-immiscible extractants. *Green Chem.*, *17*(9), 4518–4521. https://doi.org/10.1039/C5GC01451D

Ventura, S. P. M., e Silva, F. A., Gonçalves, A. M. M., Pereira, J. L., Gonçalves, F., & Coutinho, J. A. P. (2014). Ecotoxicity analysis of cholinium-based ionic liquids to Vibrio fischeri marine bacteria. *Ecotoxicology and Environmental Safety*, *102*(1), 48–54. https://doi.org/10.1016/j.ecoenv.2014.01.003

Wang, W., Ma, X., Grimes, S., Cai, H., & Zhang, M. (2017). Study on the absorbability, regeneration characteristics and thermal stability of ionic liquids for VOCs removal. *Chemical Engineering Journal*, *328*, 353–359. https://doi.org/10.1016/j.cej.2017.06.178

Wen, Q., Chen, J. X., Tang, Y. L., Wang, J., & Yang, Z. (2015). Assessing the toxicity and biodegradability of deep eutectic solvents. *Chemosphere*, *132*, 63–69. https://doi.org/10.1016/j.chemosphere.2015.02.061

Yadav, A., & Pandey, S. (2014). Densities and viscosities of (choline chloride + urea) deep eutectic solvent and its aqueous mixtures in the temperature range 293.15 K to 363.15 K. *Journal of Chemical and Engineering Data*, *59*(7), 2221–2229. https://doi.org/10.1021/je5001796

Yadav, A., Trivedi, S., Rai, R., & Pandey, S. (2014). Densities and dynamic viscosities of (choline chloride+glycerol) deep eutectic solvent and its aqueous mixtures in the temperature range (283.15-363.15)K. *Fluid Phase Equilibria*, *367*, 135–142. https://doi.org/10.1016/j.fluid.2014.01.028

Yu, G., Dai, C., Gao, H., Zhu, R., Du, X., & Lei, Z. (2018). Capturing Condensable Gases with Ionic Liquids. *Industrial and Engineering Chemistry Research*, *57*(36), 12202–12214. https://doi.org/10.1021/acs.iecr.8b02420

Yu, G., Mu, M., Li, J., Wu, B., Xu, R., Liu, N., Chen, B., & Dai, C. (2020). Imidazolium-Based Ionic Liquids Introduced into Ï-Electron Donors: Highly Efficient Toluene Capture. *ACS Sustainable Chemistry and Engineering*, *8*(24), 9058–9069. https://doi.org/10.1021/acssuschemeng.0c02273

Zhang, Q., De Oliveira Vigier, K., Royer, S., & Jérôme, F. (2012). Deep eutectic solvents: Syntheses, properties and applications. In *Chemical Society Reviews* (Vol. 41, Issue 21, pp. 7108–7146). https://doi.org/10.1039/c2cs35178a

Zhang, S., Sun, N., He, X., Lu, X., & Zhang, X. (2006). Physical properties of ionic liquids: Database and evaluation. *Journal of Physical and Chemical Reference Data*, *35*(4), 1475–1517. https://doi.org/10.1063/1.2204959

Zhao, H., Gao, H., Yu, G., Li, Q., & Lei, Z. (2019). Capturing methanol and dimethoxymethane gases with ionic liquids. *Fuel*, *241*(October 2018), 704–714. https://doi.org/10.1016/j.fuel.2018.12.010

Zhou, Z. Bin, Matsumoto, H., & Tatsumi, K. (2004). Low-melting, low-viscous, hydrophobic ionic liquids: 1-Alkyl(alkyl ether)-3-methylimidazolium perfluoroalkyltrifluoroborate. *Chemistry - A European Journal*, *10*(24), 6581–6591. https://doi.org/10.1002/chem.200400533

3. Preparation and physicochemical characterization of deep eutectic solvents and ionic liquids for the potential absorption and biodegradation of styrene vapors

3.1. Abstract

Styrene emissions can be treated by physicochemical, biological, or physicochemical/biological means. Due to its low solubility in water an alternative to eliminate styrene emissions from air is the use of two-phase partitioning bioreactors (TPPBs) which comprised a hydrophobic non-aqueous phase (NAP) which can improve mass transfer of styrene. This study was devoted to prepare and evaluate the main physicochemical characteristics of novel NAPs such as Ionic liquids (ILs), Deep Eutectic Solvents (DESs) and Natural Deep Eutectic Solvents (NADEs) as well as their toxicity and biodegradability to treat styrene vapors. Absorption experiments of styrene showed that the best NAPs were the DESs formed with Tetrabutylammonium bromide and decanoic acid and the ILs [C_6mim][FAP], [C_4mim] [NTf_2] and [C_4mim] [PF_6], since they presented a styrene partition coefficient between 0.0015 and 0.0041. Finally, the IL [C_6mim][FAP] was used as a NAP in a TPPB batch process given its high styrene affinity, low solubility in water and non-biodegradability; styrene mineralization was three times higher in the TPPB compared with the control. ILs are potential adjuvant phases in biological degradation systems, as well as other solvents like DESs and NADESs.

Keywords ILs, DESs, NADESs, styrene, biodegradation

3.2 Graphical abstract

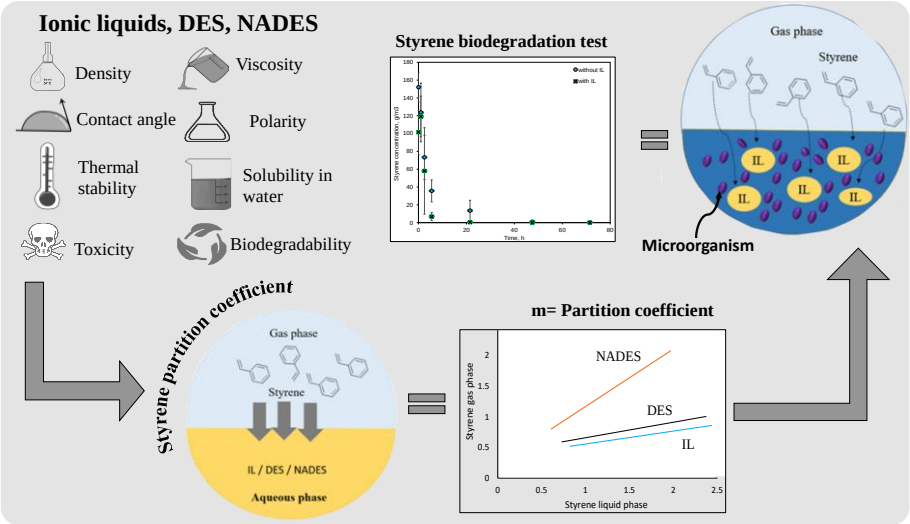

3.3. Statement of environmental implication

Styrene is a volatile organic compound widely used in the production of polystyrene plastics and resins, which is on the Right to Know Hazardous Substance and Special Health Hazard Substance lists. Thus, styrene emissions have to be controlled. In this context, this work aims to address the abatement of styrene through the application of ILs, DESs, and NADESs since they are potential phases to reduce volatile organic compounds (VOC) emissions. The application of such novel phases in partition bioreactors for VOCs abatement was also debated.

3.4. Introduction

Styrene is a volatile organic compound (VOC) boiling under normal pressure at 154 °C, with a solubility of 0.025 g /100 g water at 298 K. This VOC photodegrades in the atmosphere, with a half-life that ranges between 7 and 16 h. Styrene is used primarily to manufacture reinforced plastics, synthetic rubbers, and resins. According to the Toxics Release Inventory (TRI) from EPA in USA, 27,300,032 pounds of atmospheric styrene emissions have been released only in 2020 (EPA, 2022). Furthermore, it has been reported that 20% of styrene production is wasted as emissions and, in the best of scenarios, 60% of styrene emissions are recycled and 40% released to the atmosphere (Tan et al., 2015). Styrene emissions are known to cause serious adverse effects on human health and the environment. The Occupational

Safety and Health Administration (OSHA) reported in 2019 releases of carcinogens to air, that 47 % of the air carcinogen releases corresponded to styrene. On the other hand, the short-term exposure to styrene vapors may lead to respiratory troubles, eye irritation, and gastrointestinal effects, while chronic exposure may affect the central nervous system, causing headache, fatigue, weakness, depression, hearing loss, and peripheral neuropathy (Dimian et al., 2019). Given the wide use of styrene and its health and environmental effects, it is essential to treat its atmospheric emissions. Currently, the treatment of VOC emissions is carried out by several technologies: physical (condensation, membranes, absorption, adsorption), chemical (combustion, corrosion, oxidation) and biological (biofiltration, membrane bioreactors, biological contactors, bioscrubbers and two partition phase bioreactors) (Revah & Morgan-Sagastume, 2005). The main advantage of biological treatment methods is that they can be conducted at ambient temperatures and atmospheric pressure, and that they are easy to operate and ecologically clean, compared with physicochemical treatments. Biotechnologies for VOC emission treatments are based on the capabilities of microbial communities to use the pollutants as single carbon and energy sources resulting in the production of CO_2, H_2O and biomass. However, in the case of hydrophobic gases, like styrene, the main limitation is the low solubility of the gas in the aqueous medium, where microorganisms prevail (Rodriguez Castillo et al., 2016).To overcome such limitation, TPPBs have been proposed. Their principle consists in the absorption of a specific compound in a liquid NAP, which displays a great affinity for the hydrophobic pollutant, and coexists with the aqueous phase containing microorganisms capable to degrade the absorbed VOC (Rodriguez Castillo et al., 2016).The ideal NAP should be biocompatible, non-biodegradable, non-hazardous, have a high affinity for the target VOC, and be immiscible in water, with a low vapor pressure. Most investigated NAPs have been alkanes, perfluorocarbons, silicone oil and solid copolymers. However, the use of these NAPs presents drawbacks such as high volatility and the ability to destroy the ozone layer, as in the case of perfluorocarbons. On the other hand, operational problems have been reported when silicon oil is used, such as foam formation, adhesion to the internal walls of the reactor and emulsification, which leads to the loss of the non-aqueous phase (Muñoz et al., 2007; Muñoz et al., 2012; Quijano et al., 2009). Thus, further exploration of new NAPs is needed. ILs, DESs, and NADESs are standing out as new potential NAPs.

ILs are liquids consisting exclusively of ions. They are molten salts at room temperatures with low vapor pressure, and high thermal stability (decomposition temperatures> 150–200 °C). They remain liquid in a wide temperature range, are non-flammable, can be recycled, and have a wide range of solubilities and miscibilities (hydrophilic or hydrophobic) (Freemantle, 2009). However, ILs present environmental risks as they can be toxic to microorganisms under a range of concentrations. The natural toxicity and environmental persistence of these compounds depend on their composition. The need for a purification step during ILs synthesis is another limitation. On the other hand, DESs and NADESs are commonly prepared by mixing hydrogen bond donors (HBDs) with hydrogen bond acceptors (HBAs) and are classified into five different types (I-V). Types I-IV consist of a mixture of a quaternary ammonium halide (HBA) with an inorganic metal salt or an organic donor of hydrogen bonds (HBD), such as an amide or an alcohol. The inorganic salt or the hydrogen bond donor forms a complex with the halide anion. As a result, the charge on the anion is delocalized and the freezing point of the mixture decreases. Although most DESs are prepared from choline chloride (ChCl) as an ionic species, DESs are not considered ILs because DESs are not composed of only ionic species. Unlike types I-IV, a new type of DESs (type V) does not contain a quaternary ammonium halide as HBA, but is prepared using solely non-ionic precursors (Abranches et al., 2019). Compared to ILs, DESs have advantages such as low price, easy preparation, no purification requirement, and for most of them, good biodegradability, biocompatibility, and lack of toxicity (Muñoz et al., 2012). Like ILs, DESs are solvents that can be designed to have specific physicochemical properties, such as freezing point, viscosity, conductivity, pH, hydrophobicity, and hydrophilicity (Zhang et al., 2012). However, some obstacles for the application of DESs are still present as their viscosity, since most of DESs exhibit relatively high viscosities (35-17645 mPa/s) at room temperature, while ILs present a viscosity range between 15 to 480 mPa/s at ambient temperature (Mallakpour & Dinari, 2012; Marcus, 2016). Also, it must be considered that compared to ILs regeneration of DESs is a huge problem because DESs are mixtures rather than pure compounds, and it is difficult to regenerate the two components conserving their specific ratio, when they are dissolved in other liquid. In contrast, regeneration of ILs is much easier, since the bond between the cation and the anion is strong, thus ILs can be fully recoverable (Chen & Mu, 2021).

When DESs are obtained from natural sources, particularly through primary metabolites such as organic acids, amino acids, and sugars, they are called NADESs. The application of ILs as novel NAPs has been investigated previously in TPPBs (Quijano et al., 2013b; Quijano et al., 2011b; Rodriguez Castillo et al., 2016). Likewise, ILs have been investigated as a physical method to remove VOCs by absorption (Cheng et al., 2009; Quijano et al., 2013b; Quijano et al., 2011a; Wang et al., 2017). Moura et al. (2017) evaluated DESs for the removal by absorption of different VOCs (toluene, acetaldehyde, dichloromethane), also Chen et al., (2021) assessed toluene absorption capacities in hydrophobic DESs based on decanoic acid ([DecA]) with lauric acid ([LauA]), lidocaine, thymol, tetrabutylphosphonium bromide, and 1-octanol utilizing a bubble method. The DES [LauA][DecA] achieved the highest toluene absorption capacity, while being able to maintain such capacity during five consecutive reuse cycles after regeneration by thermal distillation at 80 ◦C, Fahri et al., (2020) prepared two DESs (ChCl/Levulinic acid or ChCl/Lactic acid, molar ratio 1:2) and valuated their affinity for toluene, dichloromethane and methyl ethyl ketone through dimensionless partition coefficient determination. The most efficient DES for the absorption of the three VOCs was ChCl/Levulinic acid (Fahri et al., 2020). Another study (Song et al., 2020) assessed toluene solubility and carried out bubble absorption experiments with tetraethylammonium chloride (TEACl) and oleic acid (OA) in a mole ratio of 1:3. Generally, in the bubble absorption experiments, toluene absorption decreased for higher flow rates and higher temperatures. Regarding absorption of chlorine volatile organic compounds, Makoś-Chełstowska et al., (2021) reported the absorption of five organochlorines (1,1,2,2-tetrachloroethane, 2,2,2-trichloroethanol, dichloromethane, chloroform and carbon tetrachloride) using the DESs formed by the mixture of camphor, guaiacol, syringole, and levulinic acid as absorbents in a bubbling column, and the highest absorption capacities for all compounds tested were obtained with the DES syringole, and levulinic acid in a 1 : 1 molar ratio (Makoś-Chełstowska et al., 2021). Similarly, Chen et al. (2022) tested the acetone solubility in hydrophobic DESs prepared from decanoic acid with two different HBAs (thymol and lauric acid), through the determination of Henry's law constant (Chen et al., 2022).

Currently, there are limited reports about absorption of VOCs with ILs and DESs/NADESs. Therefore, the objective of this study was to explore the use of ILs, DESs and NADESs as potential absorbents of styrene vapors for their application in a TPPBs process. First, the

prepared NAPs were characterized in terms of their physico-chemical properties (i.e., density, viscosity, polarity, contact angle, thermostability, partition coefficient and water solubility). Then, their biodegradability and toxicity towards activated sludge that consumes styrene vapor was evaluated as an example for a biological technique for styrene removal.

3.5. Materials and methods

3.5.1. Reagents

Styrene was purchased from Sigma Aldrich (CAS Number 100-42-5 with a purity ≥99%). The reagent used for the synthesis of 1-butyl-3-methylimidazolium hexafluorophosphate [C_4mim][PF_6], DESs and NADESs were: 1-methylimidazolium, 1-chlorobutane, potassium hexafluorophosphate, choline chloride, tetrabutylammonium bromide, tetrabutylphosphonium bromide, urea, levulinic acid, decanoic acid, 1, 2-propanediol, glucose and xylitol. Choline chloride, tetrabutylammonium bromide and tetrabutylphosphonium bromide were dried at 80 °C for 48 h before use. The ILs (Table 3.1) 1-hexyl-3-methylimidazolium tris(pentafluoroethyl)trifluorophosphate [C_6mim][FAP] (CAS Number 713512-19-7, purity ≥99%) and 1-butyl-3-methylimidazolium bis(trifluoromethylsulfonyl) imide [C_4mim][NTf_2] (CAS Number 174899-83-3, purity ≥99%) were purchased from Merck and Sigma Aldrich, respectively.

3.5.2. DESs and NADESs preparation

The selected DESs, which already exhibited high absorption capacity for VOCs in a previous study, were prepared by mixing the two components in a defined molar ratio (Table 3.2) and were kept at 80 ºC until a homogeneous colorless liquid was obtained (Moura et al., 2017). It can be noted that among the selected DESs, ChCl urea mixed in a 1:2 proportion, in absence of water, is the most historically studied, forming the well-known DES named as Reline (Nolasco et al., 2022).

The selected NADESs, whose potential for solubilisation of hydrophobic compounds has already been reported, were prepared by heating (Dai et al., 2013). In brief, distilled water and two of the listed components in Table 3.2 were mixed to achieve their respective molar ratios. Mixtures, placed in a beaker, were heated below 50 °C, and shaked until a colourless liquid was formed.

3.5.3. Synthesis of 1-butyl-3-methylimidazolium hexafluorophosphate [C_4mim] [PF_6]

Known amounts of 1-methylimidazolium and chlorobutane (1:1.2 molar ratio) were placed in a microwave reactor at 120 °C for 15 min to obtain 1-butyl-3-methylimidazolium chloride [Bmim][Cl]. The formed solution [Bmim][Cl] was dried at 100 mbar at 60 °C for 2 h to remove the excess of chlorobutane. Then, [Bmim][Cl] and KPF_6 were put in a beaker in a molar ratio 1:1.1 with 10 mL of distilled water. The mixture was agitated for 1.5 h until the formation of two phases (the oil phase is [Bmim][PF_6]). Finally, the mixture was washed with 60 mL of distilled water and dried at 90 mbar at 85 °C for 2 h. [C_4mim] [PF_6] was analyzed using ^{1}H Nuclear Magnetic Resonance to corroborate its formation (Yongqing et al., 2011).

Table 3.1 Ionic liquids

Abbreviation	Name
[C_6mim][FAP]	1-hexyl-3-methylimidazolium tris(pentafluoroethyl)trifluorophosphate
[C_4mim][NTF_2]	1-butyl-3-methylimidazolium bis(trifluoromethylsulfonyl) imide
[C_4mim][PF_6]	1-butyl-3-methylimidazolium hexafluorophosphate

Table 3.2 Deep Eutectic Solvents and Natural Deep Eutectic Solvents

	Abbreviation	HBA	HBD		Molar ratio
DES	ChCl: Urea	Choline chloride	Urea		1:2
DES	TBP-Br:Lev	Tetrabutylphosphonium bromide	Levulinic acid		1:6
DES	TBA-Br:Dec	Tetrabutylammonium bromide	Decanoic acid		1:2
NADES	ChCl:PCH	Choline chloride	1,2-propanediol	water	1:1:1
NADES	ChCl:Gluc	Choline chloride	Glucose	water	5:2:5
NADES	ChCl:Xyl	Choline chloride	Xylitol	water	2:1:3

3.5.4. Physicochemical characterization of solvents

3.5.4.1 Density and viscosity

The density of the solvents was measured with a pycnometer. The viscosity was determined with a Cannon-Fenske viscometer using glycerol as reference. All measurements were made at room temperature (20 °C) in triplicate.

3.5.4.2. Thermal stability

The thermal stability was determined through a TGA equipment (Thermo Cahn-Versa Therm High Sensivity thermo−gravimetric analyzer), under nitrogen atmosphere. Samples of 20-40 mg were used. To determine the initial decomposition temperature (T_{onset}), a dynamic mode was used. Experimental conditions were: temperature range from 20 °C to 600 °C until complete thermal degradation of sample, at a heating rate of 10 °C/min.

3.5.4.3. Polarity

Mixtures of 5–10 mL of each IL/DES/NADES and 1 mL of Nile red solution (0.5 mg mL−1 MeOH) was placed into a glass tube, then methanol was removed by evaporation at 70 °C. A Visible absorption spectrum was collected from 400 to 800 nm.

Molar transition energies ($ET_{(NR)}$) were calculated with the following formula (Haraźna et al., 2019):

$ET_{(NR)}$ kcal/mol=$hcv_{max}NA = 28\ 591/ʎ_{max}$

Where;

h= Planck's constant, ($1.58367 * 10^{-37}$, kcal*s)

c= the speed of light, ($2.99792 * 10^{17}$, nm/s)

v_{max}= wave number of maximum absorption, (nm)

NA= Avogadro's number, ($6.02214 * 10^{23}$, mol^{-1})

$ʎ_{max}$ = wavelength of maximum absorption, (nm)

An increase in $ET_{(NR)}$ indicates a decrease in polarity.

3.5.4.4. Contact angle

Contact angle measurements were performed by the contact angle of the IL, DES or NADES droplet (approximately 20 μL) on the surface of a Teflon surface with a goniometer Theta

Lite (Theta Litoptical Tensiometer, Biolin Scientific, USA). The measurements were carried out at room temperature (20°C).

3.5.4.5. Solubility of solvents in water

The aqueous solubility of the ILs was measured at room temperature (20 ºC) and atmospheric pressure in deionized water. Solutions were prepared by adding approximately 1 mL of IL to a sample vial containing 10 mL of aqueous solution (deionized water). The sample vial containing the mixture was shaken vigorously for 3 min to provide a good contact between the phases. After initial liquid–liquid contact, the sample vials were centrifuged for 15 min at 2000 rpm to achieve a good phase separation between the aqueous solution and the IL. Finally, the mixture was aged for 12 h in a water bath and then maintained close to room temperature to allow equilibration before concentration measurements. Since the imidazolium cation has a maximum absorbance at 211 nm, the UV absorbance of the mixtures were measured at 211 nm to determine the concentration of IL in aqueous solution. Blank measurement was performed using deionized water.

The aqueous solubility of the DESs/NADESs were measured following the test No. 105 guideline for the testing chemicals (OECD, 1995).

3.5.5 Toxicity test

Toxicity tests of the NAPs to microorganisms were carried out in serological bottles of 10 mL hermetically covered with mininert Teflon valves®. The bottles had a working liquid volume of 5 mL (mineral medium + inoculum + IL/DES/NADES + glucose). The IL proportion was 2, 4, 6, 8 and 10 % v/v, except in the case of DES TBA-Br:Dec, in which the concentrations evaluated were 36, 40, 45 and 50% v/v. Glucose was added at a concentration of 1 g/L. Activated sludge from a wastewater treatment plant (Parque Tangamanga I San Luis Potosí, S.L.P., Mexico) was used as inoculum. The mineral medium used was composed of: (g/L) $NaNO_3$, 6; KH_2PO_4, 3; $CaSO_4.2H_2O$ 0.25; $MgSO_4.7H_2O$, 0.38; $CaCl_2$, 0.055; and trace elements $FeSO_4.7H_2O$, 0.015; $MnSO_4.H_2O$, 0.012; $ZnSO_4.7H_2O$, 0.013; $CuSO_4.7H_2O$, 0.0023; $CoCl_2.6H_2O$, 0.0015; H_3BO_3, 0.0015. The pH of the mineral medium was adjusted to 7.

The bottles were incubated at 30 °C for 24 h and 150 rpm. After 24 h, the samples were centrifuged at 3500 rpm for 5 min and passed through a 0.4 μm filter. Then, glucose

concentration of the supernatant was measured using the phenol-sulfuric method, except for the NADES ChCl: Glc. For the NADES ChCl: Glc, the CO_2 concentration was measured in the gas phase, due to the presence of glucose as HBD in the structure of this NAP.

Experiments without the solvents were run, as well as endogenous respiration control experiments. All the experiments were carried out in triplicate. At the end, the percentage of glucose uptake *vs* the solvent concentration was plotted, and the half maximal effective concentration (EC_{50}) value was obtained with the analysis [Inhibitor] vs. normalized response -- Variable slope performed using GraphPad Prism version 9.2.0 for Windows, GraphPad Software. The statistical differences of glucose uptake (%) between solvents and control in the toxicity test were determined by ANOVA and Tukey test. Differences were considered significant at $p < 0.05$. All statistical analyses were carried out using R studio 2021.09.0.

3.5.6 Biodegradability test

The biodegradability assay was performed using serological bottles of 10 mL with a working liquid volume of 5 mL (mineral medium + inoculum + IL / DES / NADES). The proportion of IL /DES/NADES was 5 % v/v, except for DES TBA-Br: Dec (36 % v/v). The inoculum and the mineral medium used were the same as above described. The bottles were kept at 30 °C and 150 rpm. The consumption of the NAPs was measured through the chemical oxygen demand determination in the aqueous phase for 30 days. Also, the concentration of CO_2 was measured by gas chromatography in the gas phase for the same period. The experiments were carried out in triplicate.

3.5.7 Partition coefficient

Tests were carried out in 20 mL serological bottles closed with mininert Teflon valves® and 0.5 mL of NAP. Different amounts of styrene (1, 4, 7, 10 µL) were injected. The bottles were incubated at 28 °C and 140 rpm. To ensure that gas-liquid equilibrium has been reached, a sufficient time of incubation of 72 h was given before measurement of styrene gas phase concentration by gas chromatography. The selected time of 72 h has been commonly used in literature for determination of gas-liquid partition coefficients (Alonso-Campos et al., 2021; Bocquet et al., 2006; Dupuy et al., 2011; Rodriguez Castillo et al., 2019; Souchon et al., 2004). Even though this lapse of time gives very convenient margin to ensure that the equilibrium is achieved, it is not the minimum time required, and we can find reports waiting 24 and 48 h to reach equilibrium (Moura et al., 2017; Quijano et al., 2011a).

Styrene concentration in the liquid medium was calculated by subtracting the amount of styrene in the gas phase at equilibrium from the initially added styrene in the headspace. Partition coefficient is determined with the slope of curve of styrene concentration in the liquid phase versus styrene concentration in the gas phase.

CO_2 partition coefficient for the IL [C_6mim][FAP] were carried out in 10 mL serological bottles closed with mininert Teflon valves® and 0.5 mL of NAP. Different volumes (2,4, 6, 8 and 10 mL) of a gas mixture of N_2/CO_2 (80:20) were injected and followed the same procedure for styrene partition coefficient.

3.5.8 Styrene biodegradation test

Biodegradation test was performed for the IL [C_6mim][FAP] in 20 mL serological bottles closed with mininert Teflon valves®. The bottles had 10 mL of working liquid volume (mineral medium + inoculum + 5% v/v of IL). Inoculum and mineral medium were the same as described above. The bottles were injected with 1.5 µL of styrene and incubated at 30 °C and 150 rpm. CO_2 concentration in the gas phase was measured by gas chromatography for 3 days. Experiments without the IL were run, as well as endogenous respiration control experiments. The percentage of mineralization was calculated considering the ratio of the amount of CO_2 produced upon the theoretical maximum CO_2 achievable in case of complete stoichiometric oxidation of styrene carbon. The endogenous respiration (corresponding to a blank without styrene) was subtracted from the CO_2 observed. In presence of the IL, CO_2 present in the NAP was considered on the basis of the CO_2 partition coefficient previously determined.

At the end, the CO_2 in the gaseous phase *vs* time was plotted, and the results were analyzed with the Gompertz sigmoidal model.

$$H(t)=H_{max}*\exp\{-\exp[R/H_{max}(\lambda-t)+1]\} \quad \text{(Equation 1)}$$

where:

H (t): CO_2 produced through time (g/m^3)

H_{max}: Maximum CO_2 produced (g/m^3).

R: CO_2 rate production (g/m^3*h).

λ: lag phase (h).

3.5.9 Analytical methods

Styrene concentration was measured with a Gas Chromatograph (GC-Thermo Scientific TRACE 1300) equipped with a BD-624 intermediate polarity column and a flame ionization detector (FID). Nitrogen was used as the carrier gas at 3.5 mL/min and an operating pressure of 28.4 kPa. The operating temperatures for the FID are 180, 100, and 180 °C for the injector, column, and detector, respectively.

CO_2 concentration was quantified using a gas chromatograph equipped with a Hayesep D column and a thermal conductivity detector (GC, 6890N Network GC System, Agilent Technologies, Waldbronn, Germany) using nitrogen as carrier gas, with an injection port, oven and detector temperature of 250 °C, 60 °C and 250 °C, respectively.

3.6. Results and discussion

3.6.1. Physicochemical properties

3.6.1.1. Identification of 1-butyl-3-methylimidazolium hexafluorophosphate [C_4mim][PF_6] by ^{1}H RMN

The spectrum of [C_4mim][PF_6] (CDCl3, ppm) obtained by ^{1}H nuclear magnetic resonance (Fig. 3.1) showed the following peaks: δ 0.991 (triplet), 1.412 (sextet), 1.889 (quintet), 3.996 (singlet), 4.188 (triplet), 7.247 (singlet), 7.266 (singlet) and 8.636 (singlet). Those peaks corroborate the formation of the IL desired and agree with the peaks obtained by (Yongqing et al., 2011) for the same IL.

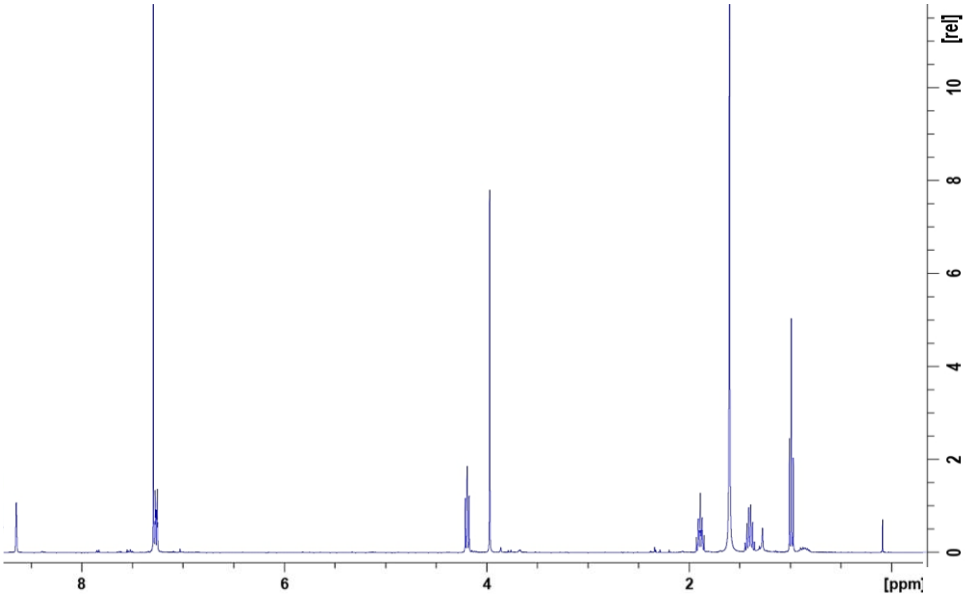

Fig. 3.1 $[C_4mim][PF_6]$ ^1H RMN spectrum using deuterated chloroform as solvent

3.6.1.2. Density and viscosity

To select the proper NAP in a TPPB process, it is important to know their physico-chemical properties (i.e., density, viscosity, etc.). Thus, it is of interest to select a NAP that has a different density than water to allow its recovery. Moreover, in the industrial scale, the density must be considered in the designs for storage systems and packaging. The densities measured experimentally of ILs, DESs, and NADESs at 20 °C were reported in Table 3.3. The densities of these solvents are higher than that of water, except for TBA-Br:Dec that has a density of 0.955 g/mL. Different studies have indicated that ILs, DESs and NADESs density values range from 0.88 to 1.6 g/cm^3 (Dietz et al., 2017; Ghaedi et al., 2017).

Different studies noticed that the densities are related to the molar masses of the ions, with ILs with heavy atoms being in general denser. Thus, the density of ILs increases with the molar mass of the anion in the approximate order $[BF_4]^-$ < $[OTf]^-$ < $[PF_6]^-$ < $[NTf_2]^-$ < [FAP]- (Jacquemin et al., 2006), which is reflected in Table 3.3, where IL with the heaviest anion ($[FAP]^-$ molar mass=445.01 g/mol) showed the highest density (1.53 g/cm^3) and the IL with the lowest molar mass anion ($[PF_6]^-$ molar mass=144.96 g/mol) showed the lowest density (1.13 g/cm^3).

The viscosity values obtained for the NAPs are shown in Table 3.3. The dynamic viscosity values for ILs ranged between 76.9 and 357.1 mPa*s, while the viscosities obtained for DESs

and NADESs ranged from 114.5 to 3451.3 mPa*s. The values reported for ILs range between 15-480 mPa, while most of the viscosities reported for DESs present values from 35 to 17645 mPa*s, at room temperature (Marcus, 2016). The viscosity of ILs is determined by their tendency to form hydrogen bonds and by the strength of electrostatic forces and Van der Waals interactions. ILs formed by anions with the capacity to generate hydrogen bonds, especially fluorinated anions will be viscous. In ILs with imidazole cations, the viscosity will increase with increase of alkyl chain, due to stronger Van der Waals interactions. Likewise, the symmetry of the anion can influence the viscosity. When the anion presents an irregular shape ($[(CF_3SO_2)\ (CF_3CO)\ N]^-$ and $[NTf_2]^-$), it tends to form ILs of low viscosity, and anions with high symmetry ($[BF_4]^-$, $[PF_6]^-$) can result in high viscosity salts (Huddleston et al., 2001). This is in accordance with our results, since the IL with anion $[NTf_2]^-$ showed the lowest viscosity, and the IL with the anion $[PF_6]^-$ presented a higher value of viscosity.

In the case of DESs and NADESs, the high viscosity is the result of a lower mobility of the molecules within DESs / NADESs, due to the extensive network of hydrogen bonds between each component. Electrostatic Van der Waals interactions also affect the viscosity of DESs and NADESs (Dietz et al., 2017). The viscosity of DESs / NADESs can also be explained by the "theory of holes"; in this theory, the viscosity is correlated with the availability of holes in the fluid that allows adequate molecule movement. Thus, viscosity is controlled primarily by volumetric factors, despite the strong intermolecular interactions developed in these systems.

The viscosity of the NAPs is an important factor to consider, since, at industrial scale, viscosity can alter the mass transport properties and affect stirring, mixing, and pumping operations. High viscosities can significantly affect rates of mass transfer and power requirements for mixing in aqueous systems.

3.6.1.3. Polarity

Polarity can be explained as the intermolecular interactions between solvent and solute that do not lead to chemical reactions. An empirical polarity parameter has been described by observing the effect of a solvent on a solvent-dependent process. Such parameter has been obtained by the rate of a chemical reaction or the absorption of light by a solvatochromic dye. Solvatochromism describes the change in UV-visible absorption spectra in molecules

such as Reichardt's betaine dye, Nile red, or phenol blue. The Nile red polar parameter (E_{RN}) has been used to represent the polarity of ILs, DESs and NADESs, as well as to evaluate whether there is any dependence of the styrene partition coefficient with polarity.

As can be seen in Table 3.3, the $ET_{(RN)}$ values found for the evaluated solvents varied between 49.2 and 53.3 kcal / mol. An increase in the $ET_{(RN)}$ value indicates a decrease in polarity, thus, the less polar solvent was the DES ChCl:glucose followed by IL [C_4mim] [PF_6] with values of 53.3 and 52.7 kcal / mol, respectively.

Regarding ILs, it has been reported that those containing the cation [C_4mim], see their polarity decrease with increasing size of the anion (Carmichael & Seddon, 2000). Such observation was not consistent with this work, since ILs ([C_4mim] [PF_6] and [C_4mim] [NTf_2]) presented $ET_{(RN)}$ values of 52.7 and 52.4 kcal / mol, respectively. On the other hand, Carmichael & Seddon, (2000) indicated that for ILs with 1-alkyl-3-methylimidazolium, the polarity is determined by the anion containing short 1-alkyl groups and by the cation containing 1-long alkyl (Carmichael & Seddon, 2000). Fletcher et al. (2001) suggested that Nile red experiences a microenvironment within [C_4mim] [PF_6], finding a similar to fairly polar behavior as water. They explained this because the $ET_{(RN)}$ value for [C_4mim] [PF_6] was similar to the one of pure water (48.17 kcal / mol) (Fletcher et al., 2001).

The DESs and NADESs formed with ChCl and sugar or alcohols remained in a range of 49.2 to 53.3 kcal / mol (Table 3.3), which is comparable to the $ET_{(RN)}$ values reported by Mulia et al. (2019), who evaluated DESs formed with ChCl and different polyalcohols, where the most polar DESs contained ethylene glycol as HBD (47.4 kcal / mol), and the least polar DES contained 1,4-butanediol as HBD (60.6 kcal / mol) (Mulia et al., 2019).

Since it is intended to link those physicochemical characteristics with the ability to absorb VOCs, specifically styrene, the $ET_{(NR)}$ value of styrene was also obtained, giving a value of 64.2 kcal / mol. Also, a correlation coefficient was calculated in order to verify if there is some association between the styrene partition coefficient and the polarity. However, no direct correlation was found between the $ET_{(NR)}$ values of the NAPs and their partition coefficient with styrene ($R^2 = 0.1750$).

3.6.1.4. Contact angle

Contact angle measurement is a tool to characterize properties like wettability and adhesion of a surface or probing liquid–solid interactions. The use of water as a probing liquid is very common, and surfaces with large water contact angles are highly hydrophobic. Teflon (PTFE), which has a highly hydrophobic surface, presents a water contact angle of 112-117°. A low contact angle of a liquid on a hydrophobic surface indicates an increase in the wetting ability of this surface and a more hydrophobic character of the liquid. The wetting angles with a Teflon surface of the 9 NAPs were determined and their values varied between 63.1° and 136.9° (Table 3.3). Low values of contact angle reveal a more hydrophobic character; thus, the trend of the solvents regarding their hydrophobic character is: [C_6mim] [FAP] >TBA-Br:Dec>TBP-Br:Lev> [C_4mim] [NTf_2] > ChCl: PCH > [C_4mim][PF_6] >Cl-Ch: Urea >ChCl: Xil >ChCl: Gluc.

In the same way, as with the polarity parameter, presence of correlation between the contact angle and the partition coefficient value was verified. A correlation coefficient of $R^2 = 0.7185$ was obtained indicating a better correlation than with polarity. In other words, 72% of the variation in the partition coefficient of styrene is explained by the hydrophobic character of the solvents.

3.6.1.5. Solubility in water

The aqueous solubility and stability data are valuable information for process design. ILs, DESs and NADESs are promising solvents for different applications; however, there is still concern especially when using ILs because of the problem of their recovery. In absence of recovery, economic problems due to high cost of ILs and environmental problems due to their toxicity can arise. ILs are non-volatile, thus the only way for them to be lost in the environment is in a wastewater stream, increasing the potential threat to the aquatic environment and organisms living there, as well as diminishing the recovery of the ionic liquid as NAP (Chen & Mu, 2021; Wong et al., 2002)

Likewise, it is important to evaluate the stability of DESs in aqueous phase, since the decomposition of ChCl:phenol DESs in aqueous phase has been reported (Shishov et al., 2020).

Experiments of solubility in water were carried out systematically for all NAPs, even though the selected ILs for this work are classified as immiscible in water. Actually, the results (Table 3.3) indicated that ILs presented some water solubility, with [C_6mim] [FAP] having the lowest solubility in water (0.38 g / L), and [C_4mim] [NTf_2] being almost 3 times more soluble in water (1.12 g / L). On the other hand, [C_4mim] [PF_6] was 1.8 times more soluble in water than [C_6mim] [FAP]. The lower solubility is explained by the hydrophobicity of the anions $[FAP]^-$ since they prevent H_2O from joining the IL and dissociating them into ion pairs (Ma et al., 2018).

According to the test guide No. 105 for Test Chemicals (OECD, 1995), results indicated that all DESs / NADESs (except TBA-Br: Dec) are miscible in water with a solubility >1000 g/L, since formation of two phases was not observed when adding water to a fixed amount of solvent. However, in the case of DES TBA-Br: Dec, the formation of two phases was noted. Also, the formation of crystals was observed at a concentration lower than 36% (v / v) of DES, indicating the breaking of hydrogen bonds between tetrabutylammonium bromide (TBA-Br) and decanoic acid and therefore the disappearance of the DES.

3.6.1.6. Thermal stability

Thermal stability analysis of the solvents allows us to determine the scope of its application since these parameters determine the temperature range in which a solvent can maintain its liquid form and the beginning of thermal decomposition.

The decomposition temperature of the NAPs is presented in Table 3.3. Among the three ILs, [C_4mim] [PF_6] is the less stable with a T_{onset} of 192 °C. On the other hand, the most stable IL is [C_4mim] [NTf_2] with a T_{onset} of 317 °C. According to literature, the thermal stability for many ILs is generally >300°C. For instance, the family of 1-alkyl-3-methylimidazolium bis(trifluoromethylsulfonyl)imide [C_nMIM][NTf_2] (n=2–8) remains stable up to 326.85 °C (Zhang et al., 2006a).

For DESs, initial decomposition temperature varies from 119 °C to 208 °C, which is consistent with previous reports where it was indicated that the thermal decomposition of mixtures of DESs at 0% water content begins around 125- 200 ºC (Delgado-Mellado et al., 2018; Dietz et al., 2017). In the cases of DES TBP-Br: Lev and NADES ChCl: 1,2-propanediol, two degradation steps are observed, where the first corresponds to the

decomposition temperature of HBD (Levulinic acid and 1, 2 propanediol) and the second belongs to the decomposition temperature of the ammonium salt (choline chloride and tetrabutylphosphonium bromide). Finally, the initial loss of mass observed at 100 °C in the NADESs corresponds to water added at the beginning, while DESs and ILs presented the same loss due to the hygroscopic nature of the solvents.

3.5.10 Toxicity test

Toxicity is defined as a molecular sequence of events from the absorption of an effective dose to the production of a specific biological response. A toxic mode of action is a set of physiological and behavioral signs that characterize an adverse biological response. Common measures of toxicity include the half maximal effective concentration (EC_{50}), which refers to the concentration which induces a response halfway between the baseline and the maximum after a specified exposure time. Table 3.4 shows the EC_{50} values obtained for ILs, DESs and NADESs.

In this study, glucose consumption by activated sludge was evaluated as a biological response in the presence of different solvents at different concentrations at a certain time (24 h), to verify if there is an adverse biological response to them. The glucose consumption at 24 h by activated sludge at different concentrations of the solvents as well as the final pH of the experiment is shown in Fig. 3.2. In the case of ILs, it is observed that in the presence of [C_6mim] [FAP] there is no inhibitory effect on glucose consumption by activated sludge, since this consumption remains between 96.5 and 99.6 % at the different concentrations of IL tested (2, 4, 6, 8 and 10% v/v) and the final pH measured indicates a slight decrease from the initial pH (7) with values between 6.5-6.9.

Table 3.3 Physicochemical characteristics of the IL, DES and NADES evaluated in this work.

	Solvent	Density*, g/cm^3	Kinematic viscosity*, cSt	Dynamic viscosity*, mPa*s	Polarity*, $ET_{(NR)}$ kcal/mol	Contact angle*	Solubility in water* (g/L)	T_{onset}, 4. °C
IL	[C_6mim][FAP]	1.53 ± 0.01	93.6 ± 1.0	145.8 ± 1.6	51.5 ± 0.1	63.1 ± 4.4	0.38 ± 0.27	290.87
IL	[C_4mim][NTF_2]	1.41 ± 0.02	54.4 ± 0.3	76.9 ± 0.4	52.4 ± 0.1	82.5 ± 7.1	1.12 ± 0.32	317.19
IL	[C_4mim][PF_6]	1.13 ± 0.06	316.9 ± 4.5	357.1 ± 5.1	52.7 ± 0.1	101.2 ± 2.3	0.72 ± 0.17	192.99
DES	Ch-Cl: Urea	1.17 ± 0.01	1377.2 ± 25	1618.3 ± 30	50.2 ± 0.1	128.3 ± 3.1	>1000	134.53
DES	TBP-Br:Lev	1.09 ± 0.01	108.2 ± 0.7	118.2 ± 0.8	49.2 ± 0.2	80.4 ± 2.2	>1000	118.95, 322.34
DES	TBA-Br:Dec	0.95 ± 0.01	573.9 ± 31	548.0 ± 30.0	51.4 ± 0.1	72.7 ± 6.7	<1**	126.71
NADES	ChCl: PCH	1.08 ± 0.02	106.4 ± 1.5	114.5 ± 1.6	50.2 ± 0.1	97.2 ± 2.3	>1000	134.03, 240.03
NADES	ChCl: Gluc	1.41 ± 0.02	2442.6 ± 319	3451.3 ± 451.4	53.3 ± 0.1	136.9 ± 6.9	>1000	154.45
NADES	ChCl: Xyl	1.17 ± 0.01	342.2 ± 2.8	400.3 ± 3.3	50.4 ± 0.1	129.7 ± 1.1	>1000	207.88

*Determination performed at room temperature (20 ºC)

**Stable in water above 36% v/v

While the IL [C_4mim] [NTf_2] causes a decrease of 14 to 16% in glucose consumption in concentrations higher than 6% v/v compared to the control (without IL), this could be explained by the decrease in pH, since at concentrations of 8 and 10% the final pH measured was 5.7 and 5.1, respectively. The IL [C_4mim][PF_6] reduces glucose consumption by 38% at a concentration of 2% v/v and causes an inhibition in glucose consumption of 80% to 99% at concentrations of 4 to 10% v/v.

Regarding ILs, [C_6mim][FAP] and [C_4mim][NTF_2], at all concentrations tested, showed no significant differences compared with the control, while [C_4mim][PF_6] showed significant differences at all tested concentrations compared with the control. Between ILs, [C_4mim][PF_6] also showed significant differences compared with the other two ILs [C_6mim][FAP] and [C_4mim][NTF_2], while between these two ILs there was no significant difference.

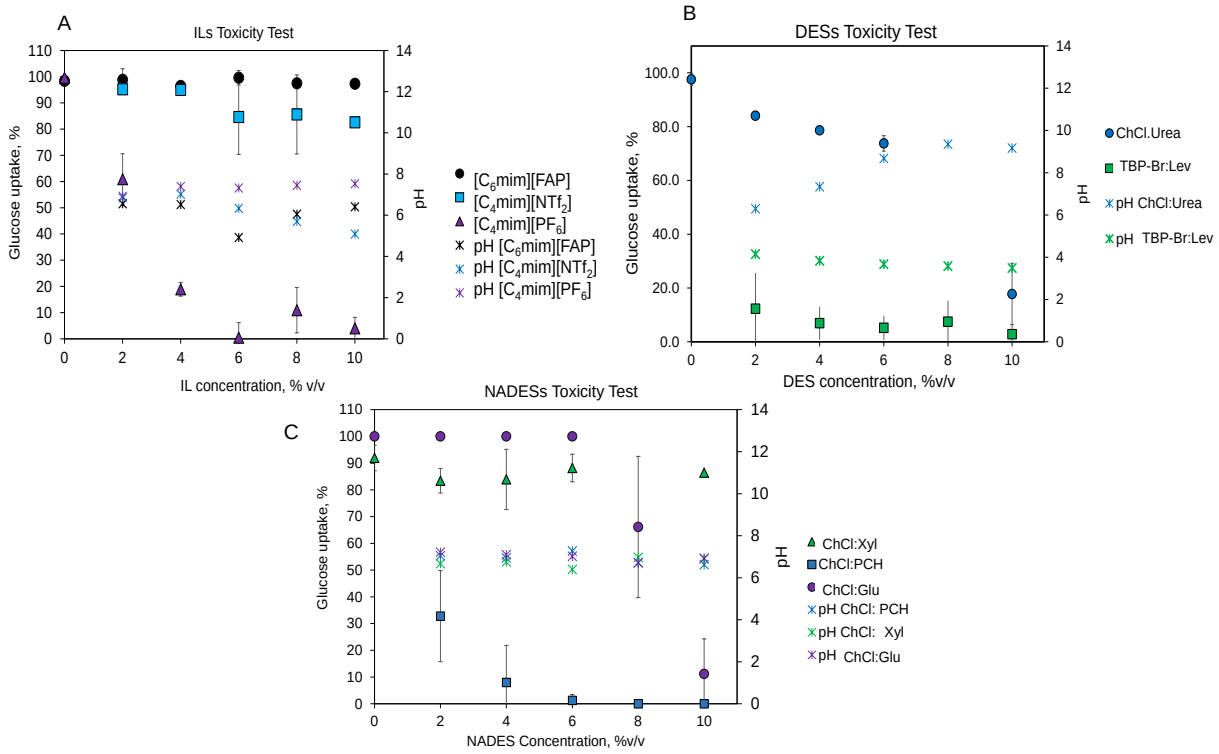

Fig. 3.2 Percentage of glucose consumed by activated sludge at different A) ILs B) DESs or C) NADESs concentrations (%) at 24 h

The presence of DES ChCl: Urea at concentrations of 2-6% v/v showed a glucose consumption of 15-26% lower than the control, while a concentration of 10% v/v of ChCl:Urea reduces glucose consumption by activated sludge up to 82% compared to the control (without DES), at concentrations above 6% the environmental pH significantly increased up to 9.1, which resulted in greater toxicity to bacteria. The DES TBP-Br:Lev at a concentration of 2% v/v showed an inhibition in glucose consumption of 87% and up to 95% in concentrations equal to or greater than 4% v/v. When the added DES is TBA-Br: Dec inhibits 100% of glucose consumption by activated sludge at all tested concentrations (Fig. 3.3). In the case of the DESs with organic acids the final pH was severely diminished from the initial pH 7 to 2.8 when decanoic acid was the HBD and a decreased from pH 7 to 4.15 when levulinic acid was the HBD, thus when organic acid is used as HBD, such pH values are far below the optimal for bacterial growth (6.5-7.5), also acid HBDs could inactivate cells by denaturing proteins located on the cell wall, resulting in loss of cell activity and death (Zhao et al., 2015). Thus, toxicity tests indicated that the control of pH is crucial when DESs are applied in continuous TPPBs. For DESs, the final pH of the toxicity experiments was function of the type of hydrogen bond acceptor or donor used to prepare these phases, as it was demonstrated, ammonium salts tended to increase the pH of the medium and by the contrary organic acids decrease the pH of the solution. In addition, the continuous biodegradation of DESs in the toxicity experiments can provoke changes in the DESs:water ratio which is a key parameter to maintain these NAP phases stable, as they can be destabilized or lost in the medium. Thus, when using DESs in TPPBs the DESs:water ratio should be maintained constant by the continuous addition of these DESs into the medium like a reloading process to reconstitute the losses due to the biodegradation of these phases during the process. For ILs and NADEs, the slight change in the final pH in the toxicity tests indicated that pH can be controlled easily when TPPBs are used. When the added NADES is ChCl: Xylitol, the glucose consumption remained above 80% in all the concentrations tested. On the other hand, when ChCl: PCH at 2% v/v was tested, an inhibition of 64% in the consumption of glucose was shown; and at concentrations of 4% to 10% v/v, the inhibition of glucose consumption varied from 91 to 100%. For ChCl:Glc in concentrations of 2 to 6% v/v the glucose uptake by the activated sludge remained close to 100% and for concentrations of 8 and 10% v/v the glucose consumption decreased up to 66 and 11%, respectively. For all

the NADESs tested the pH remain between 6.5-7.2 thus the toxic effect cannot be attributed to a change in the pH environment, but directly to the nature of the HBD, and to the hydrogen bonding between the mixture compounds that increase the toxicity through the respective charge delocalization, since chemicals having delocalized charges are more toxic than chemicals with localized charges (Wen et al., 2015).

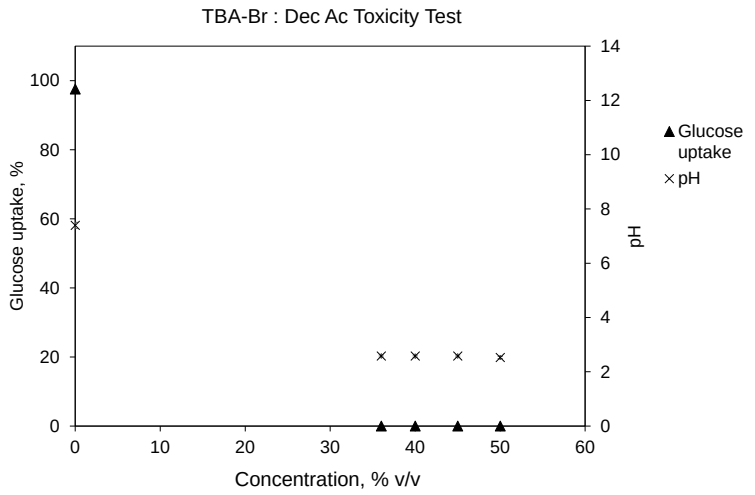

Fig. 3.3 Percentage of glucose consumed by activated sludge at different TBA-Br:Dec Ac DES concentrations (%) at 24 h

For glucose uptake using NADESs as a NAP, ChCl: Gluc (8-10 %v/v) and ChCl:PCH (at all tested concentrations) showed significant differences compared to the control. Regarding ChCl:Gluc (2-8 %v/v) and ChCl:Xyl (2-10 %v/v) no significant differences were observed, as well as between ChCl:Gluc (10 %v/v) and ChCl:PCH (2-10 % v/v).Table 3.4 shows the IC_{50} values obtained for some of the ILs, DESs and NADESs. The IC_{50} calculation for the solvents were carried out only for the solvents which presented a percentage of inhibition in glucose consumption by activated sludge greater than 50%. Therefore, solvents with relatively lower toxicity are not presented in Table 3.4 ($[C_4mim][NFT_2]$, $[C_6min][FAP]$, ChCl: Xyl), as well as the DES TBA-Br: Dec, which IC_{50} could not be determined due to its 100% toxicity at the lowest tested concentration.

Among Table 3.4 solvents, the most toxic was the DES TBP-Br: Lev, with a IC_{50} (0.123% v/v) and the least toxic was the NADES ChCl:Gluc with an IC_{50} of 8.45% v/v.

Different studies have reported the toxicity effect of various ILs to activated sludge (Quijano et al., 2011a, 2011b; Rodriguez Castillo et al., 2016). Such studies have also tested toxicity

through glucose consumption. For instance, when 10% (v/v) of [C_4mim][PF_6] and [C_4mim][NTf_2] were tested, a decrease in the metabolic activity of microorganisms (-30%) was observed, so a concentration of 5% (v/v) was considered non-toxic for microbial metabolism.

DESs or NADESs toxicity has been assessed through different methods and towards different microorganisms. For example, choline-based DESs with different HBDs (urea, acetamide, glycerol and ethylene glycol) were tested towards *Escherichia coli* (Wen et al., 2015). A severe effect on the growth of *Escherichia coli* was found at high concentrations (0.75 M) of DESs compared to low concentrations (0.075 M), finding an inhibition index of 93% at high concentration, and an inhibition index <10% at low concentrations. Another study evaluated the toxicity of DESs based on the HBA ChCl with different organic acids, as HBDs (acetic, lactic, glycolic and citric) at different molar ratios using a Microtox test, which consisted in measuring the inhibition by the luminescence of the marine bacteria *Vibrio fischer*i [43]. They found the next pattern of toxicity: ChCl:acid (2:1) < ChCl:acid (1:1) < ChCl Cl:acid (1:2), where a higher content of acid in the DESs led to a higher toxic effect toward the bacteria. Likewise, choline-based DESs has been evaluated with different HBDs (amine, alcohol, sugars and organic acids) through disk diffusion susceptibility test and growth inhibition towards two Gram-positive (*Staphylococcus aureus* and *Listeria monocytogenes*) and two Gram-negative (*Escherichia coli* and *Salmonella enteritidis*) bacteria (Zhao et al., 2015). The authors reported that only the DESs formed with organic acids presented a significant inhibitory effect on bacterial growth; however, amine-, alcohol- and sugar-based DESs did not inhibit bacterial growth. Regarding NADESs, Radošević et al. (2018) evaluated the antimicrobial activity of NADESs formed with choline chloride and different HBDs (oxalic acid, urea, xylitol and sorbitol) using a disk diffusion method towards Gram-positive bacteria (*Staphylococcus aureus*), and Gram-negative bacteria (*Escherichia coli*, *Proteus mirabilis, Salmonella typhimurium, Pseudomonas aeruginosa*), finding that only NADESs formed with oxalic acid inhibited the growth of all the tested microorganisms (Radošević et al., 2018). On the other hand, the toxicity of different choline chloride and glycerol-based NADESs at different ratios of hydrogen bond acceptor to HBDs (alcohols, sugars, or amino acids) was evaluated towards two Gram-positive and two Gram-negative bacteria, finding that only the NADESs with glycerol and arginine presented an inhibitory effect over all the

strains evaluated. They concluded that choline chloride- and glycerol- based NADESs, generally are benign solvents (Yao et al., 2017).

Even if it is not possible to make a direct comparison with our results we can relate some conclusions; like organic acid-based DESs or NADESs presented a more drastic effect over the growth or function of bacteria than those formed with sugar, alcohols or amines. This can be attributed to the pH value, which can be out of the threshold for optimal bacterial growth (6.5-7.5) (Zhao et al., 2015). It is also worth mentioning that in aqueous solution, the DESs may be partially dissociated, leading to the cholinium cation interacting with the cell wall through H-bonding or electrostatic interaction, and thus leading to cell wall distortion or disruption (De Morais et al., 2015; Wen et al., 2015).

Table 3.4 EC_{50} values obtained for some ILs, DESs and NADESs

Solvent	**IC_{50}, %v/v**	**R^2**
$[C_4mim][PF_6]$	2.345	0.9709
Cl-Ch: Urea	7.098	0.8635
TBP-Br:Lev	0.123	0.9686
ClCh: PCH	1.541	0.9338
ClCh: Gluc	8.448	0.9181

3.6.2 Biodegradability test

The results of the biodegradability tests of the different NAPs studied is shown in Fig. 3.4. All solvents had an initial concentration of 5% v/v, except for DES TBA-Br: Dec. which had a concentration of 36% v/v. The three ILs evaluated did not show CO_2 production after 30 days of incubation at 30 °C and 150 rpm in the dark.

Regarding DES, TBP-Br: Lev and TBA-Br: Dec DES did not show a CO_2 production in the 15 days of incubation. On the other hand, DES ChCl:urea and the NADESs showed an increase in CO_2 production, keeping CO_2 constant after 7 days of incubation.

According to the Test No. 301 of the OECD Guidelines for the Test of Chemical Substances (OECD, 1992), a chemical is considered readily biodegradable once 70% of the dissolved

organic carbon (DOC) is removed and 60% of the CO_2 is produced by respirometry methods in 10 days in a 28-day aerobic test under dark conditions. Thus, the three ILs and two of the DESs (DES: TBP-Br: Lev ac and TBA-Br: Dec) are considered not easily biodegradable, while the DES ChCl:urea and the three NADESs tested can be considered easily biodegradable.

The obtained results for ILs correspond to those reported in the literature. Different authors outlined that there is no biodegradation of ILs formed with 1-n-butyl-3-methylimidazolium (C_4mim) ([C_4mim] [Cl], [C_4mim] [Tf_2N], ([C_4mim] [Br], [C_4mim] [BF_4], ([C_4mim] [PF_6]) in 30-day long-term biodegradability assays (Gathergood et al., 2004; Quijano et al., 2011b). In the same way, for DESs and NADESs, it has been reported that DESs formed with choline salts such as choline chloride with different HBDs, such as urea, glucose, oxalic acid or glycerol, are easily biodegradable (Juneidi et al., 2015; Radošević et al., 2015; Wen et al., 2015). The present study confirms this trend, indicating that ChCl:urea, ChCl:Glc, ChCl:Xyl and ChCl:PCH are also easily biodegradable.

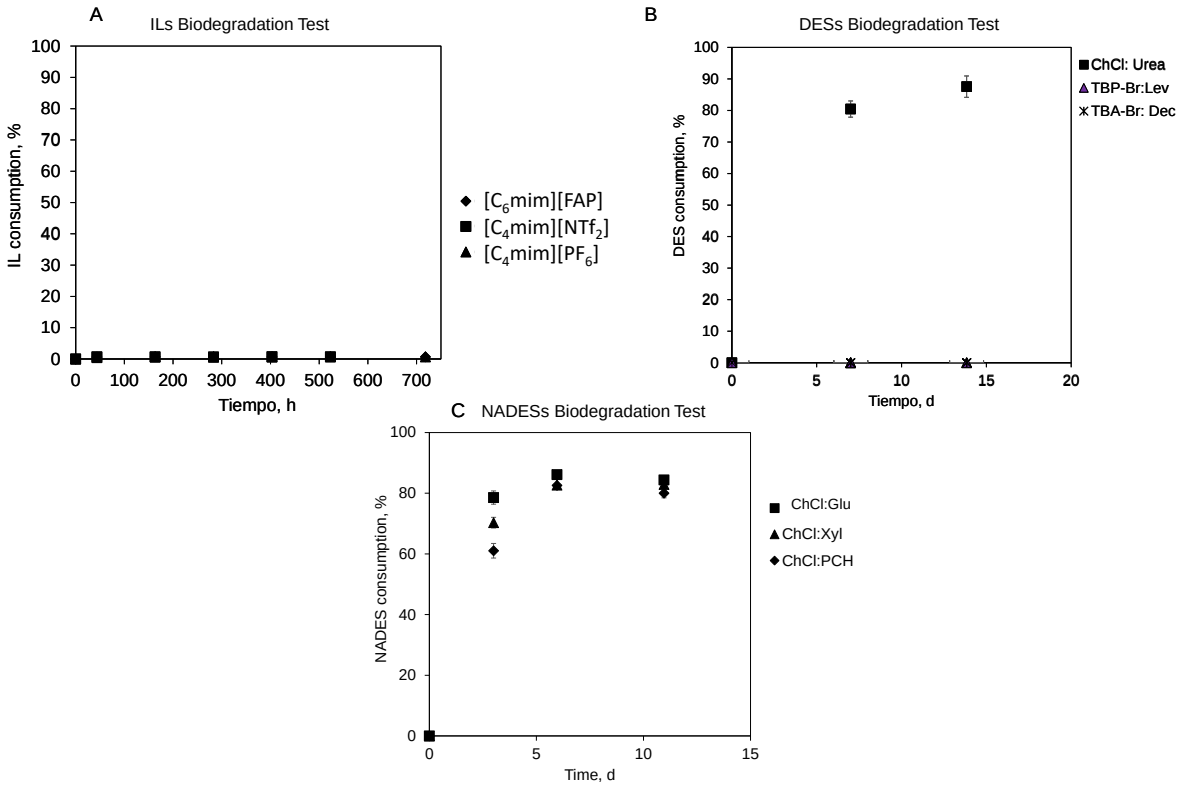

Fig. 3.4 Biodegradability test for A) ILs, B) DESs and C) NADESs

3.6.3 Styrene partition coefficient in all the solvents

Absorption process aims to transfer the pollutant from the gas to the liquid phase by intense contacting of the polluted air stream with the solvent. This mass transfer depends on the concentration of the pollutant and the partition coefficient (VOC concentration air/VOC concentration solvent). Fig. 3.5 displays the partition coefficient obtained for styrene by the static headspace method. For ILs, the values observed ranged from 0.0023-.0040, for DESs from 0.0015-0.1197, and for NADESs from 0.0579-0.1112 and finally the partition coefficient of styrene for mineral medium was 0.2. Statistically significant differences between styrene partition coefficients are indicated with different letters. The order of affinity towards styrene is as follows: (TBA-Br:Dec >[C_6mim][FAP] > [C_4mim][NTF_2] > [C_4mim][PF_6] > TBP-Br:Lev) > (ChCl:Xil > ChCl:PCH) > (ChCl: Urea> ChCl:Gluc). The order of affinity of styrene to the solvents can be explained by the general chemical principle that *like dissolves like*, to be specific, polar solvents will dissolve polar solutes, and non-polar solvents will dissolve non-polar solutes, thus the hydrophobicity of styrene makes it very soluble in non-polar solvents. All the solvents revealed a greater styrene solubility than the solubility of styrene in mineral medium. The maximum improvement was obtained with TBA-Br: Dec with a 113-fold increase. The lowest improvement was with ChCl:Glc, with a 1.6-fold increase. Comparing these results with the common NAP, silicone oil; Patel et al. (2017) performed partitioning experiments for different VOCs through mass balance method, where styrene/silicone oil (20 cSt) partition coefficient obtained was 0.0004 (Patel et al., 2017). On the other hand, Dumont et al. (2014) reported a partition coefficient for styrene/silicon oil (5 mPa s) of 0.00044 using static headspace method). Both partition coefficients are 3.5 times lower than the styrene partition coefficients obtained with the DES TBA-Br:Dec in the present study.

Since there are no studies evaluating styrene/ILs or styrene/DESs partition coefficients and the most similar molecule is toluene, we can note that for toluene the best absorbent reported is for [OctIq][NTf_2] with a partition coefficient of 0.0006 (Quijano et al., 2011a), while others have reported that toluene presents the best affinity for NTf_2 anion and isoquinolium cation (0.00022), comparing 23 ILs by a static headspace method (Rodriguez Castillo et al., 2018a). Regarding DESs and their use as VOC absorbents, Moura et al (2017) determined the partition coefficients of toluene and 7 different DESs to evaluate their efficiency in the

absorption of toluene. They noticed a 251-fold decrease at 30 °C and 654-fold decrease at 60 °C in partition coefficient for toluene in tetrabutylammonium bromide:decanoic acid compared to water, meaning that a greater amount of toluene is solubilized in these solvents than in water (Moura et al., 2017). Regarding the use of DESs as absorbents of VOC, Chen et al. (2022) reported the use of hydrophobic DESs containing thymol [Thy] and decanoic acid [DecA] with a molar ratio of 1:1 for the absorption of acetone. They observed an absorption capacity of acetone of 6.57 mg acetone per g DES at 20 ◦C (Chen et al., 2022). Some limitations in the use of all the solvents tested can be their high viscosity and in the case of ILs their high cost, therefore more research should be done to confirm the potential of these solvents in TPPB applications. In literature, there are studies with different VOCs and ILs and DESs, however as far as we know, there are no studies evaluating the styrene absorption in ILs, DESs or NADESs. This study has shown that TBA-Br:Dec, TBP-Br:Lev,[C_6mim][FAP],[C_4mim][PF_6] and [C_4mim][NTF_2] have a much greater styrene solubility than the solubility of styrene in mineral medium, thus they can be a potential NAP in a two-phase partitioning bioreactor (TPPB).

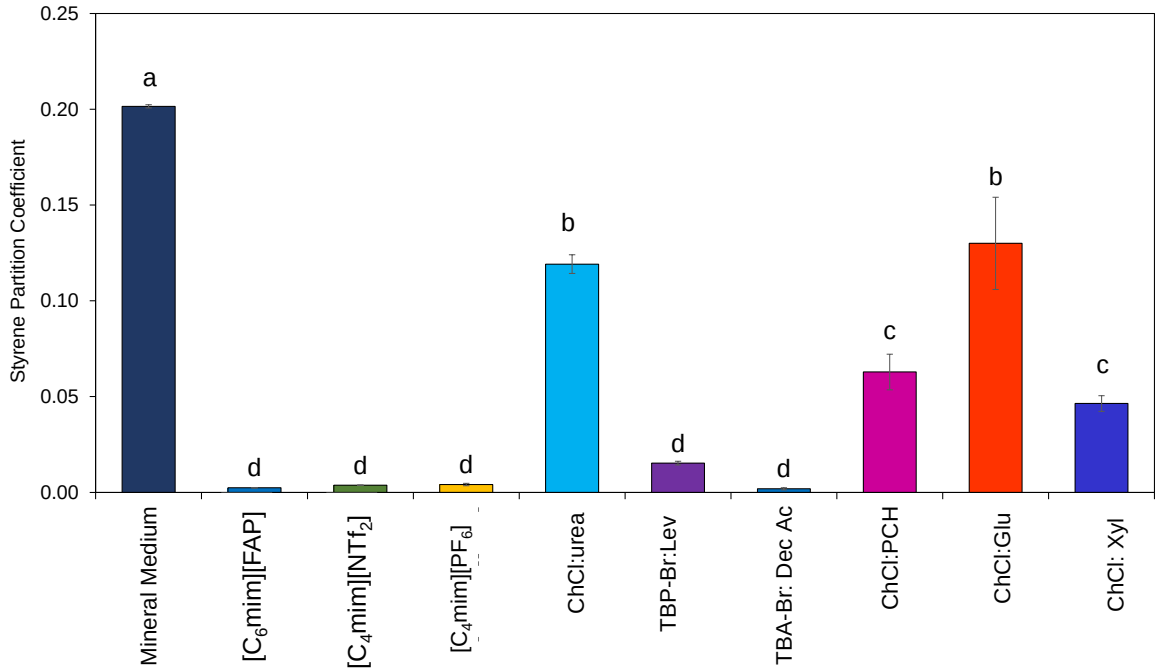

Fig. 3.5 Partitioning coefficients of different VOCs in different solvents and significant differences between partition coefficients. Tukey test performed with R 4.1.1. The same letters indicate those partition coefficients between which there are no significant differences, while between different letters indicates that there are significant differences

3.6.4 Styrene biodegradation with [C_6mim][FAP] as NAP

According to the results discussed above, [C_6mim][FAP] was selected as NAP for styrene biodegradation assays in batch TPPB process. This selection was based in the high affinity of this IL for styrene, low solubility in water, lack of activated sludge inhibition for glucose consumption and non-biodegradability. Fig 3.6 A) shows the decrease of styrene concentration in gas phase, for the assays with and without the addition of IL. As can be seen, gaseous styrene concentration in control experiment (without IL) decreased from 136 to 13.4 g/m^3 in 21 h, and by 47 h styrene has been completely removed from the gaseous phase. In presence of IL, styrene concentration decreased from 136 to 6.8 g/m^3 in 5 h, and by 21 h styrene concentration in the gaseous phase is almost zero. The faster styrene gaseous decrease in the two-phase system (with the presence of IL) is explained mainly by the greater absorption in presence of IL. This NAP is serving as a vector transfer of styrene from the gas to the liquid phase and then to the microorganisms. Styrene is absorbed in the NAP, and then some styrene molecules are slowly and continuously released for microbial consumption. The affinity of styrene to [C_6mim][FAP] was above discussed with the partition coefficient analysis, where the coefficient partition was 0.0023. On the other hand, in the case of the single-phase system (control), diminishing of styrene in the gaseous phase can only be attributed to the biodegradation process.

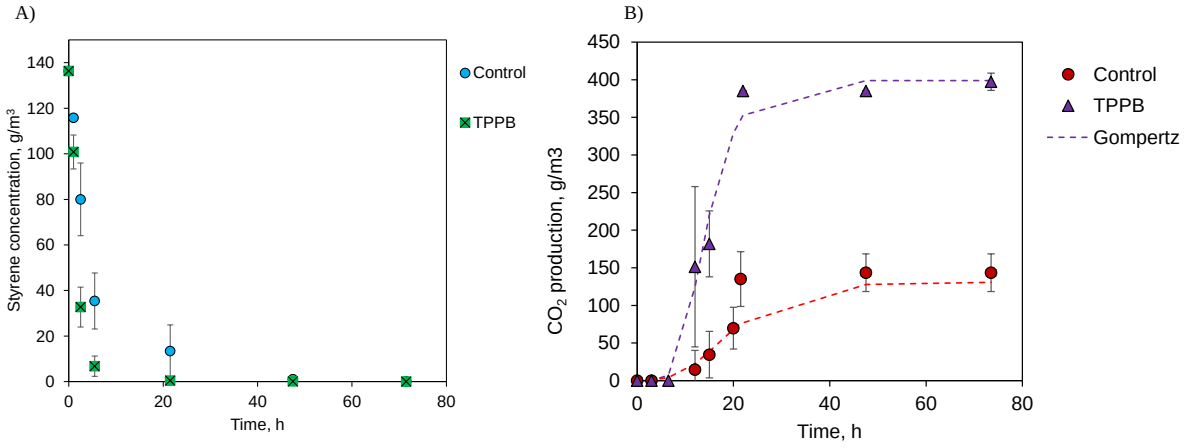

Fig. 3.6 A) Styrene consumption in the TPPB with [C_6mim][FAP] as NAP and in the control B) Production of CO_2 from the mineralization of styrene in the TPPB with [C_6mim][FAP] as NAP and in the control

Fig. 3.6 B) shows CO_2 production during styrene consumption. Assays with the presence of IL reached a much greater CO_2 production (399.0 g /m^3) compared with the control (130.7 g/m^3) at the end of the experiment (corresponding to 86.2 and 28.1 % of mineralization of styrene, respectively). The parameters obtained from the fitted Gompertz model of CO_2 production are presented in Table 3.5. Interestingly, a 3-fold increase of the maximum production of CO_2 (Hmax,g CO_2/m^3) and a 5.5 increase in the CO_2 production rate (Rmax, g CO_2/m^3 *h) were obtained in the assays when IL is used as NAP, compared with the control. Conversely, the lambda parameter that reflects the lag phase presented similar values in both treatments. Gompertz parameters obtained further corroborates the improvement of styrene consumption when the IL is used as NAP.

Table 3.5 Gompertz parameters for TPPB and the control

Gompertz parameters	**TPPB**	**Control**
H_{max}, g CO_2/m^3	399.00	130.70
R_{max}, g CO_2/m^3*h	32.94	5.95
Lambda, h	8.22	8.48
R^2	0.9847	0.9777

The studies that depict the biodegradation of styrene by activated sludge in batch tests had been performed in synthetic wastewater, for instance Babaee et al.(2010). assessed the biodegradation of styrene with activated sludge in batch test from wastewaters containing styrene as the sole carbon source (Babaee et al., 2010). They reported the biodegradation of styrene at concentrations of 50-200 mg/L in the aqueous phase using 2 types of activated sludge (industrial and municipal). They indicated that at initial concentrations of 50 mg/L and 100 mg/L, styrene was completely consumed within approximately 4 to 9 days, respectively, in the industrial activated sludge assays. Moreover, they did not observe a lag phase in styrene biodegradation when an industrial activated sludge was used at a styrene concentration up to 100 mg/L. Conversely, a lag phase was observed even at 50 mg/L styrene in the assays with municipal activated sludge; however, the rate of styrene biodegradation after the lag phase was like that achieved by the industrial activated sludge.

In the case of municipal activated sludge, a complete biodegradation at 50 mg/L of styrene was reached in 5 days. For initial styrene concentrations in the range 150–200 mg/L in the aqueous phase, the lag phase in the municipal activated sludge extended to at least 10 days. In the same way Hazrati et al., (2015) used an industrial mix culture supplied from a petrochemical complex to evaluate the styrene biodegradation in water, concentration ranges of styrene varied from 8 to 220 mg/l and they reported that total styrene biodegradation varied from 2 to 127 h for the different tested concentrations, when an initial styrene concentration of 80 mg/L was evaluated they observed that styrene is fully consumed at 27 h (Hazrati et al., 2015). Thus, since styrene biodegradation kinetics is highly dependent on the source of the activated sludge, different results could be obtained if industrial activated sludge is used in styrene biodegradation tests in the present study. One reason for the higher styrene biodegradation rates obtained in this study is that the presence of a NAP decreases the aqueous styrene concentration below the toxicity threshold level. It is also important to mention that not all styrene is mineralized, subproducts can be produced since the attack of the styrene aromatic ring by microorganisms can produce cis glycol, 3-vinylcatechol and muconic semialdehyde, and finally this last compound is converted to pyruvate and acetaldehyde. Other byproducts reported for the biodegradation of styrene are styrene oxide, 2-phenylethanol and phenylacetaldehyde (Mooney et al., 2006).

Regarding the effects of NAP in other VOC biodegradation in batch test by activated sludge, Keramati et al., (2021) assessed the biodegradation of hexane and methanol with and without silicon oil (5 and 10%) by a microbial consortium adapted to consume hexane and methanol. Initial concentrations of hexane (5−10 g m^3) and methanol (1−5 g m^3) were evaluated. The authors reported an increase in the mass transfer of hexane with the addition of silicon oil which translated into a raise in the hexane removal efficiency from 72-80% to 92-94%, while methanol removal efficiency decreased from 15-34% to 6-24% with the addition of silicon oil, due to an increase of the methanol partition coefficient from 0.00018 without silicon oil to 0.003 in the presence of silicon oil. In such case, the mineralization of the total VOCs increased from 27-29% without silicon oil to 35–43 % in the presence of oil. They concluded that best conditions for a hexane removal efficiency of 90% and a methanol removal efficiency of 24% are initial concentration of 5 g/m^3, 1 g/m^3, and 5% v/v for hexane and methanol, respectively (Keramati et al., 2021).

Even though no direct comparison with our study is possible, due to the differences in styrene measurements and conditions, we can highlight that in the present study, the use of IL as NAP is shortening the 90% styrene removal from the gaseous phase to 5 h with an initial styrene concentration of 136 g/m^3, as well as an enhancement in the mineralization of the VOC, when $[C_6mim][FAP]$ is present.

3.7. Conclusions

Physicochemical characteristics of nine different NAPs were determined, given their impact in selection of the solvent for the removal of hydrophobic VOCs from the air, as well as their affinity towards the target VOC (styrene). The densities obtained for IL and the DES TBA-Br: Dec, are different from water, thus their recovery and recyclability can be cost-effectively carried out, especially when using ILs. Nonetheless, some of the DESs and NADESs are miscible in water, and thus cannot be regenerated, most of them are biodegradable which will diminish their environmental impact. Imidazolium ionic liquids $[C_6mim][FAP]$ and $[C_4mim][NTf_2]$, as well as DESs TBP-Br:Lev and TBA-Br:Dec were suitable styrene absorbents according to their partition coefficients. Given its high styrene affinity, low solubility in water and non-biodegradability, the ionic liquid $[C_6mim][FAP]$ was used as a NAP in a TPPB batch process. This study showed that the addition of IL (5 %v/v) improved the styrene mass transfer and outperformed the control by a 3 times increase of styrene mineralization. Ionic liquids are potential adjuvant phases in biological degradation systems, as well as other solvents like DESs and NADESs, which should be evaluated for more biodegradation processes.

3.8. Acknowledgment

The authors express their sincere thanks to CONACYT for the financial support for this work [SEP-CONACYT-CB-2014-01-239622 Grant] and for the scholarship No. 787139. Also, thanks to IPICYT for the use of facilities.

3.9. References

Abranches, D. O., Martins, M. A. R., Silva, L. P., Schaeffer, N., Pinho, S. P., & Coutinho, J. A. P. (2019). Phenolic hydrogen bond donors in the formation of non-ionic deep eutectic solvents: The quest for type v des. *Chemical Communications*, *55*(69), 10253–10256. https://doi.org/10.1039/c9cc04846d

Alonso-Campos, V., Covarrubias-García, I., & Arriaga, S. (2021). Styrene bioconversion by Pseudomonas putida utilizing a non-aqueous phase for polyhydroxyalkanoate production. *Journal of Chemical Technology \& Biotechnology*, *n/a*(n/a). https://doi.org/https://doi.org/10.1002/jctb.6935

Babaee, R., Bonakdarpour, B., Nasernejad, B., & Fallah, N. (2010). Kinetics of styrene biodegradation in synthetic wastewaters using an industrial activated sludge. *Journal of Hazardous Materials*, *184*(1–3), 111–117. https://doi.org/10.1016/j.jhazmat.2010.08.012

Bocquet, S., Gascons Viladomat, F., Muvdi Nova, C., Sanchez, J., Athes, V., & Souchon, I. (2006). Membrane-based solvent extraction of aroma compounds: Choice of configurations of hollow fiber modules based on experiments and simulation. *Journal of Membrane Science*, *281*(1), 358–368. https://doi.org/https://doi.org/10.1016/j.memsci.2006.04.005

Carmichael, A. J., & Seddon, K. R. (2000). Polarity study of some 1-alkyl-3-methylimidazolium ambient-temperature ionic liquids with the solvatochromic dye, Nile Red. *Journal of Physical Organic Chemistry*, *13*(10), 591–595. https://doi.org/10.1002/1099-1395(200010)13:10<591::AID-POC305>3.0.CO;2-2

Chen, C. C., Huang, Y. H., & Fang, J. Y. (2022). Hydrophobic deep eutectic solvents as green absorbents for hydrophilic VOC elimination. *Journal of Hazardous Materials*, *424*(PB), 127366. https://doi.org/10.1016/j.jhazmat.2021.127366

Chen, C. C., Huang, Y. H., Hung, S. M., Chen, C., Lin, C. W., & Yang, H. H. (2021). Hydrophobic deep eutectic solvents as attractive media for low-concentration hydrophobic VOC capture. *Chemical Engineering Journal*, *424*. https://doi.org/10.1016/j.cej.2021.130420

Chen, Y., & Mu, T. (2021). Revisiting greenness of ionic liquids and deep eutectic solvents. *Green Chemical Engineering*, *2*(2), 174–186. https://doi.org/10.1016/j.gce.2021.01.004

Cheng, X., Yang, G., Mu, T., Guo, X., Wang, X., National, B., Sciences, C. A., & Univer-, R. (2009). *Absorption of Vinyl Chloride by Room Temperature Ionic Liquids*. *37*(3), 245–248. https://doi.org/10.1002/clen.200800188

Dai, Y., van Spronsen, J., Witkamp, G. J., Verpoorte, R., & Choi, Y. H. (2013). Natural deep eutectic solvents as new potential media for green technology. *Analytica Chimica Acta*, *766*, 61–68. https://doi.org/10.1016/j.aca.2012.12.019

De Morais, P., Gonçalves, F., Coutinho, J. A. P., & Ventura, S. P. M. (2015). Ecotoxicity of Cholinium-Based Deep Eutectic Solvents. *ACS Sustainable Chemistry and Engineering*, *3*(12), 3398–3404. https://doi.org/10.1021/acssuschemeng.5b01124

Delgado-Mellado, N., Larriba, M., Navarro, P., Rigual, V., Ayuso, M., García, J., & Rodríguez, F. (2018). Thermal stability of choline chloride deep eutectic solvents by TGA/FTIR-ATR analysis. *Journal of Molecular Liquids*, *260*, 37–43. https://doi.org/10.1016/j.molliq.2018.03.076

Dietz, C. H. J. T., Kroon, M. C., Van Sint Annaland, M., & Gallucci, F. (2017). Thermophysical Properties and Solubility of Different Sugar-Derived Molecules in Deep Eutectic Solvents. *Journal of Chemical and Engineering Data*, *62*(11), 3633–3641. https://doi.org/10.1021/acs.jced.7b00184

Dimian, A. C., Bildea, C. S., & Kiss, A. A. (2019). Styrene manufacturing. In A. C. Dimian, C. S. Bildea, & A. A. Kiss (Eds.), *Applications in Design and Simulation of Sustainable Chemical Processes* (pp. 443–481). Elsevier. https://doi.org/10.1016/B978-0-444-63876-2.00012-7

Dumont, E., Andrès, Y., & Le, P. (2014). Mass transfer coefficients of styrene into water / silicone oil mixtures : New interpretation using the ‘“ equivalent absorption capacity ”’ concept. *Chemical Engineering Journal*, *237*, 236–241. https://doi.org/10.1016/j.cej.2013.10.021

Dupuy, A., Athes, V., Schenk, J., Jenelten, U., & Souchon, I. (2011). Solvent extraction of highly valuable

oxygenated terpenes from lemon essential oil using a polypropylene membrane contactor: Potential and limitations. *Flavour and Fragrance Journal*, *26*(3), 192–203. https://doi.org/10.1002/ffj.2052

Environmental Protection Agency (EPA). (2022). *TRI Toxic tracker*.

Fahri, F., Bacha, K., Chiki, F. F., Mbakidi, J. P., Panda, S., Bouquillon, S., & Fourmentin, S. (2020). Air pollution: new bio-based ionic liquids absorb both hydrophobic and hydrophilic volatile organic compounds with high efficiency. *Environmental Chemistry Letters*, *18*(4), 1403–1411. https://doi.org/10.1007/s10311-020-01007-8

Fletcher, K. A., Storey, I. A., Hendricks, A. E., Pandey, S., & Pandey, S. (2001). Behavior of the solvatochromic probes Reichardt's dye, pyrene, dansylamide, Nile Red and 1-pyrenecarbaldehyde within the room-temperature ionic liquid bmimPF6. *Green Chemistry*, *3*(5), 210–215. https://doi.org/10.1039/b103592b

Freemantle, M. (2009). *An Introduction to Ionic Liquids*. The Royal Society of Chemistry.

Gathergood, N., Garcia, M. T., & Scammells, P. J. (2004). Biodegradable ionic liquids: Part I. Concept, preliminary targets and evaluation. *Green Chemistry*, *6*(3), 166–175. https://doi.org/10.1039/b315270g

Ghaedi, H., Ayoub, M., Sufian, S., Lal, B., & Uemura, Y. (2017). Thermal stability and FT-IR analysis of Phosphonium-based deep eutectic solvents with different hydrogen bond donors. *Journal of Molecular Liquids*, *242*, 395–403. https://doi.org/10.1016/j.molliq.2017.07.016

Haraźna, K., Walas, K., Urbańska, P., Witko, T., Snoch, W., Siemek, A., Jachimska, B., Krzan, M., Napruszewska, B. D., Witko, M., Bednarz, S., & Guzik, M. (2019). Polyhydroxyalkanoate-derived hydrogen-bond donors for the synthesis of new deep eutectic solvents. *Green Chemistry*, *21*(11), 3116–3126. https://doi.org/10.1039/c9gc00387h

Hazrati, H., Shayegan, J., & Seyedi, S. M. (2015). Biodegradation kinetics and interactions of styrene and ethylbenzene as single and dual substrates for a mixed bacterial culture. *Journal of Environmental Health Science and Engineering*, *13*(1), 1–12. https://doi.org/10.1186/s40201-015-0230-y

Huddleston, J. G., Visser, A. E., Reichert, W. M., Willauer, H. D., Broker, G. A., Rogers, R. D., & April, R. (2001). *Characterization and comparison of hydrophilic and hydrophobic room temperature ionic liquids incorporating the imidazolium cation Green Context*. https://doi.org/10.1039/b103275p

Jacquemin, J., Husson, P., Padua, A. A. H., & Majer, V. (2006). *Density and viscosity of several pure and water-saturated ionic liquids*. 172–180. https://doi.org/10.1039/b513231b

Juneidi, I., Hayyan, M., & Hashim, M. A. (2015). Evaluation of toxicity and biodegradability for cholinium-based deep eutectic solvents. *RSC Advances*, *5*(102), 83636–83647. https://doi.org/10.1039/c5ra12425e

Keramati, S., Ferdowsi, M., & Zamir, S. M. (2021). Compounds interactions during simultaneous biodegradation of hydrophobic n-hexane and hydrophilic methanol vapors in one- and two-liquid phase conditions. *Process Safety and Environmental Protection*, *147*, 283–291. https://doi.org/10.1016/j.psep.2020.09.040

Ma, C., Laaksonen, A., Liu, C., Lu, X., & Ji, X. (2018). The peculiar effect of water on ionic liquids and deep eutectic solvents. In *Chemical Society Reviews* (Vol. 47, Issue 23, pp. 8685–8720). Royal Society of Chemistry. https://doi.org/10.1039/c8cs00325d

Makoś-Chełstowska, P., Słupek, E., & Gębicki, J. (2021). Deep eutectic solvent-based green absorbents for the effective removal of volatile organochlorine compounds from biogas. *Green Chemistry*, *23*(13), 4814–4827. https://doi.org/10.1039/d1gc01735g

Mallakpour, S., & Dinari, M. (2012). Ionic Liquids as Green Solvents: Progress and Prospects. In A. Mohammad & D. Inamuddin (Eds.), *Green Solvents II: Properties and Applications of Ionic Liquids* (pp. 1–32). Springer Netherlands. https://doi.org/10.1007/978-94-007-2891-2_1

Marcus, Y. (2016). Ionic liquid properties: From molten salts to RTILs. In *Ionic Liquid Properties: From Molten Salts to RTILs*. https://doi.org/10.1007/978-3-319-30313-0

Mooney, A., Ward, P. G., & O'Connor, K. E. (2006). Microbial degradation of styrene: Biochemistry, molecular genetics, and perspectives for biotechnological applications. *Applied Microbiology and*

Biotechnology, *72*(1), 1–10. https://doi.org/10.1007/s00253-006-0443-1

Moura, L., Moufawad, T., Ferreira, M., Bricout, H., Tilloy, S., Monflier, E., Costa Gomes, M. F., Landy, D., & Fourmentin, S. (2017). Deep eutectic solvents as green absorbents of volatile organic pollutants. *Environmental Chemistry Letters*, *15*(4), 747–753. https://doi.org/10.1007/s10311-017-0654-y

Mulia, K., Fauzia, F., & Krisanti, E. A. (2019). Polyalcohols as Hydrogen-Bonding Donors in Choline Chloride-Based Deep Eutectic Solvents for Extraction of Xanthones from the Pericarp of Garcinia mangostana L. *Molecules*, *24*(3). https://doi.org/10.3390/molecules24030636

Muñoz, R., Daugulis, A. J., Hernández, M., & Quijano, G. (2012). Recent advances in two-phase partitioning bioreactors for the treatment of volatile organic compounds. In *Biotechnology Advances* (Vol. 30, Issue 6, pp. 1707–1720). https://doi.org/10.1016/j.biotechadv.2012.08.009

Muñoz, R., Villaverde, S., Guieysse, B., & Revah, S. (2007). Two-phase partitioning bioreactors for treatment of volatile organic compounds. In *Biotechnology Advances* (Vol. 25, Issue 4, pp. 410–422). https://doi.org/10.1016/j.biotechadv.2007.03.005

Nolasco, M. M., Pedro, S. N., Vilela, C., Vaz, P. D., Ribeiro-Claro, P., Rudić, S., Parker, S. F., Freire, C. S. R., Freire, M. G., & Silvestre, A. J. D. (2022). Water in Deep Eutectic Solvents: New Insights From Inelastic Neutron Scattering Spectroscopy. *Frontiers in Physics*, *10*(February), 1–12. https://doi.org/10.3389/fphy.2022.834571

OECD. (1992). OECD 301 - Ready Biodegradability. *OECD Guidelines for the Testing of Chemicals*, *301*(July), 1–62.

OECD. (1995). Test No. 105: Water Solubility. In *OECD* (Issue July). OECD Publishing. https://doi.org/10.1787/9789264069589-en

Patel, M. J., Popat, S. C., & Deshusses, M. A. (2017). Determination and correlation of the partition coefficients of 48 volatile organic and environmentally relevant compounds between air and silicone oil. *Chemical Engineering Journal*, *310*, 72–78. https://doi.org/10.1016/j.cej.2016.10.086

Quijano, G., Couvert, A., Amrane, A., Darracq, G., Couriol, C., Le Cloirec, P., Paquin, L., & Carrié, D. (2011a). Potential of ionic liquids for VOC absorption and biodegradation in multiphase systems. *Chemical Engineering Science*, *66*(12), 2707–2712. https://doi.org/10.1016/j.ces.2011.01.047

Quijano, G., Couvert, A., Amrane, A., Darracq, G., Couriol, C., Le Cloirec, P., Paquin, L., & Carrié, D. (2011b). Toxicity and biodegradability of ionic liquids: New perspectives towards whole-cell biotechnological applications. *Chemical Engineering Journal*, *174*(1), 27–32. https://doi.org/10.1016/j.cej.2011.07.055

Quijano, G., Couvert, A., Amrane, A., Darracq, G., Couriol, C., Le Cloirec, P., Paquin, L., & Carrié, D. (2013). Absorption and biodegradation of hydrophobic volatile organic compounds in ionic liquids. *Water, Air, and Soil Pollution*, *224*(5). https://doi.org/10.1007/s11270-013-1528-y

Quijano, G., Hernandez, M., Thalasso, F., Muñoz, R., & Villaverde, S. (2009). Two-phase partitioning bioreactors in environmental biotechnology. In *Applied Microbiology and Biotechnology* (Vol. 84, Issue 5, pp. 829–846). https://doi.org/10.1007/s00253-009-2158-6

Radošević, K., Čanak, I., Panić, M., Markov, K., Bubalo, M. C., Frece, J., Srček, V. G., & Redovniković, I. R. (2018). Antimicrobial, cytotoxic and antioxidative evaluation of natural deep eutectic solvents. *Environmental Science and Pollution Research*, *25*(14), 14188–14196. https://doi.org/10.1007/s11356-018-1669-z

Radošević, K., Cvjetko Bubalo, M., Gaurina Srček, V., Grgas, D., Landeka Dragičević, T., & Redovniković, R. I. (2015). Evaluation of toxicity and biodegradability of choline chloride based deep eutectic solvents. *Ecotoxicology and Environmental Safety*, *112*, 46–53. https://doi.org/10.1016/j.ecoenv.2014.09.034

Revah, S., & Morgan-Sagastume, J. M. (2005). Methods of Odor and VOC Control. In Z. Shareefdeen & A. Singh (Eds.), *Biotechnology for Odor and Air Pollution Control* (pp. 29–63). Springer Berlin Heidelberg. https://doi.org/10.1007/3-540-27007-8_3

Rodriguez Castillo, A. S., Biard, P. F., Guihéneuf, S., Paquin, L., Amrane, A., & Couvert, A. (2019). Assessment of VOC absorption in hydrophobic ionic liquids: Measurement of partition and diffusion

coefficients and simulation of a packed column. *Chemical Engineering Journal*, *360*(July 2018), 1416–1426. https://doi.org/10.1016/j.cej.2018.10.146

Rodriguez Castillo, A. S., Guihéneuf, S., Biard, P. F., Paquin, L., Amrane, A., & Couvert, A. (2018). Impact of activated sludge acclimation on the biodegradation of toluene absorbed in a hydrophobic ionic liquid. *International Journal of Environmental Science and Technology*, *15*(3), 621–630. https://doi.org/10.1007/s13762-017-1429-5

Rodriguez Castillo, A. S., Guihéneuf, S., Le Guével, R., Biard, P. F., Paquin, L., Amrane, A., & Couvert, A. (2016). Synthesis and toxicity evaluation of hydrophobic ionic liquids for volatile organic compounds biodegradation in a two-phase partitioning bioreactor. *Journal of Hazardous Materials*, *307*, 221–230. https://doi.org/10.1016/j.jhazmat.2015.12.043

Shishov, A., Gorbunov, A., Moskvin, L., & Bulatov, A. (2020). Decomposition of deep eutectic solvents based on choline chloride and phenol in aqueous phase. *Journal of Molecular Liquids*, *301*, 112380. https://doi.org/10.1016/j.molliq.2019.112380

Song, Y., Chen, S., Luo, F., & Sun, L. (2020). Absorption of Toluene Using Deep Eutectic Solvents: Quantum Chemical Calculations and Experimental Investigation. *Industrial and Engineering Chemistry Research*, *59*(52), 22605–22618. https://doi.org/10.1021/acs.iecr.0c04986

Souchon, I., Athès, V., Pierre, F.-X., & Marin, M. (2004). Liquid-liquid extraction and air stripping in membrane contactor: application to aroma compounds recovery. *Desalination*, *163*(1), 39–46. https://doi.org/https://doi.org/10.1016/S0011-9164(04)90174-9

Tan, G. Y. A., Chen, C. L., Ge, L., Li, L., Tan, S. N., & Wang, J. Y. (2015). Bioconversion of styrene to poly(hydroxyalkanoate) (PHA) by the new bacterial strain Pseudomonas putida NBUS12. *Microbes and Environments*, *30*(1), 76–85. https://doi.org/10.1264/jsme2.ME14138

Wang, W., Ma, X., Grimes, S., Cai, H., & Zhang, M. (2017). Study on the absorbability, regeneration characteristics and thermal stability of ionic liquids for VOCs removal. *Chemical Engineering Journal*, *328*, 353–359. https://doi.org/10.1016/j.cej.2017.06.178

Wen, Q., Chen, J. X., Tang, Y. L., Wang, J., & Yang, Z. (2015). Assessing the toxicity and biodegradability of deep eutectic solvents. *Chemosphere*, *132*, 63–69. https://doi.org/10.1016/j.chemosphere.2015.02.061

Wong, D. S. H., Chen, J. P., Chang, J. M., & Chou, C. H. (2002). Phase equilibria of water and ionic liquids [emim][PF6] and [bmim][PF6]. *Fluid Phase Equilibria*, *194–197*, 1089–1095. https://doi.org/10.1016/S0378-3812(01)00790-7

Yao, H., Feng, F., Jiang, J., Qiao, Y., Wu, T., Voglmeir, J., & Chen, Z.-G. (2017). Green and efficient extraction of rutin from tartary buckwheat hull by using natural deep eutectic solvents. *Food Chemistry*, *221*, 1400–1405.

Yongqing, S., Yongfu, H., Cong, L., Ping, W., Yun, Z., Limei, L., & Fei, H. (2011). Microwave-assisted synthesis and spectral identification of [Rmim]PF 6 (R = p,b,c6) ionic liquids. *Asian Journal of Chemistry*, *23*(1), 97–99.

Zhang, Q., De Oliveira Vigier, K., Royer, S., & Jérôme, F. (2012). Deep eutectic solvents: Syntheses, properties and applications. In *Chemical Society Reviews* (Vol. 41, Issue 21, pp. 7108–7146). https://doi.org/10.1039/c2cs35178a

Zhang, S., Sun, N., He, X., Lu, X., & Zhang, X. (2006). *Physical Properties of Ionic Liquids : Database and Evaluation*. *March 2005*. https://doi.org/10.1063/1.2204959

Zhao, B. Y., Xu, P., Yang, F. X., Wu, H., Zong, M. H., & Lou, W. Y. (2015). Biocompatible Deep Eutectic Solvents Based on Choline Chloride: Characterization and Application to the Extraction of Rutin from Sophora japonica. *ACS Sustainable Chemistry and Engineering*, *3*(11), 2746–2755. https://doi.org/10.1021/acssuschemeng.5b00619

4. Greenhouse gases capture applying impregnated silica with IL, DES and NADES

4.1 Abstract

To improve the quality of life and mitigate the adverse impacts of climate change, it is imperative to develop technologies aimed to capturing greenhouse gases (GHGs). Among the GHGs, carbon dioxide (CO_2) and nitrous oxide (N_2O) are the first and third GHGs most released into the atmosphere, respectively, with N_2O exhibiting a warming potential nearly 300 times greater than that of CO_2. Ionic liquids (ILs), deep eutectic solvents (DES), and natural deep eutectic solvents (NADES) have gained attention as promising candidates for GHGs capture due to their favorable attributes such as low vapor pressure, thermal stability, non-flammability, and recyclability. Nevertheless, the utilization of ILs, DESs, and NADESs for GHGs absorption present challenges like mass transfer limitations attributable to their elevated viscosity. To overcome this drawback, it is proposed the impregnation of these solvents onto a porous support material such as silica gel. This strategy takes advantage of the GHGs absorption capacity of the solvents, and the high surface area provided by the porous medium. This work is devoted to investigate the influence of the particle size of porous silica gel impregnated with IL, DES, or NADES on the efficiency of capturing CO_2 and N_2O at atmospheric pressure and temperature. The impregnated material was subjected to characterization through thermogravimetric analysis (TGA), X-ray diffraction (XRD), and Fourier-transform infrared spectroscopy (FTIR). The partition coefficient of CO_2 and N_2O was determined through a static headspace method. The FTIR analysis of the impregnated particles indicated successful impregnation of silica gel with the solvents. TGA results demonstrated that the percentage of impregnation on silica gel ranged from 36.8% to 43.0% w/w. The CO_2 partition coefficient in the impregnated silica exhibited a range of 0.46 to 4.75, whereas the N_2O partition coefficient in the impregnated silica ranged from 0.50 to 2.21. This indicates that the impregnated particles have a greater affinity for N_2O compared to CO_2. The process of impregnation demonstrated the capability to reduce solvent consumption by 60% while preserving the greenhouse gas capture capacity. The impregnation techniques offers significant advantages, such as the prevention of solvent loss, it also allows the operation of absorption columns with reduced solvent consumption. Moreover, it simplifies both the

absorption and regeneration processes, benefiting subsequent cycles of absorption. In this context, impregnation emerges as a valuable technique to enhance GHGs capture.

4.2 Graphical Abstract

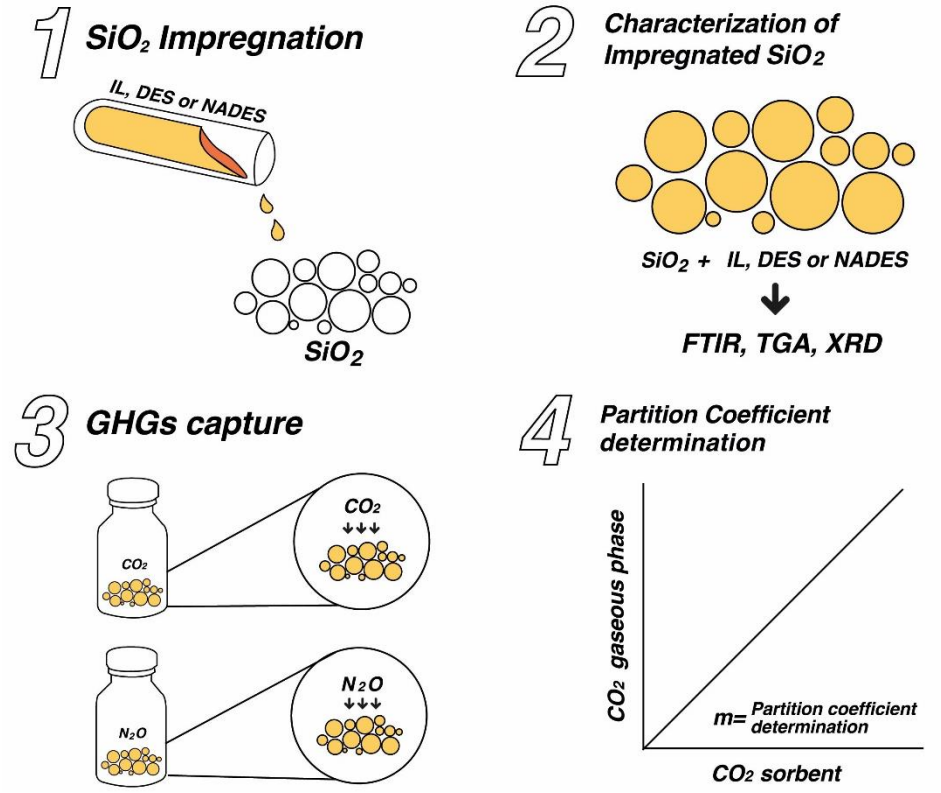

4.3 Introduction

Gases that trap heat in the atmosphere are known as greenhouse gases (GHG). The emission of these gases by human activities are responsible for global warming. Carbon dioxide (CO_2) is the main greenhouse gas emitted by human activities. Combustion of fossil fuels (coal, natural gas, and oil) is the main human activity that emits CO_2, although certain industrial processes and the land use also emit CO_2. Nitrous oxide (N_2O) is also a GHG; anthropogenic activities such as agriculture, fuel combustion, wastewater management, and industrial processes increase the amount of N_2O to the atmosphere. N_2O molecules remain in the atmosphere for an average of 114 years. The impact of 1 gram of N_2O on atmospheric warming can be 300 times greater than that of 1 gram of CO_2. Therefore, the removal of GHGs in the form of CO_2 and N_2O is vital. Ionic liquids (ILs), are gaining interest for CO_2

capture due to their special characteristics such as low vapor pressure, thermal stability, non-flammable, have a wide range of solubilities and miscibilities (hydrophilic or hydrophobic), and because they are recyclable (Salar-García et al., 2017). Experimental and simulation studies have shown high solubility of CO_2 in different ILs (Hasib-ur-Rahman et al., 2010; Janiczek et al., 2012; Sistla et al., 2012; Zareie-kordshouli et al., 2016). The high solubility could be explained by the anionic moiety that enhances interactions favoring particular distributions of CO_2 molecules around the cation (Hasib-ur-Rahman et al., 2010). CO_2 adsorption on ILs takes place by physical adsorption through weak Lewis acid-base interactions. Physical solvent-based approaches offer significant advantages when dealing with high partial pressures and concentrations of GHGs, compared to chemical solvents, the interactions between GHGs and the sorbent in physical solvent processes are weaker, resulting in reduced energy requirements for solvent recovery (Pakzad et al., 2020). The use of ILs present limitations in mass transport processes as a consequence of their high viscosity, also a large amount will be required if used directly as a liquid in an absorption process. To overcome these drawbacks, the incorporation of IL in porous support (activated carbon, zeolite, or silica) have been proposed. Expecting a synergistic effect between the high CO_2 adsorption capacity of IL and the high surface area of porous materials. Among the advantages of this strategy is the reduction in the amount of IL required and the increase in the sorption rate due to an improvement of the gas-liquid interface (Z. Zhang et al., 2009).

DESs are substances that have also been proposed as CO_2 absorbers (Ghazali et al., 2020). DES has advantages such as low price, they are easy to prepare and not require purification, apart frommost of them are biodegradable, biocompatible, and non-toxic (Zhang et al., 2012). DES consists of a mixture of a quaternary ammonium halide with an inorganic metal salt or an organic hydrogen bond donor, such as an amide or alcohol. The inorganic salt or hydrogen bond donor forms a complex with the halide anion. As a result, the charge on the anion is delocalized and the freezing point of the mixture decreases. When DES are obtained from natural sources, especially through primary metabolites such as organic acids, amino acids, and sugars, they are called NADES (Zhang et al., 2012). Studies on CO_2 and N_2O uptake with NADES are scarce, presenting a great opportunity to be explored.

Hence, the aim of this study is to impregnate three distinct solvents (IL, DES, NADES) onto a porous material like silica gel (SiO_2) using an impregnation-vaporization technique. The primary objective is to determine the partition coefficient of greenhouse gases (GHGs) in each solvent and impregnated material.

4.4 Materials and Methods

4.4.1 Reagents

Choline chloride (ChCl), tetrabutylammonium bromide (TBA-Br), decanoic acid (DecA), and 1,2-propanediol (PCH) were obtained for DES and NADES preparation. ChCl and TBA-Br were dried at 60 °C for 48 h before use. The ionic liquid bis(trifluoromethylsulfonyl)imide of 1-hexyl-3-methylimidazole [C_6mim][NTf_2] was purchased from Sigma Aldrich. The support used was silica gel (SiO_2) with different size particle 250-400 µm, 37-63 µm, and 800-1200 µm. The GHGs selected are CO_2 and N_2O.

4.4.2 DES/NADES preparation

DES was prepared by mixing TBA-Br and DecA in a molar ratio of 1:2 and kept at 80°C until a homogeneous colorless liquid was obtained (Moura et al., 2017). NADES was prepared by mixing ChCl, PCH, and water in a molar ratio (1:1:1) and heating below 50°C with stirring until a colorless liquid was formed (Dai et al., 2013).

4.4.3 Silica impregnation

The silica particles used as support did not receive pretreatment, they were used directly from the commercial supplier. The preparation of the impregnated material was done by impregnation-evaporation method, for which 6.67 g of IL/DES was mixed with 1 mL of acetone in a 50 mL vial, followed by the addition of 10 g of silica gel. The adsorbents were shaken for 2 h at 25 °C and dried at 60 °C for 6 h. The dried adsorbents were stored in a desiccator (Makoś et al., 2020). In brief, 6.67 g of NADES were added to 10 g of silica gel

4.4.4 Characterization of the impregnated silica gel

FT-IR-ATR spectra (Thermo Scientific Nicolet iS5) of the impregnated silica gel and pure compounds were taken using the following parameters: 4000-400 cm^{-1} range; 4 cm^{-1} resolution; 32 number of scans. Thermogravimetric analysis was performed on a Mettler Toledo TGA/DSC 3+ equipment workint with N_2 atmosphere, a flow rate of 50 mL/min, a temperature range of 25-600 °C and with a heating rate of 10 °C/min, 6-7 mg of sample were

used. Pure and impregnated silica gel samples were analyzed in an XRD instrument in the range of 5° to 80°in steps of 0.01° with a sample scan rate was 1° /min. Morphological properties of the materials were carried out using a Scanning Electron Microscope (Zeiss EVO MA10).

4.4.5 CO_2 and N_2O solubility measurements

The uptake of GHGs in solvents (IL, DES, and NADES) and impregnated silica particles was determined through equilibrium measurements between the concentration of GHGs in the gas phase and the liquid/solid phase (silica impregnated with solvents), respectively. The experiments were carried out in 15 mL serological bottles provided with septum seals that ensured airtightness. 0.5 g of solvent (IL, DES, NADES) or impregnated silica was placed, then different volumes of gas (CO_2 or N_2O) were injected (0.5-15 mL), to ensure atmospheric pressure since the same volume of GHG gas injected was withdrawed before the GHG injection from the bottle . The bottles were kept at a temperature of 293 K and 140 rpm, to allow equilibrium between the gas phase and the liquid or solid phase. After 24 h, gas samples were taken and analyzed by gas chromatograph. A mass balance based in the initial GHG concentration added into the bottle and the GHG concentration measured after 24 h which was considered the lapsed time to reach the absorption equilibrium, was used to obtain the amount of GHG in the sorbents.

The concentration of GHG in the sorbent was determined, using the next equation:

GHG sorbent= GHG gaseous phase initial- GHG gaseous phase at 24 h.

The partition coefficient corresponded to the slope of the curve that represents the relationship between the amount of GHG (in mg) in the headspace (Y axis) and the amount of GHG (in mg) in the sorbent (X axis). Consequently, a low partition coefficient value indicates a greater level of GHG solubility in the sorbent.

Statistical differences between the partition coefficient among the sorbents were determined using ANOVA and the Tukey test. Differences were considered significant at p-values less than 0.05. All statistical analyses were performed using R software version 4.1.1.

4.4.6 Gas chromatography

GHG concentration were measured using a gas chromatograph Varían CP 3800 equipped with a 10m MS5A column and a thermal conductivity detector (TCD). Argon was used as the carrier gas at 3.5 mL/min. The operating temperatures for the TCD are 110, 80, and 110 °C for the injector, column, and detector, respectively.

4.5 Results and Discussion

4.5.1 Characterization of impregnated silica

The amount of solvent retained in the silica was determined by thermogravimetric analysis, the amount of solvent impregnated in silica particles varied between 34 and 43% (Table 4.1). The SiO_2 particles showed weight loss between 4 and 6.45%. In the case of impregnated silica, the mass loss can be attributed to the solvent.

Table 4.1 Mass loss percentage in silica gel impregnated with different solvents.

Size	Particle	% Mass Loss
37-63 µm	SiO_2 + IL	40.61
	SiO_2 + DES	43.18
	SiO_2 + NADES	41.90
	SiO_2	6.45
250-400 µm	SiO_2 + IL	36.82
	SiO_2 + DES	40.85
	SiO_2 + NADES	40.64
	SiO_2	5.40
800-1200 µm	SiO_2 +IL	43.86
	SiO_2 + DES	34.78
	SiO_2 + NADES	36.36
	SiO_2	4.13

Decomposition temperatures (T_{onset}) and the temperature at the greatest weight loss (T_{peak}) of the different materials is observed in Table 4.2. The material with the highest thermal stability was the one impregnated with IL with a T_{onset} range of 301 to 327 °C, a temperature even higher than the T_{onset} of the pure IL. In the case of the material impregnated with DES, the T_{onset} was in a range of 114-121 °C, which is a a lower temperature than that of the pure DES (139.5 °C). When DES was impregnated in silica gel material two degradation steps were observed, the first one corresponded to the decomposition temperature of HBD (decanoic acid) and the second one belonged to the decomposition temperature of the ammonium salt,

while with a pure DES only 1 degradation step was observed which reached its maximum mass loss at 221 °C. The TG curves of the silica gel+ NADES presented a weight loss that started around 50°C, this was due to the evaporation of the water added during the preparation of the solvent. After this two more degradation steps for DES were reached, the first step corresponded to HBD (1,2-propanediol) and the second to the degradation of HBA (choline chloride).

Table 4.2 Decomposition temperature (T_{onset}) and temperature at which occur the highest mass loss (T_{peak}) for SiO_2 impregnated with different solvents at various sizes.

Sorbent	T_{onset}, °C	T_{peak}, °C
IL [C_6mim][NTf_2]	275.7	405.3
SiO_2 37-63 + IL	319.2	433.7
SiO_2 250-400 + IL	301.8	440.8
SiO_2 800-1200 + IL	326.5	422.3
DES	139.5	221.3
SiO_2 37-63 + DES	121.5	216.7
	365.0	428.2
SiO_2 250-400 + DES	114.2	217.2
	347.8	431.0
SiO_2 800-1200 + DES	118.3	216.2
	362.2	431.0
NADES	63.5	
	192.3	224.0
	253.5	298.0
SiO_2 37-63 + NADES	50.8	80.8
	111.5	160.7
	196.7	240.7
SiO_2 250-400 + NADES	52	84.8
	114	161.8
	201.3	245.3
SiO_2 800-1200 + NADES	58.2	-
	110	155
	200.2	252.0

The spectra obtained for silica gel and pure solvents were compared with the spectra obtained for silica gel impregnated with 40% (w/w) of IL, DES, or NADES (Fig. 4.1). Since the same patterns were observed for the different particle sizes of impregnated silica, only the spectra corresponding to the 37-63 µm size was presented. The spectra revealed characteristic bands

to the symmetric and asymmetric vibration of Si-O-Si around wavelengths 1060 cm^{-1} and 800 cm^{-1}, as well as Si-OH around 950 cm^{-1} for both pure and impregnated silica gel. Similar peaks were observed by Ghazali et al., (2020) and Makoś et al., (2020) for mesoporous silica gel. In the case of IL-impregnated silica gel particles, the characteristic peaks of the imidazole cation were observed at 3160.28 cm^{-1} (C-H alkene), 2800-2960 cm^{-1} (C-H alkane), 1450-1570 cm^{-1} (C=C cyclic alkene) and 1349 cm^{-1} (C-N aromatic). The [NTf_2] characteristics bands correspond to 1051-1178 cm^{-1} (C-F) and, these were overlapped with those corresponding to the Si=O 1372-1335 cm^{-1}. Finally, peaks corresponding to C-H bending were also observed in the range 740-840 cm^{-1}.

In addition to the characteristic peaks described above for pure silica, the silica gel particles impregnated with DES, also showed characteristics peaks of pure DES: 2850-2960 cm^{-1} (C-H alkane), 1726 cm^{-1} (C=O carboxylic acid), 1370-1455 cm^{-1} (O-H carboxylic acid), 1162 cm^{-1} (C-N amine), 737-880 cm^{-1} (C-H bending). The silica gel particles impregnated with NADES presented the characteristic peaks described above for pure silica and also those characteristics for pure NADES such as 3302 cm^{-1} (O-H alcohol), 2925-2970 cm^{-1} (C-H alkane), 1081 cm^{-1} (C-O alcohol), 950 cm^{-1} (C-H bending alkane), indicating that the three types of solvents have successfully adhered to the surface of the silica gel particle.

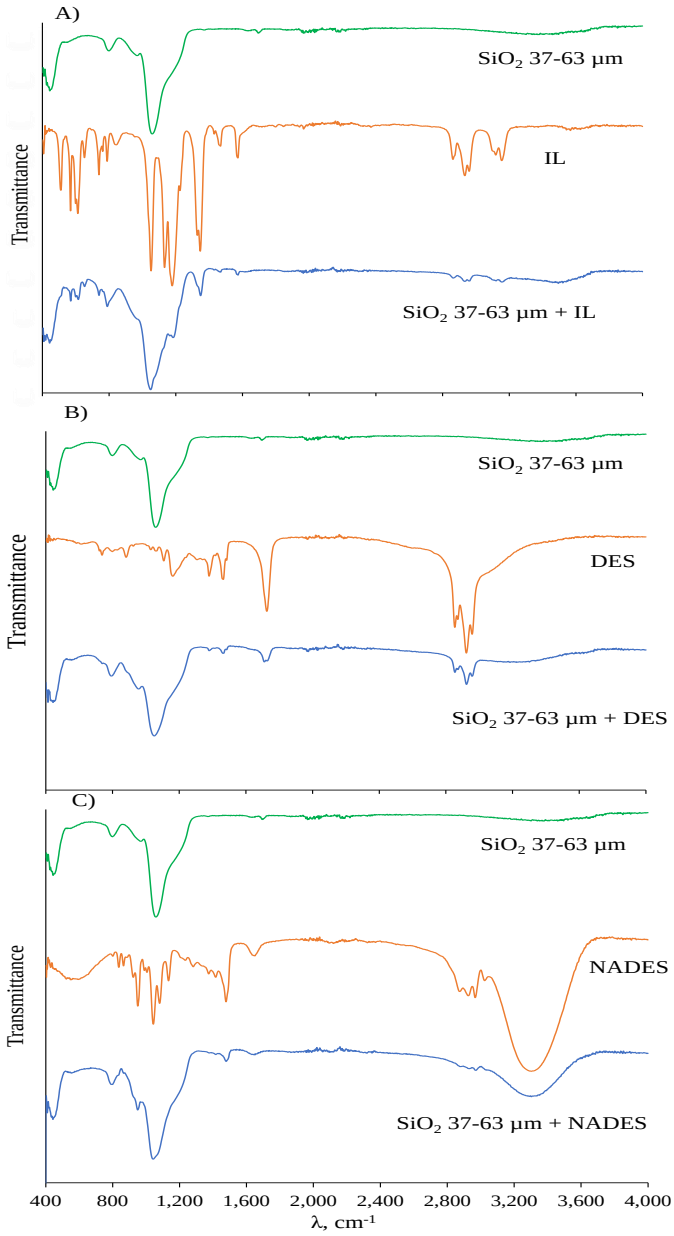

Fig. 4.1 FTIR spectra obtained for size (37-63 µm) of SiO_2 impregnated with different solvents A) SiO_2 + IL, B) SiO_2 + DES, and C) SiO_2 + NADES in addition to the spectra of pure solvents and the bare SiO_2

X-ray diffractogram of silica gel and impregnated silica gel is shown in Figure 4.2. The X-ray diffraction of the silica gel showed a broad peak between 13° and 31°, centered at 22°, distinctive of amorphous silica, confirming the absence of any ordered crystalline structure as reported by other authors (Elghniji et al., 2018; Hamoudi et al., 2008; Liu et al., 2011; Lu & Hsieh, 2012; Okoronkwo et al., 2013; Velmurugan et al., 2015). Similar pattern for

impregnated silica with IL, DES and DES suggested that the structure of the silica gel remained unaltered after the impregnation with the solvents.

.

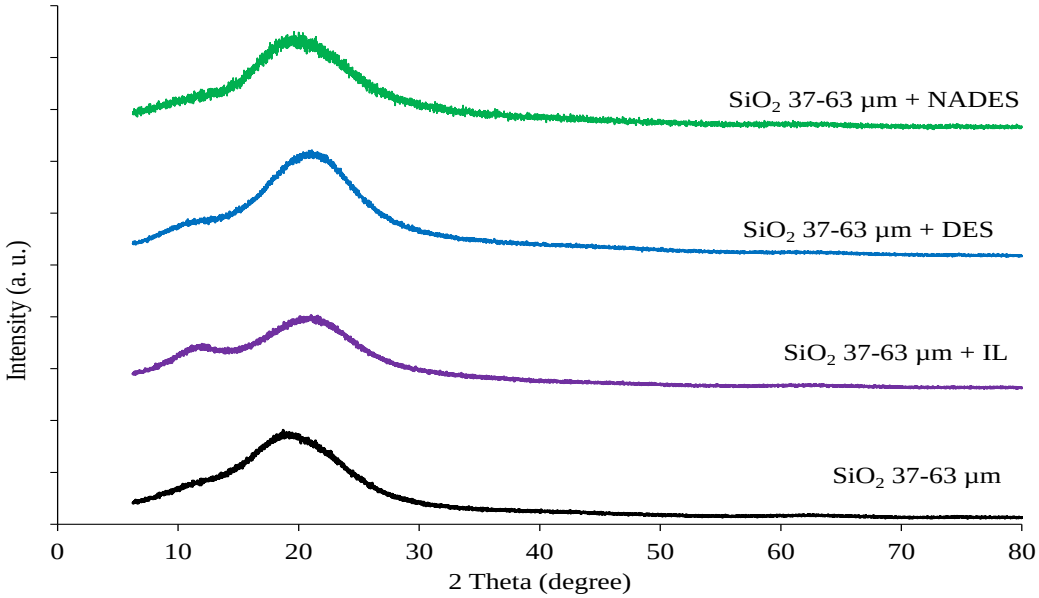

Fig. 4.2 XRD of SiO_2 and impregnated SiO_2

4.5.2 CO_2 and N_2O solubility

The CO_2 partition coefficient of the sorbents was experimentally determined at a temperature of 238 °K and under atmospheric pressure, as illustrated in Figure 4.3. A low partition coefficient (slope of GHGs in the headspace in mg vs GHGs in the sorbent in mg] value is indicative of an augmented solubility of CO_2. The hierarchical order of CO_2 partition coefficient values within the pure solvents (IL, DES, NADES) can be summarized as follows: IL < NADES < DES. This sequence suggests that CO_2 exhibits higher solubility in IL compared to NADES or DES. Specifically, CO_2 partition coefficient has a solubility that was 4.5 times greater in IL than in NADES, and 7.1 times greater in IL than in DES. The application of statistical analysis demonstrated significant differences between the CO_2 partition coefficient of IL and those of DES and NADES, as depicted in Figure 4.3.

The sequence of CO_2 solubility aligns inversely with the viscosity of the solvents, specifically IL (90.27 mPas) < NADES (114.5 mPas) < DES (548.0 mPas). This observation may provide a plausible reason for the variations in CO_2 solubility.

Concerning the impregnated silica samples, those impregnated with IL displayed the lowest CO_2 partition coefficient values, ranging from 0.46 to 0.53. Conversely, the statistical analysis did not identify any significant differences among the CO_2 partition coefficient of the three particle sizes employed. For silica impregnated with DES, the CO_2 partition coefficient values at various particle sizes ranged from 2.32 to 4.75. Notably, no significant differences were observed among the CO_2 partition coefficient values of different silica particle sizes impregnated with DES. Similarly, when the silica was impregnated with NADES, the CO_2 partition coefficient values spanned from 1.83 to 2.38. Once again, statistical analysis revealed no significant differences between the CO_2 partition coefficient values for different particle sizes of silica impregnated with NADES. The absence of significant differences observed among the various particle contained with the IL, DES, or NADES tested may be attributed to the uniform impregnation percentage applied, resulting in an equivalent sorbent quantity being present in all particles.

With respect to the control group (bare silica), it was observed that solely the silica impregnated with IL displayed a reduction in the CO_2 partition coefficient, this indicated an enhancement in CO_2 capture by a factor ranging from 3.0 to 3.9. Nevertheless, the statistical analysis demonstrates that this decrease in the partition coefficient does not yield significant differences in the CO_2 partition coefficient when comparing the bare silica and the silica impregnated with IL.

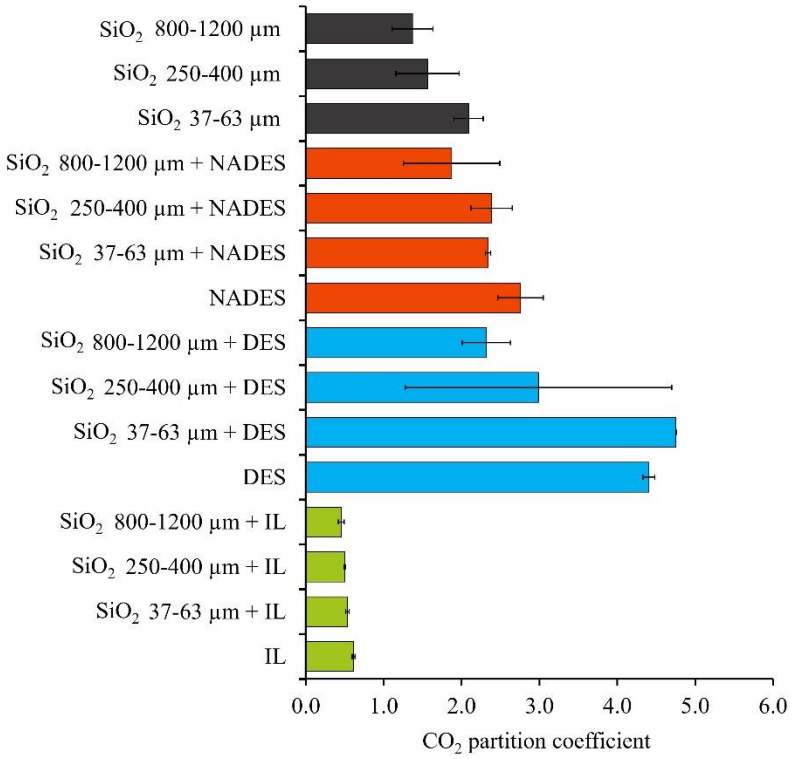

Fig. 4.3 CO_2 partition coefficient in solvents and impregnated SiO_2

The experimental N_2O partition coefficient of the sorbents at 293 K and atmospheric pressure is shown in Fig. 4.4. A low partition coefficient value is indicative of an augmented solubility of N_2O. The pure solvents (IL, DES, NADES) exhibit N_2O partition coefficient values following the next order: IL < NADES < DES. This order suggests that N_2O has higher solubility in IL compared to the NADES or DES, with N_2O being 1.4 times more soluble in IL than in NADES and 1.51 times more soluble in IL than in DES. However, the statistical analysis indicated no significant differences between the N_2O partition coefficient of IL and the N_2O partition coefficient of DES and NADES (Figure 4.4).

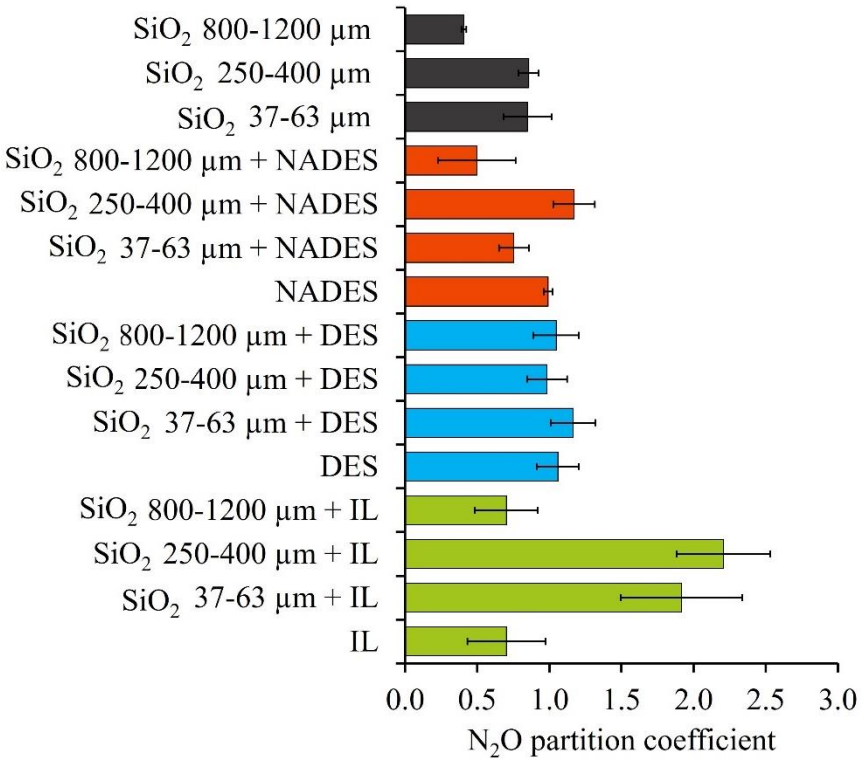

Fig. 4.4 N_2O partition coefficient in solvents and impregnated SiO_2

The N_2O partition coefficient of the three particle sizes impregnated with IL varied from 0.71 to 2.2. Similarly, for the three particle sizes impregnated with DES, the N_2O partition coefficient ranged from 0.98 to 1.16, while for the three particle sizes impregnated with NADES, the N_2O partition coefficient ranged from 0.50 to 1.17. The significant differences among the sorbents used are shown in Figure 4, where no specific trend is observed among particle sizes or differences between the solvents employed and with respect to the bare silica, it was observed no enhancement in the solubility of N_2O in the impregnated silica, given that N_2O partition coefficient of bare silica did not presented significant differences with the N_2O partition coefficient of the rest of the silica impregnated. The lack of enhancement in the impregnation can be attributed to a decrease in the available surface area, pore volume, and pore size of the silica, dueto the high pore blockage caused by the utilized solvents (Ghazali et al., 2020; Mohamedali et al., 2020; Polesso et al., 2019).

The N_2O partition coefficient in the pure solvents exhibited a range from 0.70 to 1.05, while the CO_2 partition coefficient in the pure solvents ranged from 0.61 to 4.4. Among these

solvents, IL displayed the lowest partition coefficient values for both CO_2 and N_2O. Statistical analysis indicated the absence of significant differences between the partition coefficient of CO_2 and N_2O in IL. Conversely, the partition coefficient in NADES demonstrated that N_2O is 2.8 times more soluble in NADES compared to CO_2, and the statistical analysis revealed significant differences between the partition coefficient of CO_2 and N_2O in NADES. Similarly, partition coefficient in DES revealed that N_2O is 4.2 times more soluble in DES than CO_2, with significant differences observed between the partition coefficient values of CO_2 and N_2O. The present study emphasizes the potential reduction in solvent consumption by 60% in CO_2 capture through immobilization in silica, given that the CO_2 partition coefficient of pure solvents and the CO_2 partition coefficient for silica impregnated with solvents presents no significant differences.

Table 4.3 showcases a comparison of CO_2 absorption capacities achieved by different materials impregnated with ILs or DES. In the current study, CO_2 absorption capacities of impregnated silica were found to be lower than those observed by Wu et al., (2022). This disparity comes from the fact that Wu et al. employed a dynamic method, allowing for continuous CO_2 exposure. Ghazali et al., (2020) also recorded higher CO_2 absorption capacities for mesoporous silica gel infused with DES ChCl:U:PEI (1:2:1). This divergence is attributed to those authors utilized a dynamic absorption experiment, enabling saturation as CO_2 flowed through the impregnated material facilitating the increase of CO_2-material contact. Similarly, Polesso et al., (2019) reported elevated CO_2 absorption capacity values when investigating CO_2 sorption in silica impregnated with ILs 1-(3-methylbutyl)-3-methylimidazolium bistrifluoromethanesulfonylimide [mbmim][Tf_2N] and 1-(3-methylbutyl)-3-methylimidazolium bromide. This discrepancy may be due to their experiment was conducted at a higher pressure (0.4 MPa) comparing with the present study which was carried out at 1 atm (0.101 MPa), resulting in enhanced absorption.

The interaction between ILs and CO_2, according to theoretical approaches, suggests that the amount of CO_2 dissolved in ILs is correlated with the spaces between ions, this model is known as the empty space theory. ILs containing larger and less polar ions tend to have weaker ion-ion interactions, leading to bigger empty spaces that enhance CO_2 solubility (Mota-Lima et al., 2021). These larger spaces can also facilitate the dissolution of other

molecules like, other GHGs as N_2O. Consequently, the selectivity of ILs for CO_2 is linked to the control of empty space sizes, while CO_2 solubility is influenced by the volume of inner empty spaces within the ILs (Mota-Lima et al., 2021).

The solubility of CO_2 within DESs can be comprehended through the sorbent's free volume, as evidenced by higher CO_2 solubilities in DESs containing larger cations in comparison to those with smaller cations. This relationship signifies an augmentation in the sorbent's free volume as the chain lengths of the cations extend. The nature of interactions between DES and CO_2 is influenced by the HBD used. Amines and alkanolamines as HBDs lead to chemical absorption, while other HBDs like amides, glycols, sugars, and acids result in physical absorption. Dihydric alcohols with hydroxyl groups closer together exhibit higher CO_2 absorption compared to those with groups further apart. Ethylene groups and greater free volume contribute to higher CO_2 solubility in certain DESs. The strength of interactions between functional groups and CO_2 follows this order: amide > carbonyl group > ether bond > hydroxyl group, except for glycerol-based DESs where CO_2 solubility is higher than carbonyl-based HBD DESs (Cichowska-Kopczyńska et al., 2023).

Even though it is not possible to make direct comparison with other studies regarding N_2O absorption capacities obtained in this study (Table 4.4), it is worth mentioning that Chen et al., (2014) measured the solubility of N_2O in 13 different ILs using an isochoric saturation technique, at pressures near atmospheric level, and observed that the IL [bmim][NTf_2] demonstrated the highest solubility for N_2O, and ILs with anions $[NTf_2]^-$ or bis(pentafluoroethylsulfonyl)imide $[Beti]^-$ exhibited greater N_2O absorption compared to those with other anions. This implies that N_2O solubility increases with the number of fluoroalkyl groups within the anion. They also observed that changes in the cation minimally affected N_2O solubility, while ILs containing fluoroalkyl groups exhibited higher solubility. Additionally, ILs with cations containing an oxygen atom showed improved N_2O solubility compared to cations with only alkyl groups. This is attributed to the smaller volumetric mass of these cations, leading to greater compactness and free volume within the IL, fostering favorable interactions with N_2O. Overall, the results for N_2O solubility mirror those of CO_2. The favorable interaction between the negative charge of fluorine atoms in the anion and the positive charge in N_2O is a common factor. However, this interaction is less pronounced in

N_2O due to its positive charge being distributed between two nitrogen atoms. Consequently, CO_2 generally exhibits higher solubility than N_2O across most ILs (Chen et al., 2014).

Another study, measured N_2O solubilities within imidazolium-based ILs—specifically 1-butyl-3-methylimidazolium tetrafluoroborate ([bmim][BF_4]), 1-butyl-3-methylimidazolium thiocyanate ([bmim][SCN]), 1,3-dimethylimidazolium methylphosphonate ([Dmim][MP]), 1,3-diethoxyimidazolium bis(trifluoromethylsulfonyl)imide ([$(ETO)_2$im][NTf_2]), and 1,3-dihydroxyimidazolium bis(trifluoromethylsulfonyl)imide ([$(OH)_2$im][NTf_2])— at 40°C and 40 bar pressure, and reported N_2O absorption capacities of 44 to 105 grams of gas per kilogram of IL. In this context, [$(ETO)_2$im][Tf_2N] and [bmim][BF_4] emerge as the most efficient ILs as N_2O absorbent (Revelli et al., 2010)

Table 4.3 Comparison of the CO_2 absorption capacity with reported sorbents prepared with the wet impregnation method.

Solvent	Support	Sorbent	T, K	Pressure	Sorption capacity, mg CO_2/g sorbent	Reference
IL	-	IL	298	1 atm	33.0 ± 0.7	This work
IL	SiO_2 37-63 µm	SiO_2 37-63 µm + IL			34.8 ± 0.3	
IL	SiO_2 250-400 µm	SiO_2 250-400 µm +IL			33.4 ± 0.1	
IL	SiO_2 800-1200 µm	SiO_2 800-1200 µm + IL			35.0 ± 0.3	
DES	-	DES			9.8 ± 1.4	
DES	SiO_2 37-63 µm	SiO_2 37-63 µm + DES			9.9 ± 0.1	
DES	SiO_2 250-400 µm	SiO_2 250-400 µm + DES			13.2 ± 4.7	
DES	SiO_2 800-1200 µm	SiO_2 800-1200 µm + DES			15.9 ± 2.0	
NADES	-	NADES			14.5 ± 1.9	
NADES	SiO_2 37-63 µm	SiO_2 37-63 µm + NADES			16.7 ± 0.2	
NADES	SiO_2 250-400 µm	SiO_2 250-400 µm + NADES			16.1 ± 0.8	
NADES	SiO_2 800-1200 µm	SiO_2 800-1200 µm + NADES			19.3 ± 3.7	
-	SiO_2 37-63 µm	SiO_2 37-63 µm			17.6 ± 1.2	
-	SiO_2 250-400 µm	SiO_2 250-400 µm			20.2 ± 3.7	
-	SiO_2 800-1200 µm	SiO_2 800-1200 µm			22.3 ± 2.2	
[mbmim] [Tf_2N] and [mbmim] [Br]	silica (S) and alumina (A)	Alumina (A)	318	0.4 MPa, equilibrium	61.1	Polesso et al., 2019
		A-mbmim[Tf_2N]-10%			52.1	
		A-mbmim[Tf_2N]-20			42.7	
		A-mbmim[Tf_2 N]-30			57.5	
		Silica (S)			81.7	
		S-mbmim[Tf_2 N]-10			56	
		S-mbmim[Tf_2 N]-20			55.8	

Solvent	Support	Sorbent	T, K	Pressure	Sorption capacity, mg CO_2/g sorbent	Reference
		S-mbmim[Tf2 N]-30			45.2	
[C_2OHmim][Lys]	polydivinylbenzene porous spheres GDX-103, less than 200 mesh	GDX-103	313	0.1 MPa	9.68	Wu et al., 2022
		20% [C_2OHmim][Lys]@GDX			27.72	
		30% [C_2OHmim][Lys]@GDX			40.04	
		45% [C_2OHmim][Lys]@GDX			46.2	
		60% [C_2OHmim][Lys]@GDX			56.76	
		70% [C_2OHmim][Lys]@GDX			43.12	
ChCl:U:PEI (1:2:1)	mesoporous silica gel (SG200)	SG200	298	0.1 MPa	20	Ghazali et al., 2020
		5%ChCl:U:PEI/SG200			18	
		10%ChCl:U:PEI/SG200			22	
		15%ChCl:U:PEI/SG200			29	
		20%ChCl:U:PEI/SG200			39	
		25%ChCl:U:PEI/SG200			51	
		24%ChCl:U:PEI/SG200			43	
		22%PEI/SG200			48	

Table 4.4. N_2O absorption capacity obtained with the materials prepared in this work at 298 K and atmospheric pressure.

Solvent	Support	Sorbent	Sorption capacity, mg N_2O/g sorbent
IL	-		30.8 ± 2.8
IL	SiO_2 37-63 µm	SiO_2 37-63 µm + IL	11.4 ± 1.1
IL	SiO_2 250-400 µm	SiO_2 250-400 µm +IL	11.2 ± 3.2
IL	SiO_2 800-1200 µm	SiO_2 800-1200 µm + IL	30.3 ± 1.5
DES	-		25.7 ± 0.9
DES	SiO_2 37-63 µm	SiO_2 37-63 µm + DES	22.5 ± 1.0

Solvent	Support	Sorbent	Sorption capacity, mg N_2O/g sorbent
DES	SiO_2 250-400 µm	SiO_2 250-400 µm + DES	19.2 ± 1.7
DES	SiO_2 800-1200 µm	SiO_2 800-1200 µm + DES	27.7 ± 2.0
NADES	-		29.0 ± 1.6
NADES	SiO_2 37-63 µm	SiO_2 37-63 µm + NADES	28.8 ± 1.2
NADES	SiO_2 250-400 µm	SiO_2 250-400 µm + NADES	24.7 ± 2.3
NADES	SiO_2 800-1200 µm	SiO_2 800-1200 µm + NADES	34.6 ± 6.2
-	SiO_2 37-63 µm		28.4 ± 4.2
-	SiO_2 250-400 µm		18.0 ± 2.7
-	SiO_2 800-1200 µm		37.5 ± 0.8

4.6 Conclusion

The immobilization of solvents in various silica gel particle sizes was successfully achieved through the impregnation-evaporation method, as confirmed by FTIR and TGA analyses. Comparative assessments using pure solvents revealed that IL possess the highest absorption capacity for both CO_2 and N_2O. Notably, no significant differences were observed in the partition coefficient of CO_2 and N_2O among the different particle sizes of silica gel impregnated with IL, DES, or NADES. These findings accentuate the impregnation process's ability to reduce solvent consumption by 60% while preserving the greenhouse gas capture capacity. Consequently, this approach holds promise for mitigating the presence of greenhouse gases, such as CO_2 and N_2O under atmospheric pressure and room temperature conditions.

4.7 Perspectives

Several lines of research to enhance the CO_2 and N_2O capture process can be proposed. Firstly, there is a need to investigate the recyclability of the utilized solvents in order to identify more sustainable and environmentally friendly alternatives. Furthermore, the exploration of different combinations of cations and anions in ILs and an examination of the properties of HBD and HBA components in DES and NADES are recommended to identify options with higher GHG solubility, higher thermal stability, lower viscosity, and cost-effectiveness. Moreover, it is advised to analyze the impact of different degrees of impregnation on the physical and thermal stability, as well as the solubility of greenhouse gases. Additionally, another impregnation or grafting methods utilizing ILs, DES, and NADES can also be explored. Another area of interest involves studying alternative support materials derived from waste to efficiently recycle resources and optimize the process. It's also important to assess the recyclability of this material, through absorption-desorption cycles. Lastly, it is crucial to investigate the GHG capture in a continuous process, carefully assessing its long-term viability and effectiveness.

.

4.8 References

Chen, Y., Mutelet, F., & Jaubert, J. N. (2014). Solubility of carbon dioxide, nitrous oxide and methane in ionic liquids at pressures close to atmospheric. *Fluid Phase Equilibria*, *372*, 26–33. https://doi.org/10.1016/j.fluid.2014.03.015

Cichowska-Kopczyńska, I., Nowosieslki, B., & Warminska, D. (2023). Deep eutectic solvents: Preparation, properties and applications. *Molecules*, 1–30. https://doi.org/https:// doi.org/10.3390/molecules28145293

Elghniji, K., Virlan, C., Elaloui, E., & Pui, A. (2018). Synthesis, characterization of SiO2 supported-industrial phosphoric acid catalyst for hydrolysis of NaBH4 solution. *Phosphorus, Sulfur and Silicon and the Related Elements*, *193*(12), 806–821. https://doi.org/10.1080/10426507.2018.1515946

Ghazali, Z., Suhaili, N., Tahari, M. N. A., Yarmo, M. A., Hassan, N. H., & Othaman, R. (2020). Impregnating deep eutectic solvent choline chloride:urea:polyethyleneimine onto mesoporous silica gel for carbon dioxide capture. *Journal of Materials Research and Technology*, *9*(3), 3249–3260. https://doi.org/10.1016/j.jmrt.2020.01.073

Hamoudi, A., Khouchaf, L., Depecker, C., Revel, B., Montagne, L., & Cordier, P. (2008). Microstructural evolution of amorphous silica following alkali-silica reaction. *Journal of Non-Crystalline Solids*, *354*(45–46), 5074–5078. https://doi.org/10.1016/j.jnoncrysol.2008.07.001

Hasib-ur-Rahman, M., Siaj, M., & Larachi, F. (2010). Ionic liquids for CO2 capture-Development and progress. *Chemical Engineering and Processing: Process Intensification*, *49*(4), 313–322. https://doi.org/10.1016/j.cep.2010.03.008

Janiczek, P., Kalb, R. S., Thonhauser, G., & Gamse, T. (2012). Carbon dioxide absorption in a technical-scale-plant utilizing an imidazolium based ionic liquid. *Separation and Purification Technology*, *97*, 20–25. https://doi.org/10.1016/j.seppur.2012.03.003

Liu, Y., Guo, Y., Zhu, Y., An, D., Gao, W., Wang, Z., Ma, Y., & Wang, Z. (2011). A sustainable route for the preparation of activated carbon and silica from rice husk ash. *Journal of Hazardous Materials*, *186*(2–3), 1314–1319. https://doi.org/10.1016/j.jhazmat.2010.12.007

Lu, P., & Hsieh, Y. Lo. (2012). Highly pure amorphous silica nano-disks from rice straw. *Powder Technology*, *225*, 149–155. https://doi.org/10.1016/j.powtec.2012.04.002

Makoś, P., Słupek, E., & Małachowska, A. (2020). Silica gel impregnated by deep eutectic solvents for adsorptive removal of BTEX from Gas Streams. *Materials*, *13*(8). https://doi.org/10.3390/MA13081894

Mohamedali, M., Ibrahim, H., & Henni, A. (2020). Imidazolium based ionic liquids confined into mesoporous silica MCM-41 and SBA-15 for carbon dioxide capture. *Microporous and Mesoporous Materials*, *294*(November 2019), 109916. https://doi.org/10.1016/j.micromeso.2019.109916

Mota-Lima, A., Alcantara, M. L., Pérez-Sanz, F. J., Bazito, R. C., Vidinha, P., Alves, R. M. B., & Oller Nascimento, C. A. (2021). Review—High-Pressure Carbon Dioxide Separation Using Ionic Liquids: A CO 2 -Electrocatalysis Perspective . *Journal of The Electrochemical Society*, *168*(8), 086502. https://doi.org/10.1149/1945-7111/ac085d

Okoronkwo, E. A., Imoisili, P. E., & Olisunle, S. O. O. (2013). Extraction and characterization of Amorphous Silica from Corn Cob Ash by Sol-Gel Method | Okoronkwo | Chemistry and Materials Research. *Chemistry and Material Research*, *3*(4), 68–72.

Polesso, B. B., Duczinski, R., Bernard, F. L., Ferrari, H. Z., Da Luz, M., Vecchia, F. D., De Menezes, S. M. C., & Einloft, S. (2019). Imidazolium-based ionic liquids impregnated in silica and alumina supports for CO2 capture. *Materials Research*, *22*(suppl 1), 1–10. https://doi.org/10.1590/1980-5373-MR-2018-0810

Revelli, A. L., Mutelet, F., & Jaubert, J. N. (2010). Reducing of nitrous oxide emissions using ionic liquids. *Journal of Physical Chemistry B*, *114*(24), 8199–8206. https://doi.org/10.1021/jp103734c

Salar-García, M. J., Ortiz-Martínez, V. M., Hernández-Fernández, F. J., de los Ríos, A. P., & Quesada-Medina,

J. (2017). Ionic liquid technology to recover volatile organic compounds (VOCs). In *Journal of Hazardous Materials* (Vol. 321, pp. 484–499). Elsevier B.V. https://doi.org/10.1016/j.jhazmat.2016.09.040

Sistla, Y. S., Jain, L., & Khanna, A. (2012). Validation and prediction of solubility parameters of ionic liquids for CO 2 capture. *Separation and Purification Technology*, *97*, 51–64. https://doi.org/10.1016/j.seppur.2012.01.050

Velmurugan, P., Shim, J., Lee, K. J., Cho, M., Lim, S. S., Seo, S. K., Cho, K. M., Bang, K. S., & Oh, B. T. (2015). Extraction, characterization, and catalytic potential of amorphous silica from corn cobs by sol-gel method. *Journal of Industrial and Engineering Chemistry*, *29*, 298–303. https://doi.org/10.1016/j.jiec.2015.04.009

Wu, J., Yang, Z., Xie, J., Zhu, P., Wei, J., Jin, R., & Yang, H. (2022). Porous Polymer Supported Amino Functionalized Ionic Liquid for Effective CO2 Capture. *Langmuir*. https://doi.org/10.1021/acs.langmuir.2c03217

Zareie-kordshouli, F., Lashani-zadehgan, A., & Darvishi, P. (2016). Comparative evaluation of CO2 capture from flue gas by [Emim][Ac] ionic liquid, aqueous potassium carbonate (without activator) and MEA solutions in a packed column. *International Journal of Greenhouse Gas Control*, *52*, 305–318. https://doi.org/10.1016/j.ijggc.2016.07.014

Zhang, Q., De Oliveira Vigier, K., Royer, S., & Jérôme, F. (2012). Deep eutectic solvents: Syntheses, properties and applications. In *Chemical Society Reviews* (Vol. 41, Issue 21, pp. 7108–7146). https://doi.org/10.1039/c2cs35178a

Zhang, Z., Wu, L., Dong, J., Li, B. G., & Zhu, S. (2009). Preparation and so2 sorption/desorption behavior of an ionic liquid supported on porous silica particles. *Industrial and Engineering Chemistry Research*, *48*(4), 2142–2148. https://doi.org/10.1021/ie801165u

5. Greenhouse gases solubility in fluorinated imidazolium-based ionic liquids: a computational modeling approach

5.1 Abstract

This study focuses on using molecular dynamics simulations to investigate the behavior of gases, particularly CO_2 and N_2O, in fluorinated imidazolium-based ionic liquids. The research primarily concentrates on hydrophobic anions such as [NTf_2], [PF_6], and [FAP] for greenhouse gas (GHG) reduction. The objective is to assess the potential of ILs for absorbing CO_2 and N_2O. The simulations calculate the density of various fluorinated imidazolium ILs and compare the results with experimental data to validate the selected force field. The percentage errors range from 0.61% to 8.66%, indicating a reasonable approximation of experimental density values, although with some variability. The energy interaction calculations between ion-CO_2 and ion N_2O reveal that [NTf_2] anion exhibits higher interaction energies with both CO_2 and N_2O compared to other anions or cations, suggesting its potential effectiveness for gas absorption. ILs containing the [PF_6] anion show lower Henry's law constants for CO_2, indicating their superior capacity for absorbing CO_2. Among the ILs studied, [C_6mim][FAP] demonstrates lower Henry's law constants for N_2O, highlighting its superiority as an absorbent. The study finds no significant correlation between the length of the alkyl chain in the cation and the gas absorption properties, implying that other factors, such as the anion and its interaction with the gas molecules, play a more prominent role. These findings underscore the complex nature of gas-IL interactions, emphasizing the need for further exploration and understanding of the underlying mechanisms.

5.2 Graphical abstract

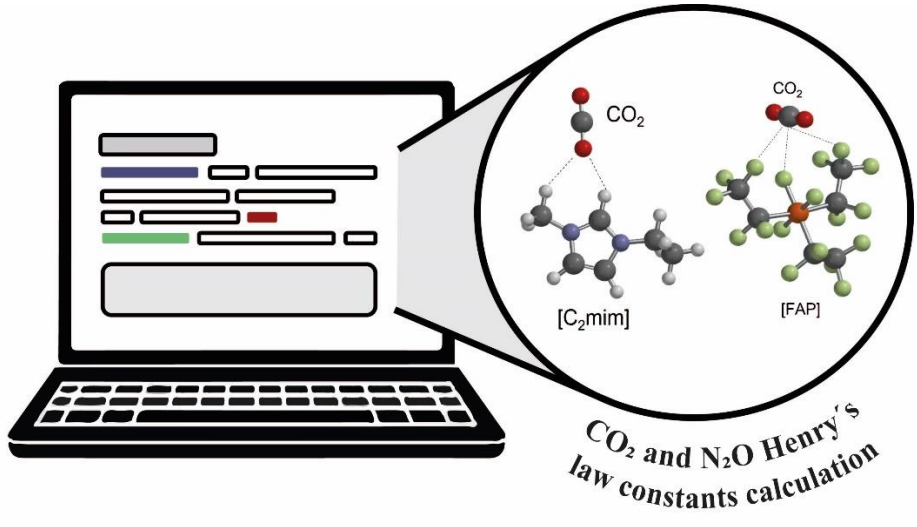

5.3 Introduction

The unregulated release of greenhouse gases such as carbon dioxide (CO_2), and nitrous oxide (N_2O) is causing a rapid increase in global warming. Since the industrial revolution, greenhouse gas emissions have been steadily rising, with CO_2 being recognized as the main contributor. Various human activities, including transportation, electricity production, industries, residential and commercial sectors, agriculture, as well as land use and forestry, contribute significantly to overall greenhouse gas emissions (Xiao & Gao, 2021). N_2O, although an inert gas, is 300 times more potent as a greenhouse gas than CO_2 and contributes 6% to the total anthropogenic radiative forcing. It remains in the atmosphere for over 100 years before natural destruction occurs. The major natural sources of N_2O are microbial denitrification and nitrification processes in oceans and tropical soils, accounting for approximately 80% of the global N_2O present in the atmosphere. However, the application of nitrogen-based fertilizers in agriculture has become a crucial and increasing source of N_2O emissions due to intensive agricultural practices (Sonwani & Saxena, 2022). Ionic liquids (ILs) possess distinct physical and chemical properties, such as negligible vapor pressure, high thermal stability, and the ability to be customized for specific purposes, making them highly suitable for gas separation. Previous studies have examined the solubility of CO_2 in various ILs, including fluorinated ILs like 1-octyl-3-methylimidazolium

bis[trifluoromethylsulfonyl]amide ([C_8mim][Ntf_2]) and 1-decyl-3-methylimidazolium bis[trifluoromethylsulfonyl]amide ([C_{10}mim][Ntf_2]) (Almantariotis et al., 2010, 2017) and CO_2 and N_2O solubility has been studied in imidazolium ILs ($C_n$mim, n = 2,4,6) with tris(pentafluoroethyl)-trifluorophosphate (FAP) anion by Almantariotis et al., (2012). Aghaie et al., (2018) reported that imidazolium-based ILs with fluorinated anions such as tetrafluoroborate $[BF_4]^-$, tris(pentafluoroethyl)trifluorophosphate $[FAP]^-$, and hexafluorophosphate $[PF_6]^-$, have shown highest CO_2 solubility. The enhanced CO_2 solubility can be attributed to the increased free volume resulting from longer alkyl chains on the cation and higher fluorination levels on the anion. For instance, the IL 1-hexyl-3-methylimidazolium tris(pentafluoroethyl) trifluorophosphate ([C_6mim][FAP]) exhibits 70% greater CO_2 solubility compared to [C_6mim][PF_6], attributed to the presence of six CF_2/CF_3 groups in $[FAP]^-$, which leads to a larger free volume. Weak interactions such as hydrogen and halogen bonding also influence CO_2 absorption. The capture mechanism of CO_2 in [C_6mim][PF_6] and [FAP] highlights the significance of electrostatic interactions in smaller and symmetrical [PF_6] anions, while van der Waals interactions play a key role in larger and asymmetrical [FAP] anions (Shukla et al., 2019).

The use of computational methods have been employed to describe the behavior of the molecules, these methods can be categorized as follows: molecular mechanics (MM), ab initio calculations, semiempirical calculations, density functional calculations (DFT) and molecular dynamics (MD). MM models molecules as atoms connected by springs (bonds). Knowing spring lengths, angles, and spring energy, energy calculations are done, and geometry optimization finds the lowest energy arrangement. Ab initio calculations comes from the Schrödinger equation which explain the electron behavior. This reveals molecular polarity and susceptibility to attacks by nucleophiles or electrophiles. Semiempirical calculations, also, utilize the Schrödinger equation whichcompile experimental data obtained by fitting calculated measures like geometry or energy. This process, termed parameterization, combines theory and experiment. While rooted in the Schrödinger equation, semiempirical methods are parameterized with empirical data. Density functional calculations (DFT) are built upon the Schrödinger equation, like ab initio and semiempirical methods. However, DFT diverges by the deriving electron distribution (electron density function) instead of a traditional wavefunction. This involves mathematical entities known

as functionals. DFT models are generally faster than ab initio but slower than semiempirical calculations. DFT's emergence is relatively recent (serious computational chemistry using DFT began in the 1980s, later than ab initio and semiempirical approaches in the 1960s). MD calculations employ physics principles to model molecular motion. This allows simulating processes such as the movement of water molecules around solute molecules, and even chemical reactions through the quantum molecular dynamics (Lewars, 2011).

Molecular dynamics (MD) have been employed to forecast the phase behavior of gas-IL systems across different temperatures and pressures (Aghaie et al., 2020; Almantariotis et al., 2010; Silveira et al., 2019; Tiwikrama et al., 2020)(Zhang et al., 2009). These simulation methods prove valuable in cases where experimental data is limited or unavailable. This approach is useful in estimating gas solubility, particularly when conflicting experimental data exists (Mellein et al., 2021). Simulations offer the advantage of providing insights into the interaction and behavior of gases within the IL medium. Due to the predominant focus on screening ILs for CO_2 capture, there is limited research available regarding the screening of ILs for N_2O. Besides most commonly hydrophobic anions such as [NTf_2], [PF_6] and [FAP] are the center of the study for GHGs, as a result, the main objective of this work is to study the molecular dynamics simulation of ILs for the reduction of GHGs including CO_2, and N_2O. For this purpose, a selection of four imidazolium cations ($C_n$mim=2,4,6,8) and three anions ([PF_6], [NTf_2] and [FAP]) were chosen.

5.4 Computational methods

Interaction energy calculations. Quantum chemistry calculations have been performed using the Spartan'20 program, version 1.1.2. The optimized structures of ions and ion-CO_2, ion-N_2O ion pairs were obtained using DFT with the B3LYP-D3 functional and the 6-311+G** basis set. The force-field parameters for $[C_n mim]^+$,$[PF_6]^-$, $[NTf_2]^-$, and $[FAP]^-$ were taken from the OPLS-AA force-field, developed by Doherty et al., (2017). The interaction energies (E_{int}) were evaluated. The interaction energy (E_{int}) is defined in equation 1 as the total energy of the relaxed complex ($E_{complex}$) minus the sum of the energies of the isolated ion and CO_2 or N_2O molecule (E_{ion}* and E_{CO2}*, respectively) corresponding to the geometries of these species obtained from the ion-CO_2 or ion-N_2O pair (X. Liu et al., 2021).

$$E_{int} = E_{complex} - (E_{ion}^* + E_{CO2}^*) \qquad \text{(Equation 1)}$$

Density. Molecular dynamic (MD) simulations were performed using Tinker 8.10 software package. Cubic boxes containing 50 ion pairs were constructed using the program Packmol. Boxes were minimized using a steepest descent algorithm for X steps. Periodic boundary conditions were applied to each box with long-range interactions handled with Particle-Mesh Ewald summations. Equations of motion were integrated using the leapfrog algorithm with a time step of 1 fs. The temperature value of 298 K was kept constant using velocity rescaling with a stochastic term (v-rescale) and a constant pressure of 1.0 bar was maintained with the Berendsen coupling during an isothermal−isobaric ensemble (NPT) simulation for 5 ns of equilibration.

CO_2 and N_2O Henry's law constant prediction. Molecular dynamic (MD) simulations were performed using Tinker 8.10 software package. A two-phase box that consists of the IL (100 ion pairs) in the middle of the simulation box, with CO_2 (40 molecules) on either side was constructed using the program Packmol. The IL box is extended in the positive and negative z-directions by 3.7 nm; thus, the cell dimensions are 3.7 nm × 3.7 nm × 20 nm in the x, y, and z directions, respectively. The CO_2 molecules diffuse in the gas phase, transfer across the interface, and diffuse through the liquid bulk.

Boxes were minimized using a steepest descent algorithm for X steps. Periodic boundary conditions were applied to each box with long-range interactions handled with Particle-Mesh Ewald summations. Equations of motion were integrated using the leapfrog algorithm with a time step of 1 fs. The temperature value of 298 K was kept constant using velocity rescaling with a stochastic term (v-rescale) and a constant pressure of 1.0 bar was maintained with the Berendsen coupling during an isothermal−isobaric ensemble (NPT) simulation for 10 ns of equilibration.

5.5 Results and Discussion

5.5.1 Optimization of molecular geometry

DFT calculations were performed to assess the affinity of CO_2 or N_2O with different cations [$C_n$mim] and anions ([PF_6], [NTf_2], [FAP]). To identify the most probable sorption sites for CO_2 or N_2O on the ions, the structures of the different ions and their complexes with CO_2 or N_2O were optimized. Additionally, to obtain the most stable geometries, the [C_2mim] cation was used as a model and CO_2 was positioned at different locations around the cation (Fig. 5.1). The position that yielded the lowest interaction energy was chosen for further optimization of the remaining [$C_n$mim]-CO_2 pairs. This is because a lower complex energy indicates a preference for existing as a complex (ion-CO_2) rather than as a single ion or a

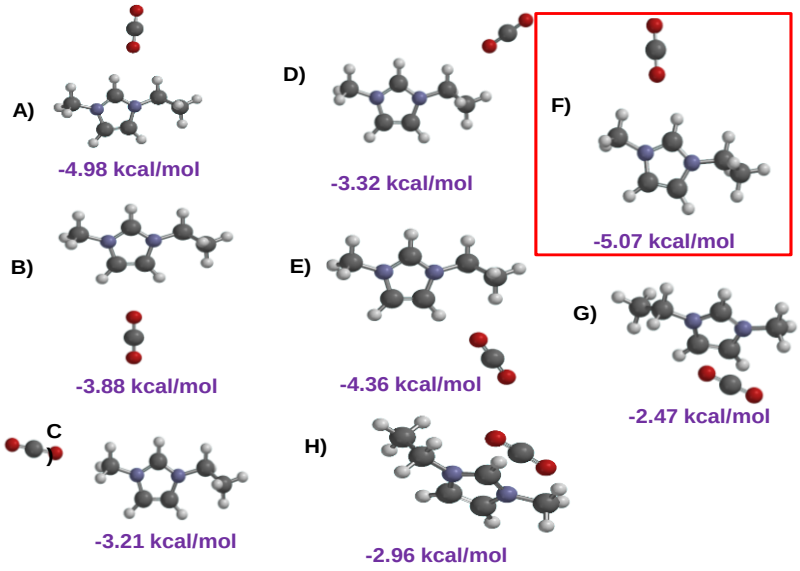

Fig. 5.1 Optimized structures of CO_2 absorbed on the [C_2mim] cation and their interaction energies. In the figure, red=oxygen, white=hydrogen, gray=carbon, and blue=nitrogen

Fig. 5.2 shows the calculated interaction energy values for different ion-CO_2 and ion-N_2O pairs, where it can be observed that the lowest interaction energy and therefore the highest affinity is obtained for the pairs formed with $[NTF_2]^-$, with values of -8.20 and -7.20 kcal/mol for CO_2 and N_2O, respectively. Similarly, it is observed that the interaction energy values are lower for the anions compared to the cations, both for CO_2 and N_2O, indicating that these molecules would prefer to interact with the anion rather than the cation in an ionic liquid.

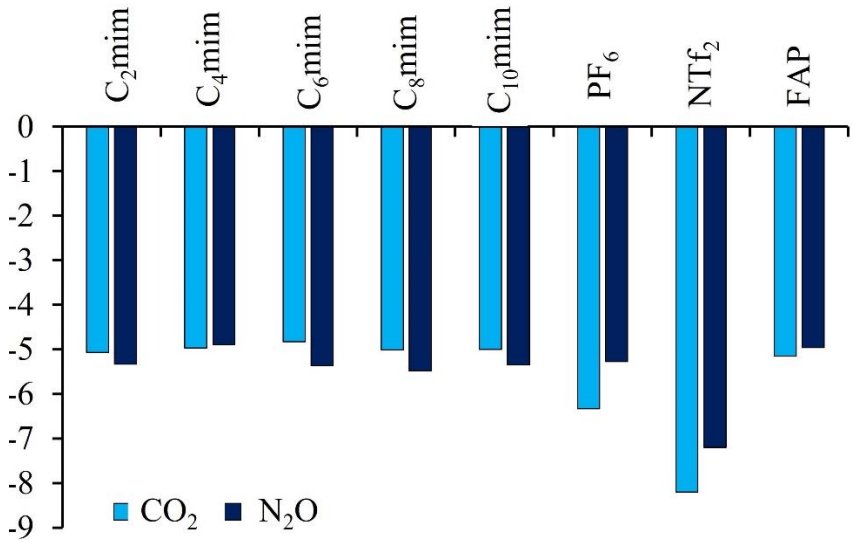

Fig. 5.2 Interaction energies for different ion-CO_2 pairs and different ion-N_2O pairs were calculated using DFT B3LYP-D3 with the 6-311+G** basis set.

5.5.2 Density

The densities of pure ILs were computed using MD simulations. These predictions were then compared to experimental values to assess the suitability of the OPLS-AA force-fields for ILs taken from Doherty et al., (2017). The densities were determined using the NPT ensemble at a temperature of 298 K, and the experimental density data for ILs were obtained from existing literature. A comparison of the experimental and computed density values is presented in Table 5.1, where the error magnitude (%E) was calculated using the following expression:

$$\%E = \left| \text{Density exp} - \text{Density calc} \right| / \text{Density exp} * 100 \qquad \text{(Equation 2)}$$

The calculated density values ranged from 1.207 to 1.582 g/mL and the average %E between the calculated and experimental densities was 3.6%. For the ILs with $[PF_6]^-$ the %E varied from 1.6% to 4.7% and for the ILs with $[NTf_2]^-$ the %E varied from 0.6 to 2.8. The highest error values were observed for ionic liquids containing $[FAP]^-$ (4.4 % to 8.7%). This %E for density calculation of imidazolium based ionic liquids with $[PF_6]^-$ and $[NTf_2]^-$ are similar to those obtained by Doherty et al., (2017) which varied from 3.5% to 4.7%. The density results imply that the OPLS-AA force-field taken from Doherty et al., (2017) used for the simulations is appropriate.

Table 5.1 Comparison between calculated and experimental density values for different fluorinated imidazolium-based ionic liquids. .

Ionic liquid	Density calc., g/mL	Density exp., g/mL	Error, %	T, K	Reference
[C_2mim][PF_6]	1.391	1.413	1.6	-	Marcus, 2016
[C_4mim][PF_6]	1.324	1.364	3.1	-	Marcus, 2016
		1.360		-	Guillermo Quijano et al., 2011a
		1.370		292.9	Jacquemin et al., 2006
		1.369		293.2	Jacquemin et al., 2008
[C_6mim][PF_6]	1.236	1.297	4.7	293.2	Ignat'ev et al., 2005
[C_8mim][PF_6]	1.207	1.251	3.5	-	Sambasivarao & Acevedo, 2009
[C_2mim][NTf_2]	1.562	1.513	2.8	-	Marcus, 2016
		1.523		292.8	Jacquemin et al, 2006
		1.523		293.2	Jacquemin et al., 2008
[C_4mim][NTf_2]	1.475	1.437	2.4		Marcus, 2016
		1.443		292.9	Jacquemin et al, 2006
		1.443		293.2	Jacquemin et al., 2008
[C_6mim][NTf_2]	1.398	1.371	1.8	-	Marcus, 2016
		1.375		293.2	Jacquemin et al., 2008
[C_8mim][NTF_2]	1.330	1.320	0.6	-	Marcus, 2016
		1.321		298.2	Zaitsau et al., 2006
		1.324		293.2	Jacquemin et al., 2008
[C_2mim][FAP]	1.582	1.732	8.7	278	Nazet et al., 2015
[C_4mim][FAP]	1.511	1.619	6.7	303	Voroshylova et al., 2018
[C_6mim][FAP]	1.489	1.557	4.4	293.2	Jacquemin et al., 2008
		1.556		293.2	Ge & Lee, 2015
		1.560		293.2	Ignat'ev et al., 2005
[C_8mim][FAP]	1.403	-	-	-	-

Table 5.3 presents a comparison between the calculated and experimental CO_2 and N_2O Henry's law constants in different fluorinated imidazolium-based ionic liquids. Error values were calculated using Eq. 2. The %E was only calculated for those ILs where the experimental Henry's constant was obtained at the same temperature. The highest %E was observed for ILs with [FAP]-, which makes sense given that the %E obtained for density also showed the highest %E. For CO_2 Henry's law constants in $[PF_6]^-$ and $[NTf_2]^-$, %E varied from 26.2 to 35.2, which is consistent with the findings reported by Silveira et al., (2019)when

studying different molecular models for CO_2 Henry's constant prediction in [emim] $[B(CN)_4]$ and [emim] $[NTf_2]$, where they obtained %E values ranging from 2.8 to 38.9.

Regarding the predicted CO_2 and N_2O Henry's law constant we can observed that CO_2 Henry's law constants values ranged from 3.38 to 4.94 MPa and the ILs with $[PF_6]^-$ exhibited lower Henry's law constants values, making them better absorbents compared to ionic liquids with $[NTf_2]^-$ and $[FAP]^-$, given that lower values of the Henry's law constants indicate higher gas solubility in the ionic liquid.

Table 5.2 Comparison between calculated and experimental Henry's law constants for CO_2 and N_2O in different fluorinated imidazolium-based ionic liquids. Calculated values were obtained at 298 K. Between parenthesis is the temperature (K) at which was obtained the experimental value.

Gas	Ionic liquid	Calculated Henry's law constant, MPa	Experimental Henry's law constant, MPa	% E	Reference
CO_2	$[C_2mim][PF_6]$	4.50	-	-	
	$[C_4mim][PF_6]$	3.94	5.34 (298)	26.2	Sarmad et al., 2016
	$[C_6mim][PF_6]$	3.69	-	-	
	$[C_8mim][PF_6]$	3.38	-	-	
	$[C_2mim][NTf_2]$	4.94	3.18 (298) 3.56 (298)	46.7	Sarmad et al., 2016 Sarmad et al., 2016
	$[C_4mim][NTf_2]$	4.28	3.3 (298) 3.43 (298)	29.6	Sarmad et al., 2016 Hasib-ur-Rahman et al., (2010)
	$[C_6mim][NTf_2]$	4.88	3.16 (298)	35.2	Sarmad et al., 2016
	$[C_8mim][NTf_2]$	4.55	-	-	
	$[C_2mim][FAP]$	4.79	2.97 (303)		Almantariotis et al., (2012)
	$[C_4mim][FAP]$	4.76	2.5 (303)		Almantariotis et al., (2012)
	$[C_6mim][FAP]$	4.81	2.28 (298) 2.51 (298)	100.9	Sarmad et al., 2016 Almantariotis et al., (2012)
	$[C_8mim][FAP]$	3.48	3.29 (313)		Sarmad et al., 2016
N_2O	$[C_2mim][PF_6]$	6.52	-	-	
	$[C_4mim][PF_6]$	4.82	-	-	
	$[C_6mim][PF_6]$	5.04	-	-	
	$[C_8mim][PF_6]$	4.37	-	-	

Gas	Ionic liquid	Calculated Henry's law constant, MPa	Experimental Henry's law constant, MPa	% E	Reference
	$[C_2mim][NTf_2]$	4.49	-	-	
	$[C_4mim][NTf_2]$	4.74	-	-	
	$[C_6mim][NTf_2]$	4.37	-	-	
	$[C_8mim][NTf_2]$	4.45	-	-	
	$[C_2mim][FAP]$	4.95	2.87 (303)		Almantariotis et al., (2012)
	$[C_4mim][FAP]$	4.80	2.37 (303)		Almantariotis et al., (2012)
	$[C_6mim][FAP]$	3.53	2.34 (303)		Almantariotis et al., (2012)
	$[C_8mim][FAP]$	3.84	-	-	

Fig. 5.2 A) illustrates the relationship between the number of carbons in the alkyl chain of the cation and the Henry's law constants value for CO_2. Only for ionic liquids with $[PF_6]^-$, an R^2 value of 0.966 was obtained, indicating that a higher number of carbons in the alkyl chain of the imidazolium cation corresponds to a lower value of the CO_2 Henry's law constants and thus a higher solubility of CO_2 in the ionic liquid. For N_2O, the Henry's law constants values ranged from 3.53 to 6.52 MPa. The ionic liquid $[C_6mim][$ FAP] exhibited lower Henry's law constants values for N_2O, suggesting this would be the best absorbent among the other ionic liquids. Fig. 5.2 shows the relationship between the number of carbons in the alkyl chain of the cation and the Henry's law constants value for N_2O. However, no correlation was found between the number of carbons of the alkyl chain of the cation and the Henry's law constants, since the highest R^2 was obtained for ionic liquids with $[PF_6]^-$ with a value of 0.74

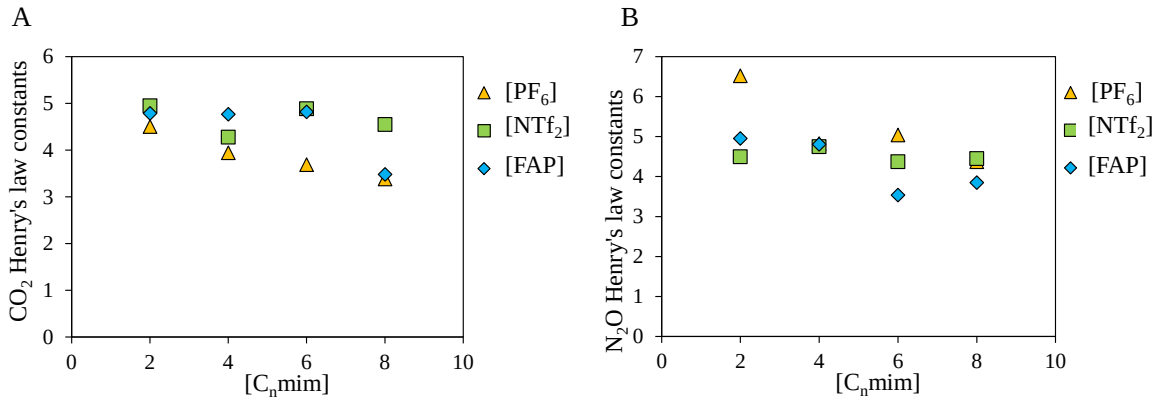

Fig. 5.1 Relation between the number of carbons in the alkyl chain of the imidazolium cation versus the Henry's law constants for CO_2 (A) and for N_2O (B)

5.6 Conclusion

Molecular dynamics simulations were employed to calculate the density of various fluorinated imidazolium ionic liquids. A comparison with experimental data revealed a range of percentage errors, ranging from 0.61% to 8.66%. These results demonstrate the ability of the simulations to reasonably approximate the density values observed experimentally, albeit with a certain degree of variability. The energy interaction calculated between ion-CO_2 and ion-N_2O suggested that both CO_2 and N_2O exhibited higher interaction energies with $[NTf_2]^-$ compared to other anions or cations used ($[PF_6]$ and [FAP]). This finding implies that ILs containing $[NTf_2]^-$ have the potential to be effective for the absorption of CO_2 and N_2O. Ionic liquids containing the $[PF_6]^-$ anion demonstrated lower Henry's law constants for CO_2, indicating their superior capacity for absorbing CO_2 compared to ionic liquids with $[NTf_2]^-$ and $[FAP]^-$. The low Henry's law constants obtained with the $[PF_6]$-based ionic liquids suggest a high affinity for CO_2 , thus, this IL could be more efficient to capture and retain CO_2. Among the various ionic liquids studied, $[C_6mim]$[FAP] demonstrated low Henry's law constants for N_2O, indicating its higher potential to absorb N_2O than $[PF_6]$-based ILs. In the investigation of numerous ionic liquids, no significant correlation was observed between the number of carbon atoms in the alkyl chain of the cation and the Henry's law constants. Other factors such as the nature of the anion, cation, and their respective interactions with the gas molecules may have a more prominent role in determining the gas absorption properties of the ionic liquids studied. These findings emphasize the complex and multifaceted nature of gas-IL interactions, urging further exploration and understanding of the underlying mechanisms governing these interactions.

5.7 References

Aghaie, M., Rezaei, N., & Zendehboudi, S. (2018). A systematic review on CO2 capture with ionic liquids: Current status and future prospects. *Renewable and Sustainable Energy Reviews*, *96*(December 2017), 502–525. https://doi.org/10.1016/j.rser.2018.07.004

Aghaie, M., Rezaei, N., & Zendehboudi, S. (2020). New insights into bulk and interface properties of [Bmim][Ac]/[Bmim][BF4] ionic liquid/CO2 systems — Molecular dynamics simulation approach. *Journal of Molecular Liquids*, *317*, 113497. https://doi.org/10.1016/j.molliq.2020.113497

Almantariotis, D., Gefflaut, T., Pádua, A. A. H., Coxam, J. Y., & Costa Gomes, M. F. (2010). Effect of fluorination and size of the alkyl side-Chain on the solubility of carbon dioxide in 1-alkyl-3-methylimidazolium bis(trifluoromethylsulfonyl) amide ionic liquids. *Journal of Physical Chemistry B*, *114*(10), 3608–3617. https://doi.org/10.1021/jp912176n

Almantariotis, D., Pensado, A. S., Gunaratne, H. Q. N., Hardacre, C., Pádua, A. A. H., Coxam, J. Y., & Costa Gomes, M. F. (2017). Influence of fluorination on the solubilities of carbon dioxide, ethane, and nitrogen in 1-n-fluoro-alkyl-3-methylimidazolium bis(n-fluoroalkylsulfonyl)amide ionic liquids. *Journal of Physical Chemistry A*, *121*(2), 426–436. https://doi.org/10.1021/acs.jpcb.6b10301

Almantariotis, D., Stevanovic, S., Fandiño, O., Pensado, A. S., Padua, A. A. H., Coxam, J. Y., & Costa Gomes, M. F. (2012). Absorption of carbon dioxide, nitrous oxide, ethane and nitrogen by 1-alkyl-3-methylimidazolium (Cnmim, n = 2,4,6) tris(pentafluoroethyl) trifluorophosphate ionic Liquids (eFAP). *Journal of Physical Chemistry B*, *116*(26), 7728–7738. https://doi.org/10.1021/jp304501p

Doherty, B., Zhong, X., Gathiaka, S., Li, B., & Acevedo, O. (2017). Revisiting OPLS Force Field Parameters for Ionic Liquid Simulations. *Journal of Chemical Theory and Computation*, *13*(12), 6131–6135. https://doi.org/10.1021/acs.jctc.7b00520

Ge, D., & Lee, H. K. (2015). Ultra-hydrophobic ionic liquid 1-hexyl-3-methylimidazolium tris(pentafluoroethyl)trifluorophosphate supported hollow-fiber membrane liquid-liquid-liquid microextraction of chlorophenols. *Talanta*, *132*, 132–136. https://doi.org/10.1016/j.talanta.2014.08.074

Hasib-ur-Rahman, M., Siaj, M., & Larachi, F. (2010). Ionic liquids for CO2 capture-Development and progress. *Chemical Engineering and Processing: Process Intensification*, *49*(4), 313–322. https://doi.org/10.1016/j.cep.2010.03.008

Ignat'ev, N. V., Welz-Biermann, U., Kucheryna, A., Bissky, G., & Willner, H. (2005). New ionic liquids with tris(perfluoroalkyl)trifluorophosphate (FAP) anions. *Journal of Fluorine Chemistry*, *126*(8), 1150–1159. https://doi.org/10.1016/j.jfluchem.2005.04.017

Jacquemin, J., Ge, R., Nancarrow, P., Rooney, D. W., Costa Gomes, M. F., Padua, A. A. H., & Hardacre, C. (2008). Prediction of ionic liquid properties. I. Volumetric properties as a function of temperature at 0.1 MPa (Journal of Chemical and Engineering Data (2008) 55 (716-726)). *Journal of Chemical and Engineering Data*, *53*(10), 2473. https://doi.org/10.1021/je800620s

Jacquemin, J., Husson, P., Padua, A. A. H., & Majer, V. (2006). *Density and viscosity of several pure and water-saturated ionic liquids*. 172–180. https://doi.org/10.1039/b513231b

Lewars, E. G. (2011). Computational chemistry: Introduction to the theory and applications of molecular and quantum mechanics. *Computational Chemistry: Introduction to the Theory and Applications of Molecular and Quantum Mechanics*, *1492*, 1–664. https://doi.org/10.1007/978-90-481-3862-3

Liu, X., O'Harra, K. E., Bara, J. E., & Turner, C. H. (2021). Solubility Behavior of CO2in Ionic Liquids Based on Ionic Polarity Index Analyses. *Journal of Physical Chemistry B*, *125*(14), 3665–3676. https://doi.org/10.1021/acs.jpcb.1c01508

Marcus, Y. (2016). *Ionic Liquid Properties*. Springer International Publishing. https://doi.org/10.1007/978-3-319-30313-0

Mellein, B. R., Scurto, A. M., & Shiflett, M. B. (2021). Gas solubility in ionic liquids. *Current Opinion in Green and Sustainable Chemistry*, *28*(4), 100425. https://doi.org/10.1016/j.cogsc.2020.100425

Nazet, A., Sokolov, S., Sonnleitner, T., Makino, T., Kanakubo, M., & Buchner, R. (2015). Densities, Viscosities, and Conductivities of the Imidazolium Ionic Liquids [Emim][Ac], [Emim][FAP], [Bmim][BETI], [Bmim][FSI], [Hmim][TFSI], and [Omim][TFSI]. *Journal of Chemical and Engineering Data*, *60*(8), 2400–2411. https://doi.org/10.1021/acs.jced.5b00285

Sambasivarao, S. V., & Acevedo, O. (2009). Development of OPLS-AA force field parameters for 68 unique ionic liquids. *Journal of Chemical Theory and Computation*, *5*(4), 1038–1050. https://doi.org/10.1021/ct900009a

Sarmad, S., Mikkola, J.-P., & Ji, X. (2016). CO2 capture with Ionic liquids (ILs) and Deep Eutectic Solvents (DESs): a new generation of sorbents. *ChemSusChem*.

Shukla, S. K., Khokarale, S. G., Bui, T. Q., & Mikkola, J. P. T. (2019). Ionic liquids: Potential materials for carbon dioxide capture and utilization. *Frontiers in Materials*, *6*. https://doi.org/10.3389/fmats.2019.00042

Silveira, A. J., Pereda, S., Tavares, F. W., & Abreu, C. R. A. (2019). A molecular dynamics study of the solvation of carbon dioxide and other compounds in the ionic liquids [emim][B(CN) 4] and [emim][NTf 2]. *Fluid Phase Equilibria*, *491*, 1–11. https://doi.org/10.1016/j.fluid.2019.03.007

Sonwani, S., & Saxena, P. (2022). Greenhouse Gases: Sources, Sinks and Mitigation. In *Greenhouse Gases: Sources, Sinks and Mitigation*. https://doi.org/10.1007/978-981-16-4482-5

Tiwikrama, A. H., Taha, M., & Lee, M. J. (2020). Experimental and computational studies on the solubility of carbon dioxide in protic ammonium-based ionic liquids. *Journal of the Taiwan Institute of Chemical Engineers*, *112*, 152–161. https://doi.org/10.1016/j.jtice.2020.06.015

Voroshylova, I. V., Ferreira, E. S. C., Malček, M., Costa, R., Pereira, C. M., & Cordeiro, M. N. D. S. (2018). Influence of the anion on the properties of ionic liquid mixtures: A molecular dynamics study. *Physical Chemistry Chemical Physics*, *20*(21), 14899–14918. https://doi.org/10.1039/c8cp01541d

Xiao, X., & Gao, M. (2021). Overview of climate change, air pollution, and human health. In *Air Pollution, Climate, and Health: An Integrated Perspective on Their Interactions*. Elsevier Inc. https://doi.org/10.1016/B978-0-12-820123-7.00003-6

Zaitsau, D. H., Kabo, G. J., Strechan, A. A., Paulechka, Y. U., Tschersich, A., Verevkin, S. P., & Heintz, A. (2006). Experimental vapor pressures of 1-alkyl-3-methylimidazolium Bis(trifluoromethylsulfonyl)imides and a correlation scheme for estimation of vaporization enthalpies of ionic liquids. *Journal of Physical Chemistry A*, *110*(22), 7303–7306. https://doi.org/10.1021/jp060896f

Zhang, X., Huo, F., Liu, Z., Wang, W., Shi, W., & Maginn, E. J. (2009). Tris (pentafluoroethyl) trifluorophosphate ([hmim][FEP]): A Molecular View by Computer Simulations. *J. Phys. Chem. B*, *113*(1), 7591–7598.

6. Global conclusions and perspectives

This work demonstrated the potential of ILs, DESs, and NADESs as effective solvents for the elimination of air pollutants, specifically VOCs like styrene. These solvents exhibit favorable physicochemical properties, biodegradability, and low toxicity towards activated sludge. The absorption experiments revealed the most suitable solvents for styrene capture, providing valuable insights for pollutant removal processes. Furthermore, the use of an IL as a non-aqueous liquid phase in a TPPB showed promising results in enhancing styrene biodegradation rates.

Additionally, this research explored the application of ILs, DESs, and NADESs for greenhouse gas capture. The impregnation of these solvents onto porous support materials, such as silica gel can offer a solution to the mass transfer limitations, due to the high viscosity presented by these solvents. The impregnated materials exhibited significant affinity for CO_2 and N_2O, with potential applications in greenhouse gas mitigation strategies. The impregnation process demonstrated a reduction in solvent consumption while maintaining the capture capacity for greenhouse gases.

Moreover, the study conducted quantum mechanics calculations to predict the Henry's law constants of CO_2 and N_2O for fluorinated imidazolium-based ionic liquids, provide valuable insights into their potential for gas capture applications. The use of these predictions could be beneficial for selecting solvents with high affinity towards target pollutants, based on parameters such as energies and Henry constants obtained through these models. These data could then be validated through practical-level experiments, thereby enabling significant savings in terms of time and financial resources.

Overall, this work contributes to the understanding of ILs, DESs, and NADESs as promising solvents for air pollution control and greenhouse gas mitigation. It highlights their advantageous properties, feasibility in pollutant removal processes, and potential for sustainable environmental applications.

This research opens up several perspectives for future work in the field of using ILs, DESs, and NADESs for air pollution control and greenhouse gas capture. Here are some potential avenues for further investigation:

1. Optimization of solvent formulations: Further research can focus on optimizing the composition of ILs, DESs, and NADESs to enhance their absorption capacities for specific pollutants. By modifying the chemical structure and ratios of the components, it may be possible to improve their selectivity, efficiency, and stability.

3. Long-term stability and recyclability: Investigating the long-term stability and recyclability of ILs, DESs, and NADESs is crucial for their practical application. Future studies can focus on evaluating the performance of these solvents over extended periods and developing efficient methods for their regeneration and reuse.

4. Process optimization in partitioning bioreactors: Further research can explore optimization strategies for partitioning bioreactors using ILs as non-aqueous phase liquids. This includes studying different reactor configurations, exploring the effects of operating parameters, and investigating the performance of various microorganisms in degrading different VOCs.

5. Development of advanced porous support materials: Exploring novel porous support materials, such as carbon-based structures or functionalized materials, with the objective todiminish the amount of solvent used, to enhance mass transfer rates and at the same timeto enhance the overall sorption capacity and efficiency of the capture process.

Finally, several applications can be listed for the utilization of the carbon dioxide that has been captured:

1.Carbon Mineralization: This involves converting captured CO_2 into stable carbonates through a chemical reaction with minerals, effectively locking up the carbon in solid form.

2. Carbonation of Concrete: CO_2 can be injected into concrete during its production, enhancing its strength and durability while sequestering the carbon.

3. Algae Cultivation: Algae can absorb CO_2 from industrial flue gases or directly from the atmosphere. The harvested algae biomass can then be used for various purposes, including biofuels, animal feed, and chemicals.

4. Carbon-to-Chemicals: CO_2 can be used as a feedstock to synthesize chemicals and fuels. For example, CO_2 can be converted into methanol, which can serve as a versatile building block for various chemical products.

These technologies are at various stages of development and implementation. Some are already being used on a small scale, while others are still in the experimental phase. As technology continues to advance, these approaches hold promise for helping to reduce CO_2 emissions and mitigate climate change.

7. Products derived from this thesis

1. Research paper

   Candia-Lomelí, M., Covarrubias-Garcia, I., Aizpuru, A., & Arriaga, S. (2023). **Preparation and physicochemical characterization of deep eutectic solvents and ionic liquids for the potential absorption and biodegradation of styrene vapors**. *Journal of Hazardous Materials*, 441(April 2022), 129835. https://doi.org/10.1016/j.jhazmat.2022.129835

2. Review

   Potential of ILs, DESs, and NADESs to enhance VOCs removal: progress and challenges. For submission

3. Research paper

   Greenhouse gases capture applying impregnated silica with IL, DES and NADES. For submission.

4. Oral presentation at a conference

   Mariana Candia-Lomelí, Sonia Arriaga, Michèle Heitz , Beatriz Delgado Cano, Antonio Avalos Ramirez (2022). **Greenhouse gases capture applying the ionic liquid impregnated onto porous silica.** *Canadian Chemical Engineering Conference*, Vancouver, British Columbia, Canada, October 22-26, 2022.

5. Research internship

   Under the direction of the Dr. Antonio Avalos Ramírez at Centre National en électrochimie et en Technologies Environnementales (CNETE) in Shawinigan, Québec, Canada and Dra. Michelle Heitz at Sherbrooke University.

8. Appendix

Table 8.1 Viscosity values and references depicted in Fig. 2.5

DES/IL	Viscosity, mPa*s	References
ChCl:EG (1:2)	35	Dietz et al., 2017
ATPB:TEG (1:10)	49.9	Hayyan et al., 2015
DEACE:Glycerol	50.4466	Siongco et al., 2013
DAC:TEG (1:4)	84.6	Hayyan et al., 2015
ChCl:Triethylene glycol (1:3)	110.4	Hayyan et al., 2015
BTPC:TEG (1:8)	116.7	Hayyan et al., 2015
MTPB:TEG (1:4)	136.1	Hayyan et al., 2015
N_{7777}-Cl:DecA (1:2)	172.87	Van Osch et al., 2015
N_{4444}-Cl:DecA (1:2)	265.26	Van Osch et al., 2015
N_{2222}-Cl:Glycolic acid (1:2)	268	Dietz et al., 2017
N_{8888}-Br :DecA (1:2)	469	Dietz et al., 2017
N_{8888}-Cl:DecA (1:2)	472.58	Van Osch et al., 2015
DEAC:Glycerol (:)	513.093	Siongco et al., 2013
N_{8881}-Br:DecA (1:2)	576.53	Van Osch et al., 2015
N_{8888}-Br:DecA (1:2)	636.36	Van Osch et al., 2015
N_{888}1-Cl:DecA (1:2)	783.41	Van Osch et al., 2015
Betaine:Levulinic acid (1:2)	838	Dietz et al., 2017
ChCl:Urea (1:2)	859.454	Shekaari et al., 2017
ChCl:Urea (1:2)	893	Dietz et al., 2017
ChCl:Glycerol (1:2)	1003.9428	Yadav et al., 2014
ChCl:Urea (1:2)	1371.9719	Yadav & Pandey, 2014
ChCl:Fructose (1.5:1)	14347.4	Hayyan et al., 2012
ChCl :Fructose (2.5:1)	17645.5	Hayyan et al., 2012
$[C_2mim][PF_6]$	15	Marcus, 2016
$[C_2mim][SCN]$	22.2	Marcus, 2016
$[C_1mim][NTf_2]$	32.9	Marcus, 2016
$[C_4mim][PF_6]$	40	Quijano et al., 2011a
$[AllylEt_2S][NTf_2]$	41.7	Rodriguez Castillo et al., 2018b
$[C_2mim][BF_4]$	52.3	Marcus, 2016
$[C_1mim][CH_3SO_4]$	72.6	Marcus, 2016
$[C_2mim][CH_3SO_4]$	78.8	Marcus, 2016
$[C_2mim][C_2H_5SO_4]$	101.3	Marcus, 2016
$[C_6mim][(C_2F_5)_3PF_3]$	119	Ge & Lee, 2015
$[C_4mim][Cl]$	161.7	Marcus, 2016
$[C_4Pyr][BF_4]$	183.7	Marcus, 2016
$[C_4mim][BF_4]$	188.1	Marcus, 2016
$[C_4mim][CH_3SO_4]$	207.6	Marcus, 2016
$[C_4mim][PF_6]$	208.3	Marcus, 2016
$[C_4mim][NTf_2]$	209	Quijano et al., 2011a, Rodriguez Castillo et al., 2018b

DES/IL	Viscosity, mPa*s	References
$[C_4mim][C_2H_5SO_4]$	214.5	Marcus, 2016
$[C_4Pyr][CF_3SO_3]$	217.6	Marcus, 2016
$[C_4Pyr][PF_6]$	231.5	Marcus, 2016
$[C_6mim][PF_6]$	241.5	Marcus, 2016
$[C_8mim][BF_4]$	254.2	Marcus, 2016
$[C_4Pyr][NTF_2]$	287.7	Marcus, 2016
$[C_4mim][NTf_2]$	291.78	Marcus, 2016
$[BMPL][(C_2F_5)_3PF_3]$	292	Ge & Lee, 2015
$[C_8mim][PF_6]$	304.1	Marcus, 2016
$[C_4mim][PF_6]$	312	Ge & Lee, 2015
$[C_4mim][C_8H_{17}SO_4]$	326.8	Marcus, 2016
$[C_8mim][NTF_2]$	360.1	Marcus, 2016
$[OctIq][NTf_2]$	451	Rodriguez Castillo et al., 2018b
$[DecIq][NTf_2]$	464.1	Rodriguez Castillo et al., 2018b
$[C_2mim][Cl]$	3530	Marcus, 2016

Table 8.2 Density values and references depicted in Fig. 2.6

DES/IL	Density, g/cm^3	References
N_{8888}-Cl:DecA (1:2)	0.8889	Van Osch et al., 2015
N_{7777}-Cl:DecA (1:2)	0.8907	Van Osch et al., 2015
N_{8881}-Cl:DecA (1:2)	0.8964	Van Osch et al., 2015
N_{4444}-Cl:DecA (1:2)	0.9168	Van Osch et al., 2015
N_{8888}-Br:DecA (1:2)	0.9298	Van Osch et al., 2015
N_{8881}-Br:DecA (1:2)	0.9422	Van Osch et al., 2015
DEACE:Glycerol (:)	1.099	Siongco et al., 2013
ChCl:Acetic acid (1:2)	1.11	Lynam et al., 2017
ChCl:Phenylacetic acid (1:4)	1.127	Altamash et al., 2017
ChCl:Phenylacetic acid (1:3)	1.138	Altamash et al., 2017
ATPB:DEG (1:16)	1.142	Ghaedi et al., 2017a
ATPB:TEG (1:16)	1.142	Ghaedi et al., 2017a
ChCl:Phenylacetic acid (1:2)	1.144	Altamash et al., 2017
ATPB:TEG (1:10)	1.155	Ghaedi et al., 2017a
ATPB:DEG (1:10)	1.156	Ghaedi et al., 2017a
ChCl :Formic acid (1:2)	1.16	Lynam et al., 2017
DEAC:Glycerol (:)	1.176	Siongco et al., 2013
ATPB:TEG (1:4)	1.187	Ghaedi et al., 2017a
ChCl :Lactic acid (1:10)	1.19	Lynam et al., 2017
ChCl:Glycerol (1:2)	1.194	Yadav et al., 2014
ATPB:DEG (1:4)	1.197	Ghaedi et al., 2017a
ChCl:Urea (1:2)	1.197	Shekaari et al., 2017
Betaine:Lactic acid (1:2)	1.2	Lynam et al., 2017

DES/IL	Density, g/cm^3	References
ChCl:Urea (1:2)	1.2	Yadav & Pandey, 2014
ChCl:Glycerol (1:2)	1.21	Abdullah & Kadhom, 2016
ChCl:Sucrose (4:1)	1.22	Craveiro et al., 2016
ChCl:Xylose (3:1)	1.22	Craveiro et al., 2016
ChCl:Xylose (2:1)	1.23	Craveiro et al., 2016
ChCl:Tartaric acid (2:1)	1.26	Craveiro et al., 2016
ChCl:Urea (1:2)	1.26	Abdullah & Kadhom, 2016
ChCl :Fructose (2.5:1)	1.26	Hayyan et al., 2012
ChCl:Glucose (1:1)	1.27	Craveiro et al., 2016
ChCl:Fructose (2:1)	1.28	Hayyan et al., 2012
ChCl:Citric acid (1:1)	1.3	Craveiro et al., 2016
ChCl:Fructose (1.5:1)	1.305	Hayyan et al., 2012
ChCl:Fructose (1:1)	1.337	Hayyan et al., 2012
ChCl:Sucrose (1:1)	1.35	Craveiro et al., 2016
Citric acid:Sucrose (1:1)	1.43	Craveiro et al., 2016
Citric acid:Glucose (1:1)	1.45	Craveiro et al., 2016
Glucose:Tartaric acid (1:1)	1.46	Craveiro et al., 2016
[C_6mim][Cl]	1.05	Ignat'ev et al., 2005
[C_4mim][$C_8H_{17}SO_4$]	1.066	Marcus, 2016
[C_4mim][Cl]	1.08	Marcus, 2016
[C_2mim][$C_2H_5SO_4$]	1.094	Marcus, 2016
[C_8mim][BF_4]	1.11	Marcus, 2016
[C_2mim][SCN]	1.116	Marcus, 2016
[C_8mim][PF_6]	1.119	Marcus, 2016
[C_1mim][Cl]	1.139	Marcus, 2016
[C_6mim][BF_4]	1.15	Ignat'ev et al., 2005
[C_1mim][SCN]	1.157	Marcus, 2016
[C_2mim][Cl]	1.186	Marcus, 2016
[C_4mim][BF_4]	1.201	Marcus, 2016
[C_2mim][CH_3SO_4]	1.205	Marcus, 2016
[C_4mim][CH_3SO_4]	1.205	Marcus, 2016
[C_4Pyr][BF_4]	1.214	Marcus, 2016
[C_4Pyr][PF_6]	1.214	Marcus, 2016
[C_4mim][$C_2H_5SO_4$]	1.232	Marcus, 2016
[C_2mim][BF_4]	1.28	Marcus, 2016
[DecIq][NTf_2]	1.2919	Rodriguez Castillo et al., 2018b
[C_6mim][PF_6]	1.292	Marcus, 2016
[C_1mim][BF_4]	1.306	Marcus, 2016
[C_4Pyr][CF_3SO_3]	1.311	Marcus, 2016
[C_8mim][NTF_2]	1.32	Marcus, 2016

DES/IL	Density, g/cm^3	References
[C_1mim][CH_3SO_4]	1.327	Marcus, 2016
[OctIq][NTf_2]	1.3282	Rodriguez Castillo et al., 2018b
[C_4mim][PF_6]	1.36	Ge & Lee, 2015
[C_6mim][$(CF_3SO_2)_2N$]	1.377	Ignat'ev et al., 2005
[C_2mim][PF_6]	1.413	Marcus, 2016
[AllylEt$_2$S][NTf_2]	1.4355	Rodriguez Castillo et al., 2018b
[C_4mim][NTf_2]	1.436	Marcus, 2016
[C_4Pyr][NTF_2]	1.442	Marcus, 2016
[C_1mim][PF_6]	1.478	Marcus, 2016
[C_2mim][Br]	1.48	Marcus, 2016
[C_2mim][NTf_2]	1.513	Marcus, 2016
[C_6mim][$(C_2F_5)_3PF_3$]	1.557	Ignat'ev et al., 2005
[C_1mim][NTf_2]	1.562	Marcus, 2016
[BMPL][$(C_2F_5)_3PF_3$]	1.589	Ge & Lee, 2015
[C_6mim][$(C_3F_7)_3PF_3$]	1.62	Ignat'ev et al., 2005
[C_2mim][I]	1.69	Marcus, 2016
[C_5mim][$(C_4F_9)_3PF_3$]	1.693	Ignat'ev et al., 2005

Table 8.3 Decomposition temperatures values and references depicted in Fig. 2.7

DES/IL	Decomposition temperature, °C	References
ChCl :EG (1:2)	84	Dietz et al., 2017
Imidazole :acetic acid (1:1)	93	Dietz et al., 2017
ChCl :EG (1:2)	107	Delgado-Mellado et al., 2018
ChCl :Malic acid (1:1)	113.15	Delgado-Mellado et al., 2018
Glucose :Tartaric acid (1:1)	117.5	Craveiro et al., 2016
Citric acid :Sucrose (1:1)	121.2	Craveiro et al., 2016
ChCl :Malonic acid (1:2)	125	Kroon & Binnemans, 2019
ChCl :Malonic acid (1:1)	126	Skulcova et al., 2017
ChCl :Sucrose (1:1)	126.8	Craveiro et al., 2016
ChCl :Glucose (1:1)	129.8	Craveiro et al., 2016
Citric acid :Glucose (1:1)	130.1	Craveiro et al., 2016
ChCl :Tartaric acid (2:1)	130.8	Craveiro et al., 2016
ATPPB :EG (1:4)	132.35, 322.29	Ghaedi et al., 2017b
ChCl :Sucrose (4:1)	141.7	Craveiro et al., 2016
N_{8888}-Br :DecA (1:2)	142	Dietz et al., 2017
N_{2222}-Cl :Glycolic acid (1:2)	143	Dietz et al., 2017
ChCl :Phenylpropionic acid (1:2)	156.45	Delgado-Mellado et al., 2018
ChCl :Levulinic acid (1:2)	158.35	Delgado-Mellado et al., 2018
ChCl :Levulinic acid (1:3)	159	Kroon & Binnemans, 2019
ChCl :Oxalic acid (1:2)	161	Kroon & Binnemans, 2019

DES/IL	Decomposition temperature, °C	References
ChCl :Xylose (2:1)	162.5	Craveiro et al., 2016
Betaine :Levulinic acid (1:2)	166	Dietz et al., 2017
ChCl :Citric acid (1:1)	171.3	Craveiro et al., 2016
ChCl :Urea (1:2)	172	Delgado-Mellado et al., 2018
ChCl :Xylose (3:1)	172.7	Craveiro et al., 2016
ChCl :Lactic acid (1:3)	173	Kroon & Binnemans, 2019
ATPPB :DEG (1:10)	173.57, 317.04	Ghaedi et al., 2018
ATPPB :DEG (1:16)	178, 315.12	Ghaedi et al., 2018
ATPPB :DEG (1:4)	178.65, 336.56	Ghaedi et al., 2018
ChCl :Phenylacetic acid (1:2)	179.05	Delgado-Mellado et al., 2018
ChCl :Glucose (2:1)	183.95	Delgado-Mellado et al., 2018
ChCl :Glycerol (1:2)	184	Delgado-Mellado et al., 2018
ChCl :Urea (1:2)	186	Dietz et al., 2017
ChCl :Phenylacetic acid (1:2)	190	Altamash et al., 2017
ChCl :Tartaric acid (1:1)	194	Skulcova et al., 2017
ChCl :Phenylacetic acid (1:4)	195	Altamash et al., 2017
ATPPB :TEG (1:16)	199.49, 311.25	Ghaedi et al., 2018
ChCl :Glycerol (1:2)	200	Abdullah & Kadhom, 2016
ChCl :Phenylacetic acid (1:3)	200	Altamash et al., 2017
ChCl :Urea (1:2)	200	Abdullah & Kadhom, 2016
ATPPB :TEG (1:4)	204.25, 326.64	Ghaedi et al., 2018
ChCl :Malic acid (1:2)	211	Kroon & Binnemans, 2019
ChCl :Lactic acid (1:1)	212	Skulcova et al., 2017
ChCl :Glycolic acid (1:3)	218	Kroon & Binnemans, 2019
ChCl :Glutaric acid (1:2)	235	Kroon & Binnemans, 2019
ATPPB :GL (1:4)	247.42, 338.35	Ghaedi et al., 2017b
ATPPB :TEG (1:10)	260.7, 315.94	Ghaedi et al., 2018
$[C_4mim][Cl]$	150	Marcus, 2016
$[C_6mim][Cl]$	253	Ignat'ev et al., 2005
$[C_8mim][BF_4]$	282	Marcus, 2016
$[C_2mim][BF_4]$	283	Marcus, 2016
$[C_2mim][Cl]$	285	Marcus, 2016
$[C_2mim][Br]$	287	Marcus, 2016
$[C_4Pyr][BF_4]$	289	Marcus, 2016
$[C_4mim][BF_4]$	293	Marcus, 2016
$[C_8mim][PF_6]$	299	Marcus, 2016
$[C_4Pyr][CF_3SO_3]$	302	Marcus, 2016
$[C_2mim][I]$	303	Marcus, 2016
$[C_6mim][BF_4]$	304	Ignat'ev et al., 2005
$[C_4Pyr][NTF_2]$	336	Marcus, 2016
$[C_4mim][C_8H_{17}SO_4]$	341	Marcus, 2016
$[C_8mim][NTF_2]$	345	Marcus, 2016
$[C_6mim][PF_6]$	361	Marcus, 2016

DES/IL	Decomposition temperature, °C	References
$[C_2mim][PF_6]$	375	Marcus, 2016
$[C_2mim][NTf_2]$	391	Marcus, 2016
$[C_4mim][NTf_2]$	403	Marcus, 2016
$[C_4mim][PF_6]$	423	Marcus, 2016
$[C_1mim][NTf_2]$	444	Marcus, 2016

Table 8.4. Log EC_{50} (μM) values and references depicted in Fig. 2.8

DES/IL	Log EC_{50} (μM)	Reference
[omim] [Cl]	0.69	Montalbán et al., 2016
[omim] $[PF_6]$	0.7	Romero et al., 2008
[omim] $[BF_4]$	0.91	Montalbán et al., 2016
[omim] [Cl]	0.94	Romero et al., 2008
[omim] $[NTf_2]$	0.99	Montalbán et al., 2016
[omim] $[PF_6]$	1.25	Montalbán et al., 2016
$[BMPy][BF_4]$	1.51	Hernández-Fernández et al., 2015
$[BMPheIM][MeSO_4]$	1.76	Hernández-Fernández et al., 2015
[hmim] $[NTf_2]$	1.82	Montalbán et al., 2016
[hmim] $[PF_6]$	2.11	Romero et al., 2008
$[BMIM][H_2SO_4]$	2.12	Hernández-Fernández et al., 2015
[hmim] [Cl]	2.18	Romero et al., 2008
[hmim] $[PF_6]$	2.36	Montalbán et al., 2016
[hmim] [Cl]	2.37	Montalbán et al., 2016
[BMIM][SCN]	2.37	Hernández-Fernández et al., 2015
Bmpy $[BF_4]$	2.44	Montalbán et al., 2016
$[Pi(_{4,4,4})_1][TOS]$	2.44	Hernández-Fernández et al., 2015
[bmim] $[NTf_2]$	2.51	Montalbán et al., 2016
$[P_{4441}][MeSO_4]$	2.64	Hernández-Fernández et al., 2015
[bdmim] $[NTf_2]$	2.87	Montalbán et al., 2016
$[MOxa][MeSO_4]$	3	Hernández-Fernández et al., 2015
$[BMIM][C_4EtSO_4]$	3.2	Hernández-Fernández et al., 2015
[bmim] $[PF_6]$	3.29	Montalbán et al., 2016
[bmim] [Cl]	3.39	Romero et al., 2008
[bmim] $[BF_4]$	3.46	Montalbán et al., 2016
[bmim] [Cl]	3.46	Montalbán et al., 2016
[bmim] $MDEGSO_4$	3.48	Montalbán et al., 2016
[HOPMIM][dca]	3.48	Hernández-Fernández et al., 2015
[HOPMIM][Cl]	3.52	Hernández-Fernández et al., 2015
[bmim] $MeSO_4$	3.57	Montalbán et al., 2016
[emim] $[NTf_2]$	3.62	Montalbán et al., 2016
[emim] [TfO]	3.74	Montalbán et al., 2016
$[Chol][H_2PO_4]$	3.76	Hernández-Fernández et al., 2015
pmim [Cl]	3.78	Montalbán et al., 2016

DES/IL	Log EC_{50} (μM)	Reference
Empy [$EtSO_4$]	3.83	Montalbán et al., 2016
[emim] [CH_3COO]	3.89	Montalbán et al., 2016
mim [Cl]	3.94	Montalbán et al., 2016
[emim] [$EtSO_4$]	4.02	Romero et al., 2008
[emim] [$EtSO_4$]	4.1	Montalbán et al., 2016
Eim [Cl]	4.16	Montalbán et al., 2016
[emim] [PF_6]	4.22	Montalbán et al., 2016
Dmim [Cl]	4.31	Montalbán et al., 2016
ETAN	4.32	Montalbán et al., 2016
[BMPyr][dca]	4.34	Hernández-Fernández et al., 2015
amim [Cl]	4.36	Montalbán et al., 2016
[emim] [Cl]	4.8	Montalbán et al., 2016
[HOPMIM][glycolate]	>5	Hernández-Fernández et al., 2015
[HOPMIM][FCH_2COO]	>5	Hernández-Fernández et al., 2015
[BMPyr][Cl]	>5	Hernández-Fernández et al., 2015
[BMPyr][TFO]	>5	Hernández-Fernández et al., 2015
Hemim [Cl]	5.34	Montalbán et al., 2016
[bmim] [NTf_2]	5.41	Mena et al., 2020
[bmim] [Cl]	6.43	Mena et al., 2020
ChCl:Citric acid (1:2)	4.51	De Morais et al., 2015
ChCl:Citric acid (1:1)	4.83	De Morais et al., 2015
ChCl:Citric acid (2:1)	4.84	De Morais et al., 2015
Cholinium:Dihydrogenocitrate	4.99	Ventura et al., 2014
ChCl:Glycolic acid (1:2)	5.02	De Morais et al., 2015
ChCl:Lactic acid (1:2)	5.06	De Morais et al., 2015
ChCl:Glycolic acid (1:1)	5.20	De Morais et al., 2015
Cholinium:Bitartrate	5.21	Ventura et al., 2014
ChCl:Glycolic acid (2:1)	5.24	De Morais et al., 2015
ChCl:Lactic acid (2:1)	5.28	De Morais et al., 2015
ChCl:Lactic acid (1:1)	5.44	De Morais et al., 2015
ChCl:Acetic acid (1:2)	5.70	De Morais et al., 2015
ChCl:Acetic acid (2:1)	6.02	De Morais et al., 2015
ChCl:Acetic acid (1:1)	6.03	De Morais et al., 2015
Cholinium:Salicylate	6.26	Ventura et al., 2014
Cholinium:Dihydrogeno phosphate	6.36	Ventura et al., 2014
Cholinium:Propanoate	6.58	Ventura et al., 2014
Cholinium:Butanoate	6.63	Ventura et al., 2014
Cholinium:Chloride	6.67	Ventura et al., 2014
Cholinium:Acetate	6.86	Ventura et al., 2014
Bzchol:Chloride	7.14	Ventura et al., 2014

Table 8.5. Dimensionless partition coefficient of different VOCs in ILs or DESs depicted in Fig. 2.9

IL/DES	VOC	Dimensionless partition coefficient,	T, K	Reference
[AllylEt$_2$S][NTf$_2$]	Toluene	0.00356	298	Rodriguez Castillo et al., 2019
	Dichloromethane	0.04914	298	Rodriguez Castillo et al., 2019
[bmim][FAP]	Styrene	0.0023	301	Candia-Lomelí et al., 2023
[bmim][NfO]	Toluene	0.01135	298	Rodriguez Castillo et al., 2019
	Dichloromethane	0.05632	298	Rodriguez Castillo et al., 2019
[bmim][NTf$_2$]	Toluene	0.00061	298	Quijano et al., 2011a
	Dimethyl Disulfide	0.0012	298	Quijano et al., 2011a
	Styrene	0.0037	301	Candia-Lomelí et al., 2023
	Dimethyl Sulfide	0.009	298	Quijano et al., 2011a
[bmim][PF$_6$]	Toluene	0.0008	293	Ma et al., 2021
	Acetone	0.0009	293	Ma et al., 2021
	Toluene	0.00096	298	Quijano et al., 2011a
	Toluene	0.0012	333	Ma et al., 2021
	Dimethyl Disulfide	0.0013	298	Quijano et al., 2011a
	Acetone	0.0014	333	Ma et al., 2021
	Styrene	0.0040	301	Candia-Lomelí et al., 2023
	Toluene	0.00976	298	Rodriguez Castillo et al., 2019
	Dimethyl Sulfide	0.011	298	Quijano et al., 2011a
	Dichloromethane	0.04226	298	Rodriguez Castillo et al., 2019
[bmim][Tf$_2$N]	Toluene	0.00581	298	Rodriguez Castillo et al., 2019
	Dichloromethane	0.04671	298	Rodriguez Castillo et al., 2019
[BMPyrr][NTf$_2$]	Toluene	0.0071	298	Rodriguez Castillo et al., 2019
	Dichloromethane	0.04242	298	Rodriguez Castillo et al., 2019
[BMTriaz][NTf$_2$]	Toluene	0.00384	298	Rodriguez Castillo et al., 2019
	Dichloromethane	0.05699	298	Rodriguez Castillo et al., 2019
[Butenylmim][NfO]	Toluene	0.01262	298	Rodriguez Castillo et al., 2019
	Dichloromethane	0.02109	298	Rodriguez Castillo et al., 2019
[Butenylmim][NTf$_2$]	Toluene	0.00771	298	Rodriguez Castillo et al., 2019
	Dichloromethane	0.04841	298	Rodriguez Castillo et al., 2019
[Butenylmim][PF$_6$]	Toluene	0.01477	298	Rodriguez Castillo et al., 2019
	Dichloromethane	0.04331	298	Rodriguez Castillo et al., 2019
[CF$_3$CF$_2$BTriaz][NTf$_2$]	Toluene	0.00231	298	Rodriguez Castillo et al., 2019
	Dichloromethane	0.0686	298	Rodriguez Castillo et al., 2019
[CNC$_3$mim][NTf$_2$]	Toluene	0.0126	298	Rodriguez Castillo et al., 2019
	Dichloromethane	0.06244	298	Rodriguez Castillo et al., 2019
[DecIq][NTf$_2$]	Toluene	0.00211	298	Rodriguez Castillo et al., 2019
	Dichloromethane	0.02052	298	Rodriguez Castillo et al., 2019
[emim][BF$_4$]	Styrene	0.0018	303	Ma et al., 2019
	Chlorobenzene	0.0024	303	Ma et al., 2019
	Ethyl acetate	0.12	303	Ma et al., 2019
	Toluene	0.15	363	Ma et al., 2019
	Hexane	0.28	303	Ma et al., 2019
[EtOEmim][NTf$_2$]	Toluene	0.0067	298	Rodriguez Castillo et al., 2019
	Dichloromethane	0.04954	298	Rodriguez Castillo et al., 2019

IL/DES	VOC	Dimensionless partition coefficient,	T, K	Reference
[EtOEMMorph][NTf_2]	Toluene	0.00325	298	Rodriguez Castillo et al., 2019
	Dichloromethane	0.06825	298	Rodriguez Castillo et al., 2019
[iPentmim][NTf_2]	Toluene	0.00254	298	Rodriguez Castillo et al., 2019
	Dichloromethane	0.04499	298	Rodriguez Castillo et al., 2019
[iPentmim][PF_6]	Toluene	0.01031	298	Rodriguez Castillo et al., 2019
	Dichloromethane	0.04315	298	Rodriguez Castillo et al., 2019
[MeOEIq][NTf_2]	Toluene	0.00554	298	Rodriguez Castillo et al., 2019
	Dichloromethane	0.05023	298	Rodriguez Castillo et al., 2019
[MeOEmim][NfO]	Toluene	0.00316	298	Rodriguez Castillo et al., 2019
[MeOEmim][NTf_2]	Toluene	0.00775	298	Rodriguez Castillo et al., 2019
	Dichloromethane	0.06259	298	Rodriguez Castillo et al., 2019
[MeOEMMorph][NTf_2]	Toluene	0.00301	298	Rodriguez Castillo et al., 2019
	Dichloromethane	0.03772	298	Rodriguez Castillo et al., 2019
[MeOEOEmim][NTf_2]	Toluene	0.00816	298	Rodriguez Castillo et al., 2019
	Dichloromethane	0.05234	298	Rodriguez Castillo et al., 2019
[nPrmim][NTf_2]	Toluene	0.00295	298	Rodriguez Castillo et al., 2019
	Dichloromethane	0.05026	298	Rodriguez Castillo et al., 2019
[OctIq][NTf_2]	Toluene	0.00022	298	Rodriguez Castillo et al., 2018
	Toluene	0.00201	298	Rodriguez Castillo et al., 2019
	Dichloromethane	0.04016	298	Rodriguez Castillo et al., 2019
ChCl:ET (1:2)	Acetaldehyde	0.0001	303	Moufawad et al., 2022
	Acetaldehyde	0.0009	303	Moura et al., 2017
	Acetaldehyde	0.0009	333	Moura et al., 2017
	toluene	0.005	333	Moura et al., 2017
	Dichloromethane	0.01	333	Moura et al., 2017
	n-heptane	0.018	303	Moufawad et al., 2022
	toluene	0.022	303	Moura et al., 2017
	toluene	0.022	303	Moufawad et al., 2022
	Dichloromethane	0.034	303	Moufawad et al., 2022
	Dichloromethane	0.034	303	Moura et al., 2017
	Methyl ethyl ketone	0.084	303	Moufawad et al., 2022
	1-decene	0.64	303	Moufawad et al., 2022
ChCl:Glycerol (1:2)	Acetaldehyde	0.00005	303	Moufawad et al., 2022
	Acetaldehyde	0.0009	303	Moura et al., 2017
	Acetaldehyde	0.0009	333	Moura et al., 2017
	n-heptane	0.018	303	Moufawad et al., 2022
	Methyl ethyl ketone	0.023	303	Moufawad et al., 2022
	Dichloromethane	0.037	303	Moura et al., 2017
	Dichloromethane	0.037	303	Moufawad et al., 2022
	toluene	0.054	303	Moufawad et al., 2022
	toluene	0.054	303	Moura et al., 2017
	Dichloromethane	0.121	333	Moura et al., 2017
	toluene	0.185	333	Moura et al., 2017
	1-decene	1.1	303	Moufawad et al., 2022
ChCl:Lactic acid (1:2)	Methyl ethyl ketone	0.0098	303	Fahri et al., 2020
	toluene	0.0101	303	Fahri et al., 2020

IL/DES	VOC	Dimensionless partition coefficient,	T, K	Reference
	Dichloromethane	0.0211	303	Fahri et al., 2020
ChCl:levulinic acid (1:2)	Acetaldehyde	0.0004	303	Moufawad et al., 2022
	Acetaldehyde	0.0009	303	Moura et al., 2017
	Acetaldehyde	0.0009	333	Moura et al., 2017
	toluene	0.004	303	Moura et al., 2017
	toluene	0.0045	303	Fahri et al., 2020
	toluene	0.005	303	Moufawad et al., 2022
	Methyl ethyl ketone	0.0065	303	Moufawad et al., 2022
	Methyl ethyl ketone	0.0066	303	Fahri et al., 2020
	Dichloromethane	0.008	303	Moufawad et al., 2022
	Dichloromethane	0.008	303	Moura et al., 2017
	Dichloromethane	0.0105	303	Fahri et al., 2020
	toluene	0.025	333	Moura et al., 2017
	Dichloromethane	0.028	333	Moura et al., 2017
	1-decene	0.029	303	Moufawad et al., 2022
	n-heptane	0.27	303	Moufawad et al., 2022
ChCl:urea (1:2)	Acetaldehyde	0.00001	303	Moufawad et al., 2022
	Methyl ethyl ketone	0.046	303	Moufawad et al., 2022
	Dichloromethane	0.055	303	Moufawad et al., 2022
	toluene	0.096	303	Moufawad et al., 2022
	1-decene	1.2	303	Moufawad et al., 2022
	n-heptane	11	303	Moufawad et al., 2022
	Acetaldehyde	0.0009	303	Moura et al., 2017
	Acetaldehyde	0.0009	333	Moura et al., 2017
	toluene	0.096	303	Moura et al., 2017
	Dichloromethane	0.124	303	Moura et al., 2017
	Dichloromethane	0.143	333	Moura et al., 2017
	toluene	0.18	333	Moura et al., 2017
Chol-C_6-Lac	Toluene	0.0028	303	Fahri et al., 2020
	Methyl ethyl ketone	0.0067	303	Fahri et al., 2020
	Dichloromethane	0.0141	303	Fahri et al., 2020
Chol-C_6-Lev	Toluene	0.0021	303	Fahri et al., 2020
	Methyl ethyl ketone	0.0068	303	Fahri et al., 2020
	Dichloromethane	0.009	303	Fahri et al., 2020
Chol-C_8-Lac	Toluene	0.002	303	Fahri et al., 2020
	Methyl ethyl ketone	0.0062	303	Fahri et al., 2020
	Dichloromethane	0.0109	303	Fahri et al., 2020
Chol-C_8-Lev	Toluene	0.0016	303	Fahri et al., 2020
	Methyl ethyl ketone	0.0051	303	Fahri et al., 2020
	Dichloromethane	0.0071	303	Fahri et al., 2020
[EtOEIq][NTf_2]	Toluene	0.00212	298	Rodriguez Castillo et al., 2019
	Dichloromethane	0.04951	298	Rodriguez Castillo et al., 2019
TBA-Br:Decanoic acid (1:2)	Acetaldehyde	0.0004	303	Moufawad et al., 2022
	1-decene	0.0004	303	Moufawad et al., 2022
	Acetaldehyde	0.0009	303	Moura et al., 2017
	toluene	0.0009	303	Moufawad et al., 2022

IL/DES	VOC	Dimensionless partition coefficient,	T, K	Reference
	toluene	0.001	303	Moura et al., 2017
	toluene	0.001	333	Moura et al., 2017
	Acetaldehyde	0.001	333	Moura et al., 2017
	n-heptane	0.0033	303	Moufawad et al., 2022
	Methyl ethyl ketone	0.004	303	Moufawad et al., 2022
	Dichloromethane	0.005	303	Moura et al., 2017
	Dichloromethane	0.005	303	Moufawad et al., 2022
	Dichloromethane	0.007	333	Moura et al., 2017
TBP-Br:ET (1:2)	Acetaldehyde	0.00013	303	Moufawad et al., 2022
	1-decene	0.0011	303	Moufawad et al., 2022
	toluene	0.0018	303	Moufawad et al., 2022
	Dichloromethane	0.004	303	Moufawad et al., 2022
	Methyl ethyl ketone	0.013	303	Moufawad et al., 2022
	n-heptane	0.047	303	Moufawad et al., 2022
TBP-Br:Glycerol (1:1)	Acetaldehyde	0.0009	303	Moura et al., 2017
	Acetaldehyde	0.0009	333	Moura et al., 2017
	Dichloromethane	0.002	333	Moura et al., 2017
	toluene	0.004	303	Moura et al., 2017
	toluene	0.005	333	Moura et al., 2017
	Dichloromethane	0.005	303	Moura et al., 2017
TBP-Br:Glycerol (1:2)	Acetaldehyde	0.00004	303	Moufawad et al., 2022
	Methyl ethyl ketone	0.0023	303	Moufawad et al., 2022
	toluene	0.004	303	Moufawad et al., 2022
	Dichloromethane	0.0053	303	Moufawad et al., 2022
	n-heptane	0.11	303	Moufawad et al., 2022
	1-decene	0.123	303	Moufawad et al., 2022
TBP-Br:Levulinic acid (1:2)	Acetaldehyde	0.00017	303	Moufawad et al., 2022
	toluene	0.0013	303	Moufawad et al., 2022
	1-decene	0.0015	303	Moufawad et al., 2022
	Methyl ethyl ketone	0.004	303	Moufawad et al., 2022
	Dichloromethane	0.006	303	Moufawad et al., 2022
	n-heptane	0.034	303	Moufawad et al., 2022
TBP-Br:Levulinic acid (1:6)	Acetaldehyde	0.0009	303	Moura et al., 2017
	toluene	0.001	303	Moura et al., 2017
	Acetaldehyde	0.001	333	Moura et al., 2017
	toluene	0.005	333	Moura et al., 2017
	Dichloromethane	0.006	303	Moura et al., 2017
	Dichloromethane	0.015	333	Moura et al., 2017

Referencias

Abdullah, G. H., & Kadhom, M. A. (2016). Studying of two choline chloride's deep eutectic solvents in their aqueous mixtures. In *International Journal of Engineering Research* (Vol. 12, Issue 9).

Altamash, T., Atilhan, M., Aliyan, A., Ullah, R., Nasser, M., & Aparicio, S. (2017). Rheological, Thermodynamic, and Gas Solubility Properties of Phenylacetic Acid-Based Deep Eutectic Solvents. *Chemical Engineering and Technology*, *40*(4), 778–790. https://doi.org/10.1002/ceat.201600475

Candia-Lomelí, M., Covarrubias-Garcia, I., Aizpuru, A., & Arriaga, S. (2023). Preparation and physicochemical characterization of deep eutectic solvents and ionic liquids for the potential absorption and biodegradation of styrene vapors. *Journal of Hazardous Materials*, *441*(April 2022), 129835. https://doi.org/10.1016/j.jhazmat.2022.129835

Craveiro, R., Aroso, I., Flammia, V., Carvalho, T., Viciosa, M. T., Dionísio, M., Barreiros, S., Reis, R. L., Duarte, A. R. C., & Paiva, A. (2016). Properties and thermal behavior of natural deep eutectic solvents. *Journal of Molecular Liquids*, *215*, 534–540. https://doi.org/10.1016/j.molliq.2016.01.038

De Morais, P., Gonçalves, F., Coutinho, J. A. P., & Ventura, S. P. M. (2015). Ecotoxicity of Cholinium-Based Deep Eutectic Solvents. *ACS Sustainable Chemistry and Engineering*, *3*(12), 3398–3404. https://doi.org/10.1021/acssuschemeng.5b01124

Delgado-Mellado, N., Larriba, M., Navarro, P., Rigual, V., Ayuso, M., García, J., & Rodríguez, F. (2018). Thermal stability of choline chloride deep eutectic solvents by TGA/FTIR-ATR analysis. *Journal of Molecular Liquids*, *260*, 37–43. https://doi.org/10.1016/j.molliq.2018.03.076

Dietz, C. H. J. T., Kroon, M. C., Van Sint Annaland, M., & Gallucci, F. (2017). Thermophysical Properties and Solubility of Different Sugar-Derived Molecules in Deep Eutectic Solvents. *Journal of Chemical and Engineering Data*, *62*(11), 3633–3641. https://doi.org/10.1021/acs.jced.7b00184

Fahri, F., Bacha, K., Chiki, F. F., Mbakidi, J. P., Panda, S., Bouquillon, S., & Fourmentin, S. (2020). Air pollution: new bio-based ionic liquids absorb both hydrophobic and hydrophilic volatile organic compounds with high efficiency. *Environmental Chemistry Letters*, *18*(4), 1403–1411. https://doi.org/10.1007/s10311-020-01007-8

Ge, D., & Lee, H. K. (2015). Ultra-hydrophobic ionic liquid 1-hexyl-3-methylimidazolium tris(pentafluoroethyl)trifluorophosphate supported hollow-fiber membrane liquid-liquid-liquid microextraction of chlorophenols. *Talanta*, *132*, 132–136. https://doi.org/10.1016/j.talanta.2014.08.074

Ghaedi, H., Ayoub, M., Sufian, S., Hailegiorgis, S. M., Murshid, G., & Khan, S. N. (2018). Thermal stability analysis, experimental conductivity and pH of phosphonium-based deep eutectic solvents and their prediction by a new empirical equation. *Journal of Chemical Thermodynamics*, *116*, 50–60. https://doi.org/10.1016/j.jct.2017.08.029

Ghaedi, H., Ayoub, M., Sufian, S., Shariff, A. M., & Lal, B. (2017). The study on temperature dependence of viscosity and surface tension of several Phosphonium-based deep eutectic solvents. *Journal of Molecular Liquids*, *241*, 500–510. https://doi.org/10.1016/j.molliq.2017.06.024

Hayyan, A., Mjalli, F. S., Alnashef, I. M., Al-Wahaibi, T., Al-Wahaibi, Y. M., & Hashim, M. A. (2012). Fruit sugar-based deep eutectic solvents and their physical properties. *Thermochimica Acta*, *541*, 70–75. https://doi.org/10.1016/j.tca.2012.04.030

Hayyan, M., Aissaoui, T., Hashim, M. A., AlSaadi, M. A. H., & Hayyan, A. (2015). Triethylene glycol based deep eutectic solvents and their physical properties. *Journal of the Taiwan Institute of Chemical Engineers*, *50*, 24–30. https://doi.org/10.1016/j.jtice.2015.03.001

Hernández-Fernández, F. J., Bayo, J., Pérez de los Ríos, A., Vicente, M. A., Bernal, F. J., & Quesada-Medina, J. (2015). Discovering less toxic ionic liquids by using the Microtox® toxicity test. *Ecotoxicology and Environmental Safety*, *116*, 29–33. https://doi.org/10.1016/j.ecoenv.2015.02.034

Ignat'ev, N. V., Welz-Biermann, U., Kucheryna, A., Bissky, G., & Willner, H. (2005). New ionic liquids with tris(perfluoroalkyl)trifluorophosphate (FAP) anions. *Journal of Fluorine Chemistry*, *126*(8), 1150–1159. https://doi.org/10.1016/j.jfluchem.2005.04.017

Kroon, M. C., & Binnemans, K. (2019). Degradation of Deep-Eutectic Solvents Based on Choline Chloride and Carboxylic Acids [Research-article]. *ACS Sustainable Chemistry & Engineering*, *7*, 11521–11528. https://doi.org/10.1021/acssuschemeng.9b01378

Lynam, J. G., Kumar, N., & Wong, M. J. (2017). Deep eutectic solvents' ability to solubilize lignin, cellulose, and hemicellulose; thermal stability; and density. *Bioresource Technology*, *238*, 684–689. https://doi.org/https://doi.org/10.1016/j.biortech.2017.04.079

Ma, X., Wang, W., Sun, C., & Sun, J. (2021). Comprehensive evaluation of ionic liquid [Bmim][PF6] for absorbing toluene and acetone. *Environmental Pollution*, *285*, 117675. https://doi.org/10.1016/j.envpol.2021.117675

Ma, X., Wu, M., Liu, S., Huang, J., Sun, B., Zhou, Y., Zhu, Q., & Lu, H. (2019). Concentration control of volatile organic compounds by ionic liquid absorption and desorption. *Chinese Journal of Chemical Engineering*, *27*(10), 2383–2389. https://doi.org/10.1016/j.cjche.2018.12.019

Marcus, Y. (2016). *Ionic Liquid Properties*. Springer International Publishing. https://doi.org/10.1007/978-3-319-30313-0

Mena, I. F., Diaz, E., Palomar, J., Rodriguez, J. J., & Mohedano, A. F. (2020). Cation and anion effect on the biodegradability and toxicity of imidazolium– and choline–based ionic liquids. *Chemosphere*, *240*. https://doi.org/10.1016/j.chemosphere.2019.124947

Montalbán, M. G., Hidalgo, J. M., Collado-González, M., Díaz Baños, F. G., & Víllora, G. (2016). Assessing chemical toxicity of ionic liquids on Vibrio fischeri: Correlation with structure and composition. *Chemosphere*, *155*, 405–414. https://doi.org/10.1016/j.chemosphere.2016.04.042

Moufawad, T., Costa Gomes, M., & Fourmentin, S. (2022). Deep eutectic solvents as absorbents for VOC and VOC mixtures in static and dynamic processes. *Chemical Engineering Journal*, *448*(June), 137619. https://doi.org/10.1016/j.cej.2022.137619

Moura, L., Moufawad, T., Ferreira, M., Bricout, H., Tilloy, S., Monflier, E., Costa Gomes, M. F., Landy, D., & Fourmentin, S. (2017). Deep eutectic solvents as green absorbents of volatile organic pollutants. *Environmental Chemistry Letters*, *15*(4), 747–753. https://doi.org/10.1007/s10311-017-0654-y

Quijano, G., Couvert, A., Amrane, A., Darracq, G., Couriol, C., Le Cloirec, P., Paquin, L., & Carrié, D. (2011). Potential of ionic liquids for VOC absorption and biodegradation in multiphase systems. *Chemical Engineering Science*, *66*(12), 2707–2712. https://doi.org/10.1016/j.ces.2011.01.047

Rodriguez Castillo, A. S., Biard, P. F., Guihéneuf, S., Paquin, L., Amrane, A., & Couvert, A. (2019). Assessment of VOC absorption in hydrophobic ionic liquids: Measurement of partition and diffusion coefficients and simulation of a packed column. *Chemical Engineering Journal*, *360*(October 2018), 1416–1426. https://doi.org/10.1016/j.cej.2018.10.146

Rodriguez Castillo, A. S., Guihéneuf, S., Biard, P. F., Paquin, L., Amrane, A., & Couvert, A. (2018). Physicochemical properties of some hydrophobic room-temperature ionic liquids applied to volatile organic compounds biodegradation processes. *Journal of Chemical Technology and Biotechnology*, *93*(1), 215–223. https://doi.org/10.1002/jctb.5343

Romero, A., Santos, A., Tojo, J., & Rodríguez, A. (2008). Toxicity and biodegradability of imidazolium ionic liquids. *Journal of Hazardous Materials*, *151*(1), 268–273. https://doi.org/10.1016/j.jhazmat.2007.10.079

Shekaari, H., Zafarani-Moattar, M. T., & Mohammadi, B. (2017). Thermophysical characterization of aqueous deep eutectic solvent (choline chloride/urea) solutions in full ranges of concentration at T = (293.15–323.15) K. *Journal of Molecular Liquids*, *243*, 451–461. https://doi.org/10.1016/j.molliq.2017.08.051

Siongco, K. R., Leron, R. B., & Li, M. H. (2013). Densities, refractive indices, and viscosities of N,N-

diethylethanol ammonium chloride-glycerol or -ethylene glycol deep eutectic solvents and their aqueous solutions. *Journal of Chemical Thermodynamics*, *65*, 65–72. https://doi.org/10.1016/j.jct.2013.05.041

Skulcova, A., Majova, V., Haz, A., Kreps, F., Russ, A., & Jablonsky, M. (2017). Long-term isothermal stability of deep eutectic solvents based on choline chloride with malonic or lactic or tartaric acid. *International Journal of Scientific & Engineering Research*, *8*(7), 2249–2252.

Van Osch, D. J. G. P., Zubeir, L. F., Van Den Bruinhorst, A., Rocha, M. A. A., & Kroon, M. C. (2015). Hydrophobic deep eutectic solvents as water-immiscible extractants. *Green Chemistry*, *17*(9), 4518–4521. https://doi.org/10.1039/c5gc01451d

Ventura, S. P. M., e Silva, F. A., Gonçalves, A. M. M., Pereira, J. L., Gonçalves, F., & Coutinho, J. A. P. (2014). Ecotoxicity analysis of cholinium-based ionic liquids to Vibrio fischeri marine bacteria. *Ecotoxicology and Environmental Safety*, *102*(1), 48–54. https://doi.org/10.1016/j.ecoenv.2014.01.003

Yadav, A., & Pandey, S. (2014). Densities and viscosities of (choline chloride + urea) deep eutectic solvent and its aqueous mixtures in the temperature range 293.15 K to 363.15 K. *Journal of Chemical and Engineering Data*, *59*(7), 2221–2229. https://doi.org/10.1021/je5001796

Yadav, A., Trivedi, S., Rai, R., & Pandey, S. (2014). Densities and dynamic viscosities of (choline chloride+glycerol) deep eutectic solvent and its aqueous mixtures in the temperature range (283.15-363.15)K. *Fluid Phase Equilibria*, *367*, 135–142. https://doi.org/10.1016/j.fluid.2014.01.028